UNIVERSITY OF OKLAHOMA

GRADUATE COLLEGE

OBSERVATIONS OF X RAYS PRODUCED BY STRONG ELECTRIC FIELDS IN THUNDERSTORMS

A Dissertation

SUBMITTED TO THE GRADUATE FACULTY

in partial fulfillment of the requirements for the

degree of

Doctor of Philosophy

By

KENNETH BRYAN EACK

Norman, Oklahoma

1997

UMI Number: 9806320

UMI
300 North Zeeb Road
Ann Arbor, MI 48103

OBSERVATIONS OF X RAYS PRODUCED BY STRONG ELECTRIC FIELDS IN THUNDERSTORMS

A Dissertation APPROVED FOR THE

DEPARTMENT OF PHYSICS AND ASTRONOMY

BY

William H. Beasley

William H. Beasley, Advisor

W David Rust

W. David Rust

Bruce A. Mason

Bruce Mason

David Branch

Dave Branch

M B Johnson

Matthew Johnson

Susan Postawko

Susan Postawko

Acknowledgments

I would like to thank first my advisor, Dr. William Beasley for his support throughout my time as a graduate student. He went beyond the call of duty (pardon the cliche) in not only his advice on academics and research but also for his help and understanding in all the non-science trials in my life.

I appreciate the advice that Dave Rust gave me for initial instrument planning and the access to the Balloon Barn facilities he provided. I thank Dennis Nealson and Paul Griffin for maintaining the barn and mobile ballooning facilities. I would also like to thank Monte Bateman for his help on numerous instrumentation issues (especially for his advice to let go of the instrument when the balloon flew off), and Tom Shepherd who provided many insightful comments on ballooning and instrumentation, not to mention some very humorous conversations. Tom Marshall and Maribeth Stolzenburg provided the electric-field instrumentation, data and diligence that made this research possible and I greatly appreciate their efforts. I thank Michael McCarthy for his advice on x-ray spectrometers, Megan Maddox for her navigational skills that placed us where we needed to be in the storms and Dr. Steve Schery of the New Mexico Tech Radon Lab for his assistance in calibrating the detectors and for involving me in research as an undergraduate. My work in the Radon Lab provided me with the preparation needed to design the detectors used in this research.

Finally I would like to thank Dr. William Winn and Dr. Charles Moore for their help in instrument testing and especially for creating and maintaining a unique research facility. The work done at the Irving Langmuir Laboratory for Atmospheric Research has been an inspiration to me.

This work was supported by grant ATM-9414122 from the Physical Meteorology Program in the Atmospheric Sciences Division of the National Science Foundation. Additional support was also provided by the Department of Physics and Astronomy through a three-year graduate student fellowship and by the Graduate College. Facilities, equipment, and personnel support were provided in part by the National Severe Storms Laboratory and the Irving Langmuir Laboratory for Atmospheric Research. The support received from these groups is greatly appreciated.

Thanks to my best friend, Mary Walsh for always being there for me and for showing me that astronomy wasn't the only reason to look up at the sky! Although last in this list, the most important individuals in this entire acknowledgment are my parents, Thad and Mary Eack. Without them and their unwavering support and Love I could never have achieved as much as I have. Thank you just is not enough!

Table of Contents

List of Tables

List of Figures

Abstract

A balloon-borne x-ray spectrometer was developed to fly on free balloons into thunderstorms in order to test hypotheses that strong electric-fields could accelerate cosmic-ray secondary electrons and produce bremsstrahlung x rays. Five flights were made over a period of two years into the stratiform regions of mesoscale convective systems. The x-ray spectrometer flew with an electric-field meter and a meteorological radiosonde. In four instances, increases in x-ray intensity were observed during these flights. All were observed in conjunction with strong electric fields. Both negative and positive polarities (referenced to the vertical field) produced x rays. These events lasted on the order of 10's of seconds. In three of the cases, the increased x-ray intensity returned to near background levels when lightning flashes reduced the local electric field. These two observations appear to indicate that the increases in x-ray intensity observed are associated with the strong electric field present in thunderstorms. However, the time resolution of these observations does not allow any conclusions to be made about the production of x-rays by lightning

Chapter 1
Introduction

In 1924, C.T.R. Wilson hypothesized that the strong electric fields known to occur in thunderstorms should be able to accelerate β particles (electrons) to high energies [*Wilson*, 1925]. In his work, Wilson assumed β emissions from radium to be the source of the energetic electrons and that at some point the electric field inside the cloud must approach the sparking limit (where dielectric breakdown occurs), which for air at sea level is about 3000 kV m^{-1}. He further assumed that some x and γ radiation should be produced as these β particles pass through the air (bremsstrahlung radiation), since whenever a charged particle is accelerated it will produce electromagnetic radiation. In this case energetic electrons (β particles) are accelerated during interactions with the air molecules. Although the full theoretical details are not presented in *Wilson* [1925], the basic physical principles are discussed. The more recent detailed theoretical work is based on these principles. *Wilson* [1925] noted that "It would be of interest to test by experiment whether a thundercloud does emit any measurable amount of extremely penetrating radiation of the β- or γ-ray type."

1.1 Ground-based measurements

To test Wilson's hypothesis, researchers over the years have tried to observe increases in x-rays or electrons during thunderstorms by making measurements at or near the ground. *Suszcynsky et al.* [1996] provides an excellent review of these efforts and

Table 1.1 provides a summary of the observational results. Although some of these measurements indicated a correlation between thunderstorm activity and increased β and γ radiation [*Schonland and Viljoen*, 1933; *Appleton and Bowen* 1933; *Halliday*, 1934; *Clay et al.*, 1952; *Whitmire* 1979 and *D'Angelo*, 1987], they were still inconclusive because of limited temporal resolution and because no clear source could be identified. Other investigations found no increases in radiation levels from background. For example *Hill* [1963] placed photographic emulsions near lightning strike points on a 300 meter tower and found no evidence of enhanced radiation levels.

Table 1.1 Previous ground-based experiments for energetic electrons or x rays from thunderstorms and lightning. Adapted from *Suszcynsky et al.* [1996].

Experiment	Location	Instrument	Source Distance	Source Type
Schonland [1930]	ground	ionization chamber	>250 m	none observed
Schonland and Viljoen [1933]	ground	Geiger (G-M) tube	20-60 km	lighting/Storm
Appleton and Bowen [1933]	ground	G-M tube	2000-3000 km	lightning
Halliday [1934, 1941]	ground	expansion cloud chamber	0 to 40 km	lightning
Macky [1934]	balloon	photographic plate	in cloud	none observed
Clay et al. [1952]	ground	ionization tubes	few km	thunderstorm
Hill [1963]	300ft tower	dosimeters	tower strike	none observed
Shaw [1963]	mountain top	NaI scintillator	0 to few km	thunderstorm
Whitmire [1979]	1800ft tower	dosimeters	tower strike	thunderstorm
D'Angelo [1987]	ground	diffusion cloud chamber	~100 m	lightning

Shaw [1967] used sodium iodide (NaI) scintillation detectors to look at the gamma emissions (with energies greater than 500 keV) produced by the energetic electrons. The emissions are relatively weak, since for an electrons with energies of a few MeV only a few percent of the energy loss is due to bremsstrahlung. Bremsstrahlung emissions provide an indirect method to look for the existence of energetic electrons in thunderstorms. The chance for success in measuring gamma-ray emissions is higher because they have a much longer attenuation length than electrons and should be more easily detected than the electrons themselves. The detectors were placed on a mountain top in Arizona at an altitude of 2800 m MSL (above mean sea level). Measurements of electric field and corona current were also made. No correlations were found between lightning flashes and increases in the gamma-ray count rates. Although there was an increase in count rate of about 5 percent that occurred with a time constant of about 10 minutes, *Shaw* [1967] was not able to draw any conclusions about the source of this increase. *Suszcynsky et al.* [1996] found similar increases during thunderstorms that appear to be correlated with the rain-out of radioactive particles from the air.

A problem with all ground-based measurements is that if the region in which the energetic electrons are produced is distant from the detector, the x-ray and electron fluxes will be strongly attenuated. For example, if the source is located near the bottom of the thunderstorm about two kilometers above the ground, the x-ray flux would be attenuated by a factor of about 10^5 and the electron flux by 10^{86}. This assumes an attenuation distance of about 150 m for 100 keV x rays, and about 10 meters for 1 MeV electrons [*McCarthy and Parks*, 1985], and no geometrical effects on the flux between source and detector. These attenuation distances are for air at an altitude of about 8000 m. If the measurements are made near the surface, the attenuation would be even greater due to the increased air density. The x-ray count rate due to an energetic electron source would have to be significantly greater than the background rate observed. For a background of order 10 counts per second (cps) and an attenuation of 10^5, the source strength would have to be of the order 10^6 cps. Again this assumes no geometrical effect on the x-ray flux. Because of the ambiguous results of ground observations made to date, it seems reasonable to infer that x-ray sources in thunderstorms, when they occur, are rarely intense enough to be observed at great distances. Clearly, to test Wilson's hypothesis, measurements have to be made closer to the source.

1.2 Airborne measurements

Macky [1934] made an attempt to detect electrons inside a thunderstorm using photographic plates attached to balloons. He found no evidence of increased levels of β radiation. It was not until the 1980's when the first definitive measurements were made. *Parks et al.* [1981] and *McCarthy and Parks* [1985] found increases of one to two orders of magnitude above background in the x-ray count rate inside thunderstorms. These increases lasted for periods on the order of a few seconds. In some cases, the count rate would abruptly return to background at about the time of a lightning flash, while for other events, the rate decreased slowly over a period of a few seconds. The occurrence of lightning flashes was determined by pilot observations, optically by a photo diode, or by a commercially available lightning detection avionics. Although no electric-field measurements were available for comparison, they believed that the increases were a result of the strong electric field in the thunderstorm increasing or maintaining the energy of energetic cosmic-ray electrons [*McCarthy and Parks*, 1985; and *McCarthy and Parks*, 1992].

1.3 New measurements

To fully test Wilson's hypothesis, measurements of x-ray intensity and electric field are needed. The goal of my research was to measure simultaneously the x-ray intensity and the electric field in thunderstorms to test the hypothesis that a significant population of energetic electrons (and the accompanying bremsstrahlung x rays) could be produced by the thunderstorm electric field. Previous thunderstorm x-ray measurements did not have electric-field data to accompany them [*Parks et al.*, 1981 and *McCarthy and Parks*, 1985]. A proven balloon-borne electric-field instrument has been in use by Marshall and Rust for over a decade [*Marshall et al.*, 1995a]. Using this instrument, *Stolzenburg et al.* [1994] found that a fairly uniform vertical electric-field, sometimes in excess of 100 kV m^{-1}, can exist over large horizontal distances for relatively long periods of time in the stratiform region of a mesoscale convective system (MCS). These types of storms provide an ideal laboratory in which to test Wilson's hypothesis because:

1. The extensive electrified region in MCS storms makes it more likely to get balloon-borne instruments into an electrified region inside the storm.
2. Previous measurements of electric fields in MCS thunderstorms suggests that strong fields (greater than 50 kV m^{-1}) will be observed during these flights.

3. The stratiform region of MCS storms has a relatively low lightning flash rate in comparison to the convective region of the storm. This makes it easier to determine the relationship between electric field and x-ray production.
4. The stratiform region, where these strong and wide-spread electric fields have been observed, has relatively calm conditions (low wind speed, and no large hail). This improves the chance that both the launch and flight will be successful.

In the next chapter, two basic models will be presented that demonstrate the plausibility of energetic electron and x-ray production in thunderstorms, along with some possible implications of effects they might have on the thunderstorm. Chapter 3 discusses the instrumentation used for this study. Chapters 4 and 5 present the observations made on five balloon flights and discuss those observations in context with the current models reviewed in Chapter 2. The final chapter comprises a summary, concluding remarks and some ideas about what to do next.

Chapter 2

Theory and Implications

As background for the presentation of the observations, which are the focus of this study, a short review of the theories and models that have been advanced to explain thunderstorm x-ray production is in order. There are two distinct types of energetic electron models: those that involve runaway electrons and those that do not. Runaway electrons and their production of electron avalanches were considered later because of the apparent failure of the non-runaway model to explain the x-ray observations of *McCarthy and Parks* [1985].

2.1 Non-Runaway Model (Electron "Gathering")

Although *Wilson* [1925] described the first model for gamma ray production in a thunderstorm environment, *McCarthy and Parks* [1992] provided the first quantitative model based on direct measurements of x rays inside thunderstorms. *McCarthy and Parks* [1992] used a one-dimensional model, using only the vertical component of both electric field and electron motion. They assumed a constant electric field over a region between 5 and 10 km in altitude. This electric field allowed energetic electrons, produced continuously by cosmic rays and radioactive decay, to travel over a much greater distance than they would without the field present. A result of this is that the electron flux near the positive charge region in the thunderstorm would be greatly enhanced [*McCarthy and Parks*, 1992]. In other words electrons are "gathered," from other places in the atmosphere because the electric field reduces the net energy loss per unit path length in air. This results in a localized increase in the electron flux.

Both *Wilson* [1925] and *McCarthy and Parks* [1992] assumed that electrons from radioactive decay were present but the latter stated that the dominant source of energetic electrons at the altitudes of interest is cosmic-ray secondaries. In *McCarthy and Parks* [1992], monoenergetic electrons are uniformly distributed in the altitude range from 9 to 14 km MSL. The model predicts the number of x rays per electron produced in the altitude range from 9 to 10 km. As the electric field is increased from zero, the x-ray production rate increases weakly until the breakeven field (E_{BE}) is reached. The breakeven field is the electric field in which a 1 MeV electron is at an energy balance between the frictional losses from interactions with the air and the gain from the electric field. A 1 MeV electron is chosen since it loses the least energy per unit path length in air. In their simulation, *McCarthy and Parks* [1992] found that x-ray production increased by nearly 3 orders of magnitude when the electric-field reaches the breakeven field strength.

McCarthy and Parks [1992] used the x-ray production simulation to determine the number of electrons required to produce the observed x-ray flux of 50 cm^{-2} s^{-1} sr^{-1} [*McCarthy and Parks*, 1985], assuming that all x-rays originate within 1 km of the detector. They found that radioactive decay provides an electron source that is a factor of 300 too small. Cosmic ray secondaries are found to provide a factor of 8 fewer electrons than are thought to be required [*McCarthy and Parks*, 1992] but the authors point out that the approximations used in the model and its one-dimensional nature do not allow them to rule out cosmic-ray secondary electrons as the source of the x-ray production they observed. An important result in *McCarthy and Parks* [1992] is that their prediction of x-ray fluxes requires that an electric field of at least 2/3 E_{BE} must exist over an altitude range of about 1 km. However, the predicted x-ray flux from this model was 50 times less than those observed by airborne instruments flown through thunderstorms.

2.2 Runaway Electron Model

Although *McCarthy and Parks* [1992] point out that most of the energy loss an electron under 100 MeV experiences is due to ionizing processes, they did not suggest what happens to the knock-off electrons that are produced as a result. *Gurevich et al.* [1992] suggests that these electrons may contribute to the production process and that a runaway electron avalanche, initiated by cosmic ray secondaries, may take place. *Roussel-Dupre et al.* [1994] modeled the temporal evolution of such an avalanche, and estimated the x-ray emissions from it. Furthermore, *Gurevich et al.* [1994] extended the model yet again to include spatial structure of the breakdown. The details in the model of *Roussel-Dupre et al.* [1994] require a detector with time resolution better than one microsecond, a spatially uniform electric field, and a uniform and continuous source of energetic "seed" electrons. *Gurevich et al.* [1994] addresses a runaway breakdown from a single breakdown pulse (a single energetic "seed" electron) and examines the spatial structure of the pulse. The results of these latter two models cannot be compared with the observations presented here that were made with a single detector and with low temporal resolution. However the earlier work of *Gurevich et al.* [1992] provides the basic physics behind the later works and a basic model that can be used to compare with the observational data presented here.

As in *McCarthy and Parks* [1992], *Gurevich et al.* [1992] uses the concept of the breakeven field (E_{BE}) and introduces a dimensionless parameter δ_o, which is defined as the magnitude of the electric field divided by the breakeven field value. The minimum energy loss occurs at an electron energy of about 1 MeV, and so only electrons with energy greater than 1 MeV are considered in *Gurevich et al.* [1992]. As electron energy increases above 1 MeV, the frictional loss slowly increases. If the electron has energy lower than 1 MeV, the frictional loss increases with decreasing electron energy. At δ_o=1 only the 1 MeV electrons have no net energy gain or loss. Higher energy electrons will lose energy until they reach 1 MeV or are removed from the electron population by collisions. Electrons with energies less than 1 MeV will slow down. Since all electrons with energy other than 1 MeV experience a net energy loss, any ionization process that results in an energetic knock-off electron will result in the loss of both electrons. In this scenario, no avalanche can occur, since there is no additional electron production.

More interesting events occur when δ_o>1. Not only will the equilibrium energy be greater than 1 MeV, depending on the value of δ_o, but electrons with lower energy than the equilibrium energy will also be able reach equilibrium. These conditions will allow knock-off electrons with sufficient energy to accelerate to the equilibrium energy. As a result, electron multiplication can occur. As a result, if δ_o>1 occurs over a distance that exceeds the runaway length, approximately 20 m for $\delta_o \approx 1.2$, an avalanche of runaway electrons can occur [*Gurevich et al.*, 1992; *M.P. McCarthy*, private communication]. The runaway length is the exponential scale length for electron multiplication and is a function of the electric field, so that as δ_o increases, the runaway length decreases (for δ_o=1.5 the scale length is 12 meters).

A problem arises when the electron multiplication models are used to predict runaway breakdown and x-ray production in thunderstorms. The model predictions use a δ_o approximately equal to 2 [*Roussel-Dupre et al.*, 1994]. In the five flights presented here, as well as the 23 flights without x-ray data presented in *Marshall et al.* [1996b], the electric field rarely exceeds E_{BE} (δ_o=1) by any significant amount. However, there have been rare observations of extremely strong electric fields in thunderstorms. For example *Winn et al. [1974]* measured a field approximately 4 times breakeven at 6 km MSL. Similarly, *Marshall et al.* [1995c] also measured fields above breakeven, but only in a few cases and for only short time periods before a lightning discharge reduced the local electric field. Although not impossible, conditions such as those used in the model predictions are observed relatively infrequently.

2.3 Some Effects of Increased Numbers of Energetic Electrons in Thunderstorms

Besides producing energetic electrons and x-rays, what is the impact of the runaway electron mechanism on the thunderstorm or on the atmosphere in general? Large numbers of energetic (1 MeV or greater) electrons may serve to limit the electric field found inside thunderstorms in at least two ways. First, since electrons are removed from air molecules and moved towards the positive charge regions in the storm, they may transport significant amounts of charge inside the thunderstorm and reduce the electric field. Second, any energetic ions produced will be stopped in a short distance, since the minimum energy loss occurs at much higher energies for heavier particles (about 1500 MeV for protons) *Evans* [1955]. The increased ionization of the air may help to provide leakage paths for the thunderstorm charge to move through, limiting the growth of the electric field. Although these possibilities are only hypothetical, there is some experimental evidence that the electric field is limited to magnitudes near the threshold for runaway electron multiplication to occur [*Marshall et al.*, 1995a]. The runaway electron mechanism is one theory that has been proposed to explain the increased x-ray levels observed in thunderstorms [*Gurevich et al.*, 1992].

There are no known observations of electric fields in thunderstorms strong enough (on the order of 1000 kV m^{-1}) to cause dielectric breakdown. As a consequence, it is not clear how lightning is initiated. The runaway mechanism has been invoked as a way to initiate lightning [*Gurevich et al.*, 1994; *Roussel-Dupre et al.*, 1994], since it requires an electric field an order of magnitude less than dielectric breakdown. Fields of this magnitude are commonly observed in thunderstorms [*Marshall et al.*, 1995a].

The runaway mechanism has also been invoked [*Roussel-Dupre and Gurevich*, 1996] to explain recently observed optical phenomena, called Red Sprites and Blue Jets, that occur above some thunderstorms [*Sentman et al.*, 1995; *Wescott et al.*, 1995]. These are luminous events that occur over thunderstorms at altitudes between 20 and 80 km MSL. Red Sprites appear to occur simultaneously with positive cloud-to-ground lightning flashes that remove hundreds of coulombs of charge from the cloud [*Lyons*, 1995; *Pasko et al.*, 1995; *Roussel-Dupre et al.*, 1996]. Although there are only a few observations, Blue Jets do not appear to be associated with cloud-to-ground lightning [*Wescott et al.*, 1995].

Although the physical mechanism that produces Sprites and Jets is unknown, most models use a lightning discharge to produce an electric-field transient above the thunderstorm that heats mesospheric electrons to energies of a few eV [*Pasko et al.*, 1995] or drives a runaway breakdown initiated by energetic electrons produced by cosmic rays [*Roussel-Dupre et al.*, 1996]. Some experimental evidence consistent with runaway breakdown has been found in the form of gamma-ray bursts detected both by satellite [*Fishman et al.*, 1994] and by balloon instrumentation [*Eack et al.*, 1996a].

Because the experimental evidence is limited, the existence of these or other effects on the atmosphere and on the thunderstorm environment is unproven. More experimental and theoretical work is needed to verify and characterize runaway breakdown in the atmosphere before its effects can be reasonably understood or predicted.

Chapter 3
Instrumentation

3.1 Design Considerations

Instruments designed to fly on small balloons into thunderstorms have some significant design restrictions. First, they must be light. This translates into limits on size as well as power consumption, since battery power available is restricted by the mass of the batteries to be used. Second, they must function in both cold and wet environments (-40 °C or colder at the top of thunderstorms). Third, they must be shielded from a harsh electrical environment. Shielding must exclude strong electric fields and radio-frequency interference from lightning to prevent interference with signals and destruction of onboard electronics.

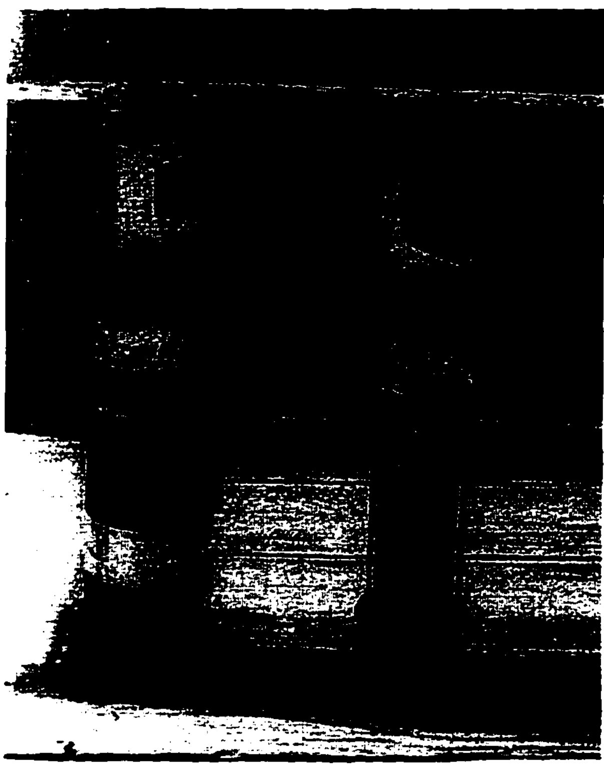

Figure 3.1. Picture of two assembled x-ray spectrometers. The instrument on the left is partially encased in its outer housing.

3.2 X-ray spectrometer overview

The x-ray spectrometer consists of two main sections: the NaI detector, and the support electronics. The entire system is mounted in an aluminum framework and covered with four thin aluminum cans that form the outer shield. Additional shielding measures are described later. The assembled detector is 50 cm long, 8.25 cm in diameter, and has a mass of 1.1 kg. Figure 3.1 is a picture of two instruments without complete outer shields. Figure 3.2 is a schematic diagram of the complete detector. Appendix A has more detailed information on the x-ray instrument components.

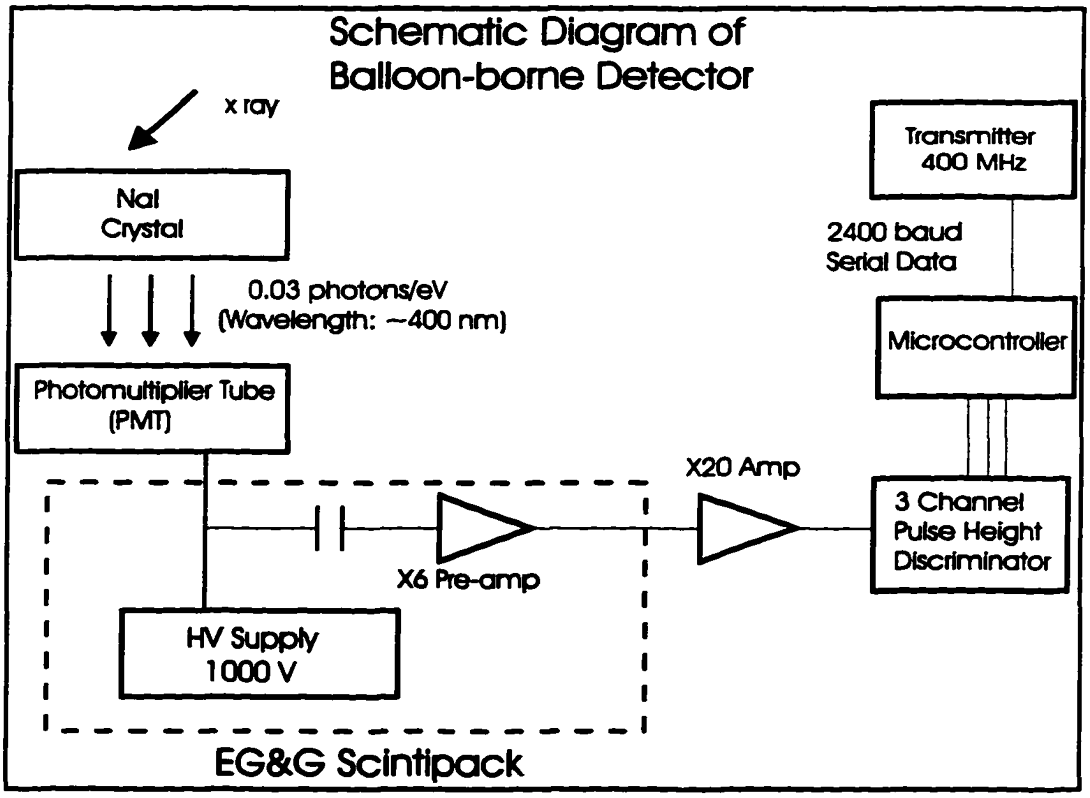

Figure 3.2. Schematic diagram of x-ray detector. Signal path begins with incident x ray and ends at the transmitter. After transmission, the data is converted into RS-232 level serial data and then recorded and time stamped by a computer on the ground.

3.2.1 Sodium Iodide Scintillation Detector

The detector uses a 5 cm diameter by 2 mm thick scintillation crystal with a 1 mil thick aluminum entrance window. The crystal is optically coupled to a Hamamatsu R1847 10-stage photomultiplier tube (PMT). The PMT bias is provided by an EG&G ScintiPack which also incorporates a pre-amplifier. As a precaution to prevent arcing in the PMT socket supplied on the ScintiPack, it was removed to allow hardwiring of the PMT. Because the instrument needs to function at reduced pressures (100 mb or lower), all high voltage sections were potted in GE Silicone RTV to prevent arcing. The mixed RTV was placed in a vacuum chamber to remove any air bubbles entrained during mixing, and then poured carefully into the mold to avoid the introduction of new bubbles. As a result of potting in RTV, the PMT and High Voltage (HV) supply are one unit and are mounted together in a thin wall aluminum tube that provides mechanical protection as well as shielding from light and electric fields. The NaI crystal is then affixed to the PMT with optical grease and held in place using black self-vulcanizing tape. After mounting the detector assembly into the instrument framework, the crystal sides are insulated with foam to prevent thermal shock and to protect from vibration during transportation. The entrance window is covered by 2.5 cm thick styrofoam to protect it from damage during transit and handling and from ice particles in storms, as well as from rapid temperature changes (Figure 3.3). Returned instruments had no damage to the crystal, indicating that the protection was adequate. This arrangement allows the detector to view a 120 degree cone, resulting in a geometry factor of 64 cm^2-sr. To save weight, a lead collimator is not used. As a result, the geometry factor will be larger for higher

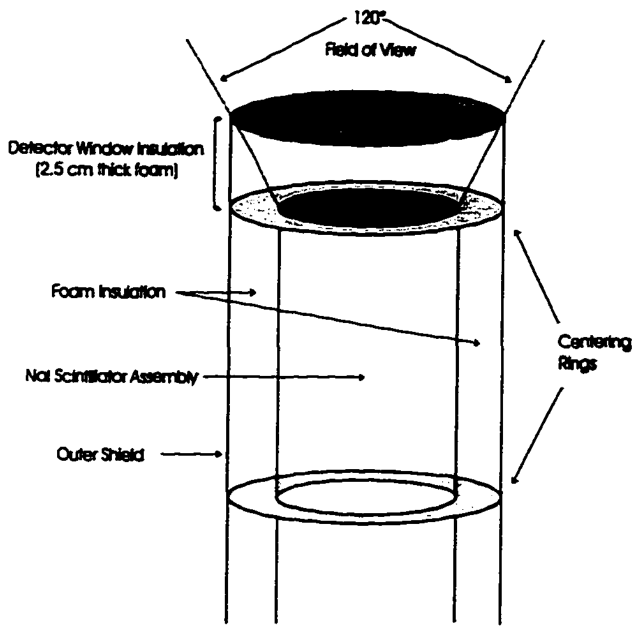

Figure 3.3. Schematic of the detector window. This arrangement results in the detector having a 120-degree field of view.

energy x rays due to their greater ability to penetrate the outer shield. This could effectively widen the viewing angle to as much as 180 degrees, increasing the geometry factor by a factor of 2 (due to the increase in solid angle viewed). Angles greater than 180 degrees are more heavily shielded by the instrument structure and electronics. For the energies of interest, little if any contribution to the x-ray flux would be made from angles outside the 180 degree field of view.

Two categories of counting efficiency, absolute and intrinsic, are commonly used to describe a detector. Absolute efficiencies are dependent on both the properties of the detector and the counting geometry [*Knoll*, 1979]. The intrinsic efficiency is dependent primarily on the detector material, detector thickness, and the energy of the photon. *Knoll* [1979] points out that although the absolute counting efficiency is strongly dependent upon the geometry, the intrinsic efficiency is not for cases in which the source is far from the detector. Since the thunderstorm source is presumed to be large in comparison to size of the detector (on the order of 10's of meters based on the current thunderstorm x-ray production models) and the source region is more than a few meters from the detector, the intrinsic efficiency is the appropriate specification. Each of these categories can be further divided into two categories: total efficiency (a measure of all events detected) and peak efficiency (only events that deposit the full energy of the incident radiation into the detector are counted). Because the detector observes a continuous spectrum from bremsstrahlung radiation and not a source with defined peaks in the energy spectrum (like a radioactive source), the calibration should be reported as a total intrinsic efficiency. The easiest method to compute the total intrinsic efficiency is to use the linear absorption coefficients [*Knoll*, 1979] for NaI. For each energy channel, the average absorption coefficient for each energy range was used (44 cm^{-1} for 42 keV, 11 cm^{-1} for 73 keV, and 5.5 cm^{-1} for 104 keV) [*Evans*, 1955]. Using these, the probability of absorption in the 2 mm thick NaI crystal was calculated for angles of incidence from 0 to 60 degrees. The probabilities were then corrected for the absorption of x rays in the 2.5 cm thick foam layer in front of the detector window (also corrected for the angular dependence of the path length). The result of this is plotted in Figure 3.4. Both the 30 to 60 keV and the 60 to 90 keV channels have relatively minor variations in efficiency with respect to incident angle and have average efficiencies of 0.94 and 0.88 respectively. The high energy channel (90 to 120 keV) shows a significantly lower efficiency for normal incidence, with an average efficiency of 0.69.

As verification that the detector was working properly, tests using calibrated point sources (the 31 keV x ray from ^{133}Ba and the 24 keV x ray of ^{109}Cd) gave *absolute total* efficiencies of about 0.14. The source to detector separation was 2.5 cm. *Knoll* [1979] reports a theoretical calculation of the absolute total efficiency for this geometry of 0.15.

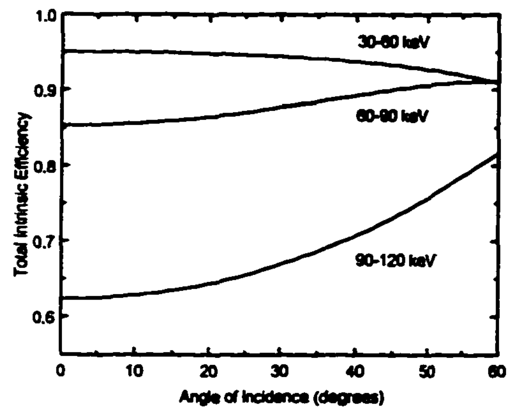

Figure 3.4. Plot of total intrinsic efficiency vs. Angle of incidence, corrected for absorption by the styrofoam protective shield. The average efficiency for channel 1 (30 to 60 keV) is 0.94, 0.88 for channel 2 (60 to 90 keV) and 0.69 for channel 3 (90 to 120 keV).

3.2.2 Support Electronics

The support electronics package consists of a signal amplifier, a pulse discriminator, a microcontroller and an FM transmitter. The crystal-controlled transmitter is from a meteorological radiosonde and operates on a frequency near 404 MHz. A Blue Earth Micro-485 was used for the microcontroller. Three 16-bit counter/timers built into the microcontroller were used to accumulate x-ray counts in the energy bands set by the discriminator. The counting time of 0.25 s is controlled by the onboard clock. At the end of each counting interval, the microcontroller sends the number of counts in each of the three channels, along with a checksum over its serial port to the transmitter. The data is transmitted in ASCII form at 2400 baud. Although an ASCII data stream is inefficient, data quality can be checked easily and in most cases, errors in one or two bytes per spectrum could be corrected.

The signal amplifier is a simple non-inverting amplifier, without any separate pulse shaping filter. The signal from the detector's charge amplifier decays with a time constant of 50 μs. At high count rates where the average time between incoming x rays is comparable to the amplifier time constant, a pulse "pile up" can occur. This results in fewer x rays counted than were incident to the detector and also each x ray is reported to have a greater energy than it actually had. Pulse shaping (high pass filtering) from the charge amplifier reduces this problem. For this instrument, count rates greater than 10000 cps where not expected. This was based on previous observations of count rates on the order of 1000 cps [*McCarthy and Parks*, 1985]. Therefore, since space on the circuit board was limited no pulse shaping was used.

The amplified signal is sent to an array of voltage comparators. The reference voltage for the comparators is set by a voltage divider network. Metal-film resistors with a tolerance of 1% and a temperature coefficient of ±100 ppm / °C were used in the divider network Each comparator output is connected to a non-retriggerable monostable multivibrator (one-shot) that has an output pulse duration of 1.7 μs. Additional digital logic after the one-shots determines which channel the x-ray event is in and increments the proper microcontroller counter. Each counter input was protected from voltage transients by a transorb connected to ground. The entire support electronics package is wrapped with a metalized plastic then with a layer of aluminum foil in contact with the metal framework and outer housing (chassis ground). The microcontroller is wrapped with an additional layer of metalized plastic and grounded foil.

3.2.3 Flight configuration

The x-ray detectors were suspended from a 1200-g helium balloon in the typical flight configuration shown in Figure 3.5. The x-ray detector can look upward or downward, depending on how it is rigged. The viewing direction will be a factor in determining the characteristics and location of the source. Initial flights used a downward looking detector to reduce the chance that water would enter the instrument through the styrofoam insulation. In addition to the x-ray detector, the balloon carries a standard meteorological radiosonde and an electric-field meter (EFM). The radiosonde provides temperature, pressure, humidity, and LORAN position data. LORAN or Long Range Aid to Navigation is a system of 100 kHz radio beacons used to determine geographic location. From these parameters, altitude, windspeed and wind direction are determined. The electric-field meter measures the vertical and horizontal electric field (the direction of the horizontal component is undetermined). This EFM is based on one developed by Winn *et al.*[1978; 1981]. *Stolzenburg* [1993] reports an error of about 7 percent for the electric field data from these instruments. More details of the EFM and its data are presented in Appendix B.

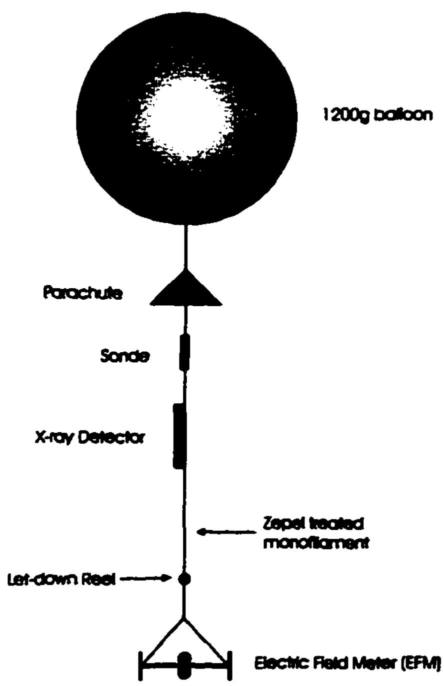

Figure 3.5. Typical flight configuration for making simultaneous x ray and electric-field soundings.

3.3 Calibration and Testing

3.3.1 Calibration

Each x-ray detector received two different calibrations. The first was the initial calibration of the NaI detector assembly. A multichannel analyzer was used to determine the peak location and area (number of counts in the entire peak) for the 59.6 keV gamma produced by an ^{241}Am source. The analyzer used has 1024 energy bins. The high voltage of each unit was adjusted to match the gains of the PMT tubes. This results in the same pulse height for a given x ray energy to be the same for all detectors, and the peak count rate to be in the same analyzer bin. Then using a counting time of two minutes, the area of the peak was found with the styrofoam protective cover in place. This was then divided by 2 (to determine the number of x-ray counts in the peak above 60 keV) and then by 480 (the number of 0.25 s intervals in the two minute counting time). The result is the number of counts expected in the 60 to 90 keV channel for a 0.25 second counting time.

Even a monochromatic x-ray source will produce a spectral peak that has spread due to instrumentation effects (spectral broadening due to the characteristics of the source is much smaller than those due to this instrument). A pulser was connected to the pre-amplifier of the detector to simulate a purely monochromatic signal from the PMT. The pulser signal is adjusted until the output of the pre-amp falls into the 60 keV bin of the multichannel analyzer. The voltage of this peak can then be easily measured on an oscilloscope to find the pulse height produced by a 60 keV x ray. Because the output of an NaI is linear with incident x-ray energy, the relationship between incident energy and peak height can be determined.

The second calibration was to set the discriminator to the desired energy ranges of 30 to 60, 60 to 90 and 90 to 120 keV. The resistor values of the voltage divider were selected to give each bin a width of 30 keV. A variable resistor was used to fine tune the network, so that the number of counts in the 60 to 90 keV channel matched the number expected from the first calibration. ^{133}Ba and ^{109}Cd (producing x rays with energy 31 keV and 24 keV respectively) sources were also used in addition to the ^{241}Am were to check the calibration of the instrument. No sources with x ray energies between 60 and 120 keV were readily available for these tests.

Before flight, the x-ray detector is rechecked with the ^{241}Am source used in the bench calibrations. This was done to be sure that no damage to the instrument had occurred between final assembly and launch and that the calibration did not change.

3.3.2 Testing

To verify that the instruments are not subject to electromagnetic interference, two instruments were tested on the ground at The Irving Langmuir Laboratory for Atmospheric Research (near Socorro, New Mexico). One of the instruments was blinded by removing the NaI crystal, but was otherwise identical to the active instrument. During several thunderstorms the inactive detector reported no counts, while the active detector observed only normal background x-ray levels. The x-ray count rate increased from background over a period of about 20 to 30 minutes during the storms and in a manner consistent with the rainout of radioactive particles by precipitation [*Lockhart et al.*, 1959]. No independent data are available for comparison, but because of the time scale of the increases they were clearly not caused by electromagnetic or other interference.

Two additional tests were performed in the laboratory to determine the effects of strong electric fields on the instrument. The first test used a small plate (0.4 by 0.4 m) connected to a high-voltage supply. The instrument was grounded and suspended over the plate with the detector window facing it. With the spacing between the instrument and plate set at 11.5 cm, the plate voltage was raised slowly over a period of eight minutes to 4000 V. No variation from background levels of x-ray counts was observed. The separation was then reduced to 1.5 cm, and the plate voltage was raised over a period of 5 minutes from 0 V to 2700 V, at which time a discharge occurred between the plate and the instrument. From small burn marks in the styrofoam, the discharge was found to have connected with the instrument at the bottom of the outer metal housing, near the detector window. Again, no variation in the x-ray count from background was observed at any time.

The second high voltage test was performed at Langmuir Laboratory using a large (3 by 3 m) plate suspended over the ground. An insulating line, which ran through the plate, was used to suspend the instrument, with the detector window facing the upper plate. In addition, an electric-field mill was recessed in the ground plate under the center of the top plate to provide a direct measurement of the electric field. The upper plate was positioned 1.2 meters above the ground plane and connected to a high voltage supply. The voltage was slowly increased to 125 kV, giving a measured electric field strength of 120kV/m, with no increase in the x-ray count rate (Figure 3.6). This procedure was repeated with opposite polarity of the electric field, again with no change in x-ray rates from background..The plate separation was then reduced to 1 meter, and a wire corona point was placed in the field of view of the detector. The electric field was increased to

170 kV/m causing corona to be emitted from both the wire and the instrument. This was done with the instrument measuring background x rays and then repeated with an x-ray source placed on the detector window. No variations from the combined natural background and source x-ray levels were observed (Figure 3.7).

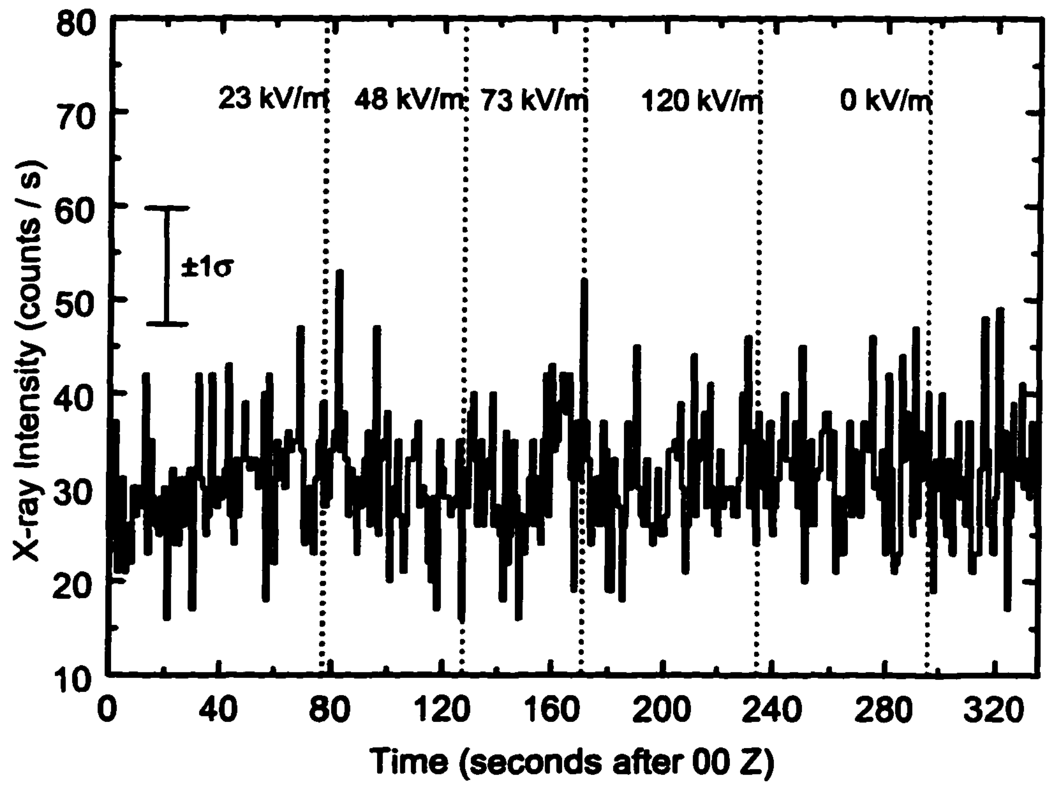

Figure 3.6. Measurement of x-ray background (at Langmuir Laboratory, elevation approximately 3200 meters) during high-voltage testing of the instrument. Vertical dashed lines indicate points where electric field was measured. Error bar represents one standard deviation in count rate.

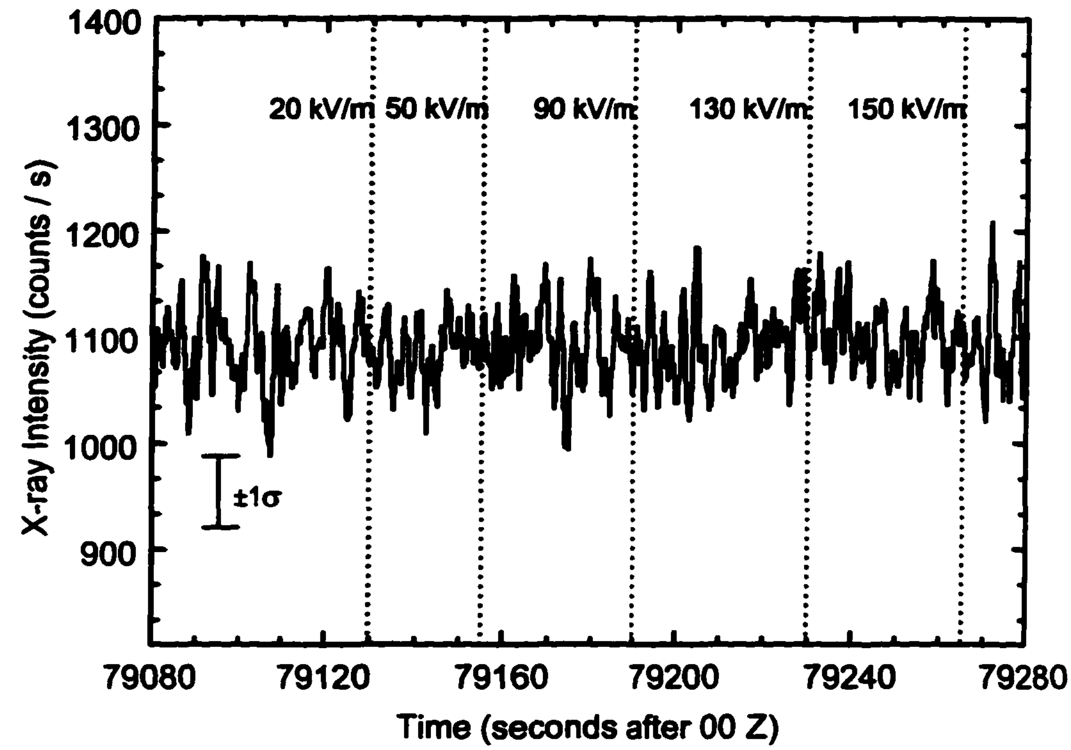

Figure 3.7. Measurement of x-ray background and a ^{241}Am source combined during high-voltage testing of the x-ray instrument at Langmuir Laboratory. Vertical dashed lines indicate points of electric-field measurement. Error bars represent one standard deviation in count rate.

Chapter 4
Observations

Five balloon flights were made during the 1994 and 1995 thunderstorm seasons. The only flight in 1994 was partially successful, since the instrument failed shortly after launch. Because the instrument was not recovered, the exact cause of the failure is not known. In 1995, four successful flights were made in to MCS storms in Oklahoma. Three flights were made from Norman, while the fourth was launched from the Oklahoma Panhandle.

Although all launches were made into stratiform regions of MCS storms, the only launch criterion used was an on-the-spot judgement of the electrical state of the storm made from observations of nearby lighting activity. This was done in an effort not to launch into a storm that was near the end of its life-time. This criterion, although qualitative, worked quite well, with two of the four 1995 flights observing large increases in x-ray intensity. The fourth 1995 flight did not observe any in-cloud x-ray increases. This flight was launched into a relatively inactive portion of an MCS (as compared to previous flights).

The polarity of the electric field data is plotted according to the polarity of the vertical electric field. A positive vertical field has field vectors that point upward. The horizontal electric field can be estimated using the "width" of the trace [*Stolzenburg*, 1996]. More details about this are given in Appendix B.

4.1 Flight 0: 27 May 1994

Flight 0 was launched near Ralls, Texas on May 27, 1994 at 0326 UTC (coordinated universal time). After reaching an altitude of about 3.5 km MSL at 0334 UTC, the signal modulation ended with the carrier still present. The carrier signal strength was strong during the entire ascent to 17 km. The electric-field meter and radiosonde operated normally throughout the flight. Later, during high-voltage testing of an x-ray instrument, it was found that in high electric fields the transmitter would sometimes "lock-up" and produce a good carrier signal with no modulation.

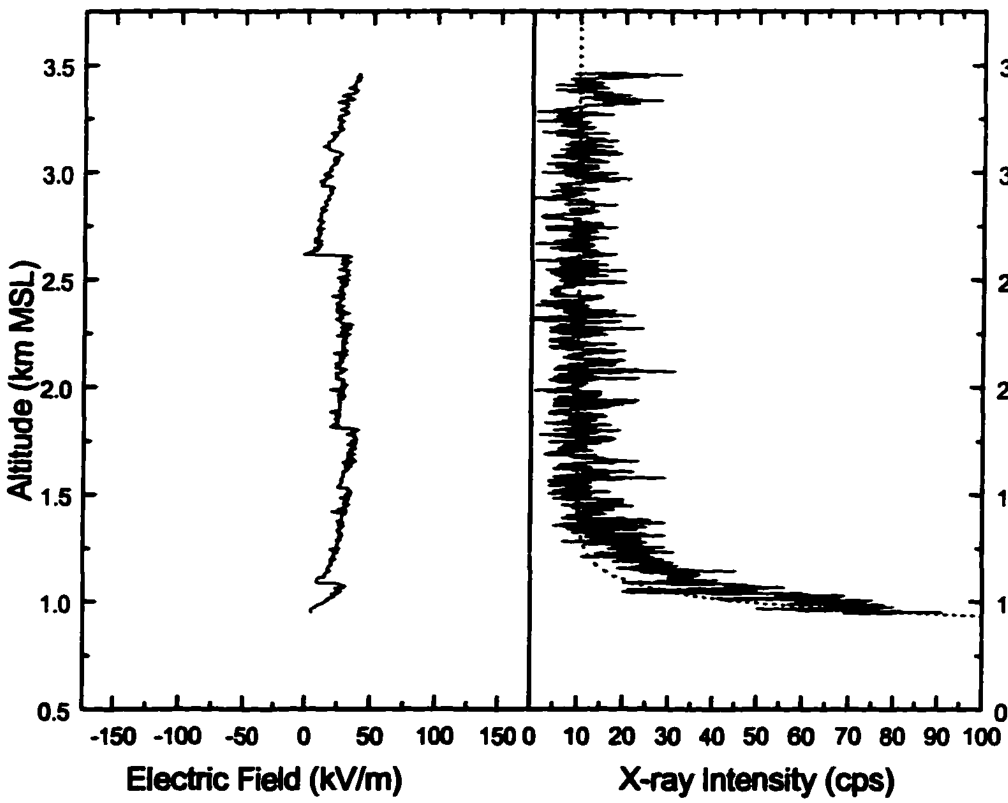

Figure 4.1. Plot of x-ray and electric-field sounding for Flight 0 made from Ralls Texas on 27 May, 1994. The dotted line in the right-hand plot shows the expected x-ray profile for a 70 cps (counts per second) source of 75 keV x rays located at the ground, superimposed on a constant source of 10 cps.

Figure 4.1 shows the data from the portion of Flight 0 when the transmitter was still operating properly. Note that there is a nearly exponential decay in x-ray intensity as the balloon ascends. This profile can be reproduced using a simple model: assume a source located at the ground that produces an intensity (as measured at the ground) of 70 counts per second (cps). Such a source could be a result of the decay of Radon and its daughter products. These radioactive nuclei are more highly concentrated near the Earth's surface (within 10 to 100 meters above ground) [*Schery et al.*, 1992]. Added to this is a constant source of 10 cps due to the cosmic-ray background. Both sources are assumed to be monochromatic at 75 keV. If the ground source is attenuated by the air (assumed to have constant density) between it and the detector as the balloon ascends, the dashed line on Figure 4.1 results.

Although this model is extremely simple, it fits the observed profile surprisingly well. As a result, it is assumed that the initial exponential decay in x-ray intensity is due to the detector moving away from a ground source. This "signature" was found to be present on all five flights.

4.2 Flight 1: 24 May 1995

Flight 1 was launched into a MCS that passed over Norman Oklahoma on 24 May 1995. Frequent intra-cloud lightning was observed before and during the flight. This flight was launched at 0047 UTC and reached a maximum altitude of 5.1 km MSL (above mean sea level) after an ascent time of less than 20 minutes. The flight was short because the balloon burst prematurely. Although no specific cause for the balloon burst is known for this flight, common reasons are hail and lightning strikes to the balloon. Figure 4.2

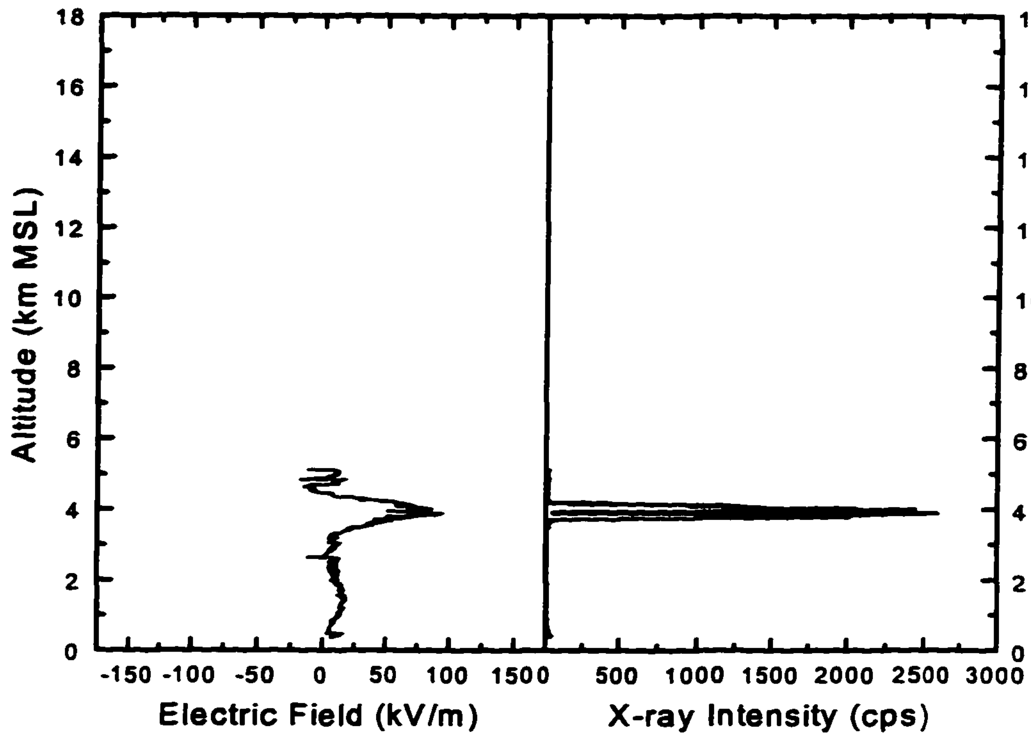

Figure 4.2. Sounding of x-ray intensity and electric field for Flight 1 made from Norman, Oklahoma on 24 May 1995. This, and the plots for the three additional flights that follow are all plotted on the same scale for easier comparison

shows the complete sounding of both x-ray intensity and electric-field for Flight 1. The instruments were recovered in October east of Moore, Oklahoma.

During the ascent, the balloon passed through one region with a positive electric field near 4 km MSL. While in this region, an increase in x-ray intensity was observed. When the balloon reached 3.9 km MSL, a lightning flash reduced the measured electric field, and at the same time the x-ray intensity quickly returned to near background levels. Lightning flashes are determined by fast (over one data point) changes in the electric field.

4.3 Flight 2: 24 May 1995

Flight 2, launched at 0141 UTC, was in the same storm as Flight 1. At the time of launch, the lightning activity was less frequent than at the time of the launch of Flight 1. The balloon reached an altitude of 7 km MSL at 0210 UTC and began to float (neither ascending or descending), most likely because of ice loading on the balloon (freezing level occurred at 3.9 km MSL). The balloon descended to about 2 km MSL (pressure 850 mb) at 0253 UTC, and then climbed back to 7.2 km MSL at 0320 UTC. Again, presumably loaded with ice, it began to descend again. At 0341 UTC, flight recording was terminated with the balloon still descending. Although the flight lasted over 2 hours with multiple ascents and descents, only the data from the initial ascent are shown. Data from later portions of the flight are considered to be unreliable due to very poor telemetry. Figure 4.3 shows the data from the first ascent of Flight 2. The instrument packages from Flight 2 were recovered in southeast Kansas a few weeks after launch.

Electric fields of both polarities were observed during this flight. However only a very small increase in x-ray intensity was observed near 4.2 km MSL in a region of negative electric field.

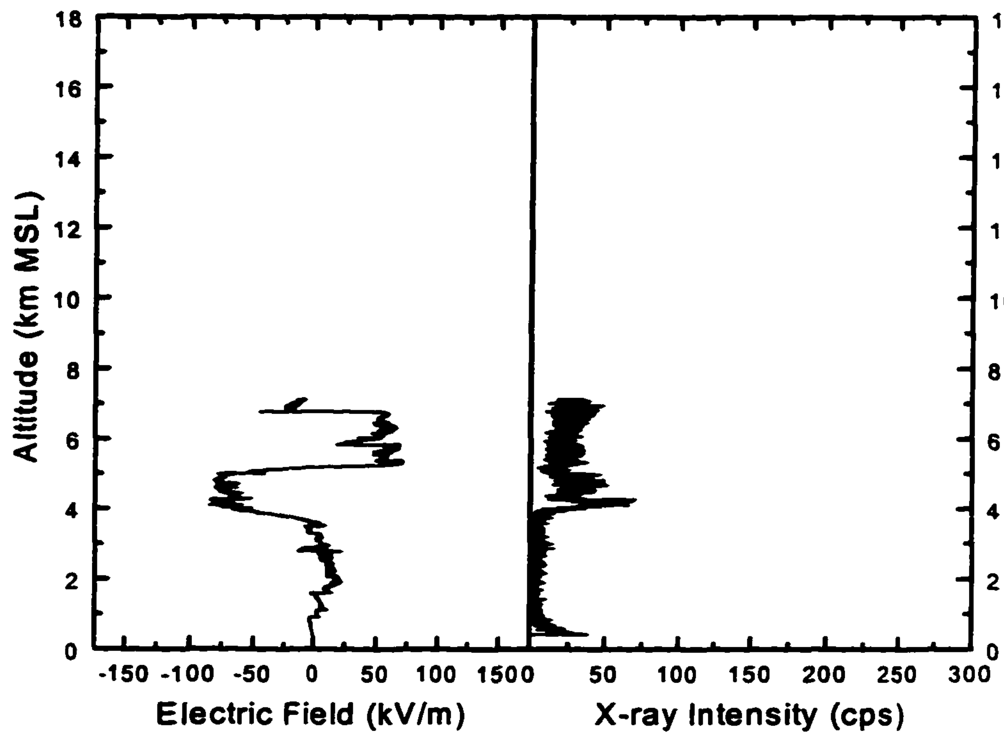

Figure 4.3. Flight 2 sounding of x-ray intensity and electric field.

4.4 Flight 3: 27 May 1995

Flight 3 was launched from Norman Oklahoma at 0605 UTC on 27 May 1995. The balloon reached a maximum altitude of about 18.5 km (71 mb pressure) at approximately 55 minutes after launch. At about 12 km MSL and at an ambient temperature of about -60 °C, the mercury switch on the electric-field meter froze. Although this switch is used to determine the polarity of the electric field, it does not affect measurement of the field magnitude. No significant electric fields were observed above 10 km MSL. During this flight, two regions with an electric field exceeding 50 kV m^{-1} were observed, one of each polarity (Figure 4.4). In both cases, significant enhancements in x-ray intensity were observed. The x-ray intensity quickly returned to near background levels at the time of a lightning flash.

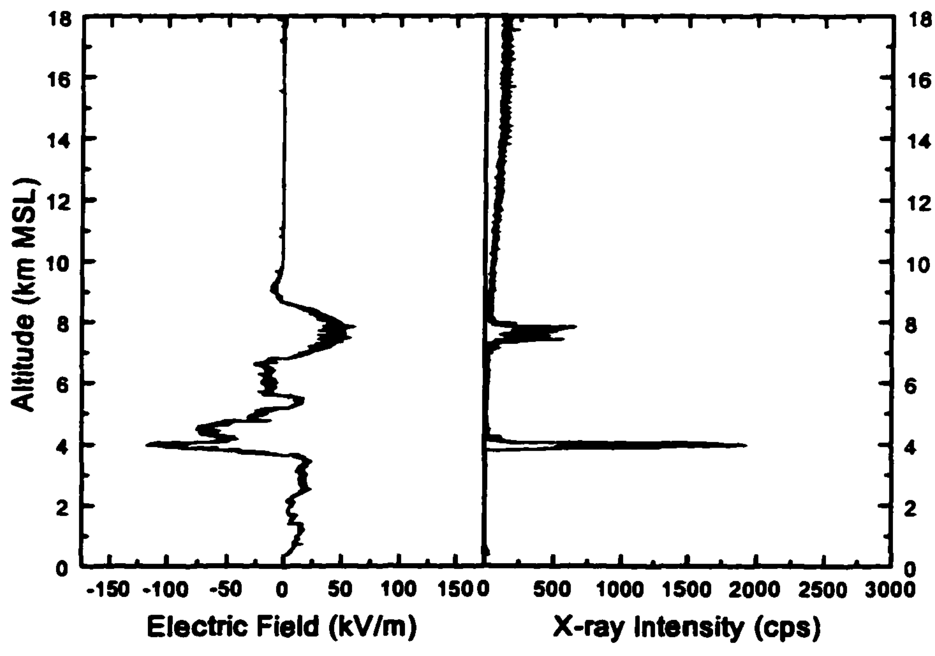

Figure 4.4. X-ray and electric-field sounding for Flight 3. Flight 3 was made from Norman, Oklahoma on 27 May 1995.

4.5 Flight 4: 29 June 1995

The final flight of 1995 was made in the Oklahoma Panhandle near Hardesty (east of Guymon). The balloon was launched at about 0600 UTC and reached a maximum altitude of 17.5 km MSL after 75 minutes of flight time. Figure 4.5 shows the sounding of electric field and x-ray intensity. Four regions of strong (magnitude of about 50 kV/m or greater) electric field were observed on this flight, two of each polarity. Although no increase in x-ray intensity was observed in the thunderstorm, x-ray pulses with a duration of about 1 second were observed near 15 km MSL. No significant electric field was observed at the time of the pulses. *Eack et al.* [1996a] could not draw any conclusions about the origin of these pulses. Appendix C discusses these pulses in further detail.

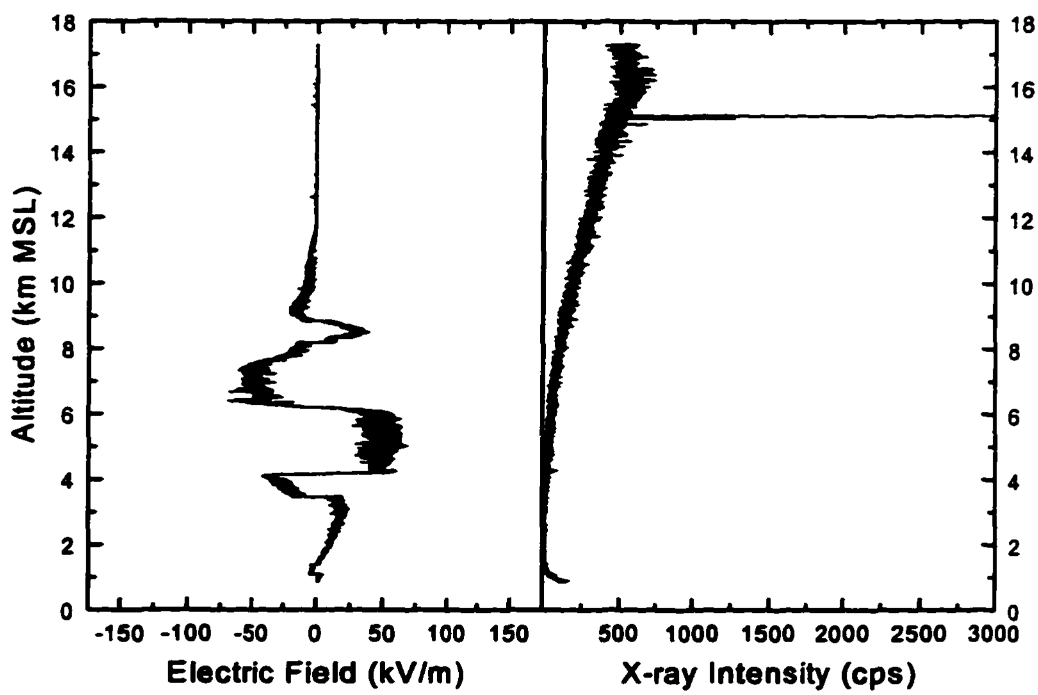

Figure 4.5. X-ray and electric-field sounding from Hardesty Oklahoma (Flight 4) made on 29 Jun 1995. The x-ray spike at 15 km MSL is one of three x-ray pulses described in *Eack et al.* [1996a].

Chapter 5
Discussion

This chapter contains a discussion of the balloon observations introduced in Chapter Three. On three of the four flights in 1995 significant increases in x-ray intensity were observed. Two x-ray events were associated with positive electric fields, and one with a negative electric field. There was one less significant event, with poorer counting statistics. There were also three cases in which electric fields larger than 50 kV m^{-1} (two positive, the other negative) were observed but where no x-ray increases were observed. For each x-ray event, a source-to detector distance is estimated. The electric field at this distance is computed using a simple charge distribution based on the vertical and horizontal electric field measured by the EFM. In all the x-ray data presented, 3σ error bars are shown, where $\sigma=N^{1/2}$ and N is the number of counts detected (Poisson or counting statistics) [*Taylor*, 1982].

5.1 Source-to-detector Distance Estimates and Electric Field at X-ray Source

The ultimate goal of x-ray measurements in thunderstorms is to understand what mechanism is at work and to discover what effects the mechanism may have on the thunderstorm itself. In order to do this, a direct measurement of the source electrons would be ideal, however so far only x-ray emissions caused by these electrons have been observed. Therefore, as a tentative first step towards understanding the source mechanism, the distance from the source to the detector will be estimated from the x-ray data. The source location and intensity cannot be uniquely determined using only a single detector. To estimate the source-to-detector distance, two methods are used. These look at either (1) the behavior of the x-ray event increase and decrease as the balloon ascends and (2) the relative intensity of each energy channel. Both methods use atmospheric absorption of x rays and do not include Compton scattering. Although important, calculating the scattering effects on x-ray intensity and spectrum requires a Monte Carlo computer code [*McCarthy and Parks*, 1992] and is beyond the scope of this work. The purpose here is to determine whether or not the observations and models (Chapter 2) are consistent. Eventually, a more detailed analysis should be undertaken.

After making an estimate of the source-to-detector distance, the next step is to estimate the electric field that may have occurred at the source location. In context of the current models, the question to be answered is: could realistic charge distributions allow the electric field at the estimated distance of the source to exceed breakeven (E_{BE}). To estimate this, the horizontal component of the measured electric field is used. In doing this, the only assumption that is made is that the horizontal field is due to a single uniform spherical charge distribution located at the estimated source distance from the balloon path. This charge is centered at the altitude of observed peak x-ray intensity. From this distribution, the electric field at the source and at the balloon is calculated and compared with the breakeven field and the actual electric-field measurement.

5.1.1 Distance Estimation

Attenuation of x rays in matter is an exponential process [*Evans*, 1955]. The attenuation length is dependent on the energy of the x ray and for this case the density of air. As in calculating the efficiency of the detector, the average value of the attenuation length, in this case for x rays in air, for each of the three energy bins will be used. Of the four x-ray events observed, three occurred at 4 km and the fourth at 8 km MSL. At 4 km the attenuation lengths are: 65 m, 87 m, and 131 m and at 8 km: 107 m, 143 m, and 216 m for channels 1,2 and 3 respectively. The attenuation at distance r for each channel is given by:

$$I_n = S_n \exp(-r/\mu_n) \qquad n = 1,2,3 \qquad (1)$$

where n is the spectrometer channel number, μ_n is the attenuation length for channel n, and I_n and S_n are the x-ray intensities at the detector and source respectively. The total x-ray intensity at the detector is then given by:

$$I_{total} = S_{total} \sum_{n=1}^{3} I_n \qquad (2)$$

where S_{total} is the source intensity. The distance r is that due to the vertical separation, which changes as the balloon ascends, and the horizontal separation that is assumed to be constant. The horizontal separation is defined as the source-to-detector distance when the source and detector are at the same altitude. The vertical separation is assumed to be zero at the point where the peak x-ray intensity is observed.

To estimate the horizontal distance, the S_n's are set to 0.55, 0.28, and 0.16 for n=1,2, and 3. These values were calculated by *Gurevich et al.* ["Theory of x-ray emission and fast preconditioning associated with thunderstorms", submitted to *J. Geophys. Res.*, 1997] for bremsstrahlung emissions from energetic electrons produced in thunderstorm electric fields. The exact spectrum of x-ray emission depends on the energy spectrum of the electrons, which is in turn dependent upon the electric field. Electric field values of about 1.2 E_{BE} were used for the calculation of the x-ray spectrum.

Distance estimates using the rate of rise to and fall from peak intensity essentially involves fitting equation (2) to the observed data. Two rate of rise methods were used. The first is a trial and error method where only S_{total} and the horizontal separation are varied. The source strength is set so that the peak height of the calculated curve is the same as the peak height of the observed. Varying the horizontal separation changes the width of the calculated curve and its curvature. The horizontal distance is varied until the curve best matches the observed data. The second method uses a chi-square minimization using the same parameters and equation. Plots of the first method are included in this chapter, while the chi-square plots are shown in Appendix D.

The second way to estimate the horizontal separation is to compare the predicted I_n's (equation 1) to the spectral intensities measured at the total x-ray intensity peak. Two comparisons are made. The first is with a calculation made by *Gurevich et al.* ["Theory of x-ray emission and fast preconditioning associated with thunderstorms", submitted to *J. Geophys. Res.*, 1997]. However I believe that this calculation is not correct, and so I have calculated my own version of this and use it for the second comparison. My calculations are included in Appendix D. The results of all methods are included in the discussion of each event and are summarized in Table 5.1 at the end of this chapter.

5.1.2 Simple Charge Distribution

After estimating the source-to-detector distance, the electric field at the estimated source location is calculated. This is based on the measured electric field using both the vertical and horizontal electric components. See Appendix B for details. Most MCS charge analyses result in uniform horizontally extensive (considered to be infinite) charge layers [*Stolzenburg*, 1996]. This charge structure will produce only a vertical electric field, resulting in a thin trace on the electric-field plot (Figure 5.1). The electric-field data shown in Chapter 4 indicates that there is a horizontal component present. This means that there is some inhomogeneity in the charge layer, either in charge density or in

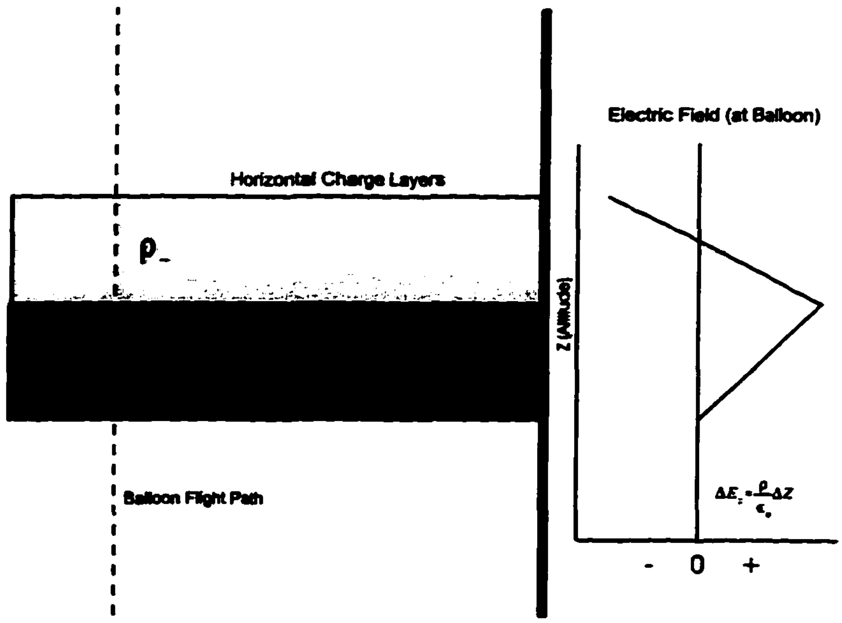

Figure 5.1. Schematic diagram of horizontal charge layers in the stratiform region of an MCS. Note that in the qualitative electric field schematic, the trace is thin indicating that there is no horizontal component to the electric field. The equation at the bottom of the field plot is Gauss's law in one dimension, and is used to determine the charge density in the layers from an electric field sounding.

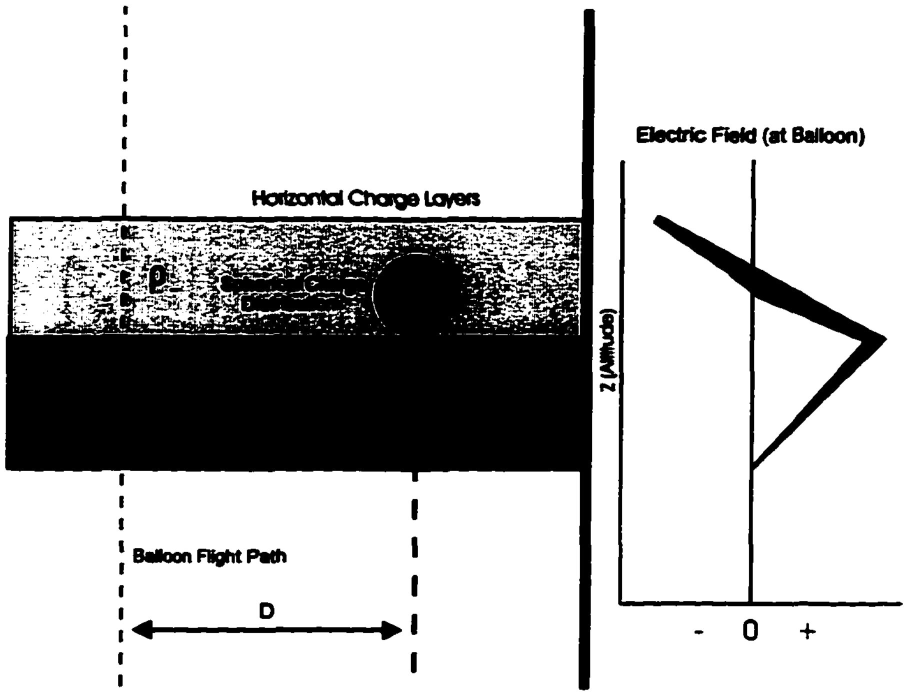

Figure 5.2. Schematic diagram of charge distribution with spherical charge "inhomogeneity" in charge layers. Note that the electric field schematic is relatively wide, indicating the presence of a horizontal component in the electric field.

distribution or thickness of the layer. For these purposes, a spherical discontinuity in the charge density in one of the layers is used. This is an extremely simple distribution, but, as the results show, serves as a good test for these calculations. The variation in charge density can be viewed as a spherical charge embedded in a horizontal charge layer (Figure 5.2). This spherical charge is centered at the source-to-detector distance estimated for each case. The total charge in the spherical region is determined from the estimated horizontal electric field. The sphere is allowed to have a radius no larger than the source-to detector distance, since any charge located outside this distance would not contribute to the horizontal field. As a result, the field of the spherical charge observed at the balloon is the same as a point charge located at the center of the sphere. The density of the horizontal layers is calculated by a one-dimensional Gauss's law approximation as described by *Stolzenburg* [1993]

After the total charge in the spherical distribution is determined, the electric field from the spherical charge and the horizontal layers is calculated along a vertical path that goes through the center of the spherical charge (thick dashed line in Figure 5.2). These are plotted for each of the four x-ray events and provide an estimate of the field in the source region. Finally the electric field from this simple charge distribution calculated along the actual balloon path (thin dashed line in Figure 5.2) is plotted for comparison with the observed electric field.

5.2 Flight 1: 24 May 1995

5.2.1 Discussion of X-ray Event

Figure 5.3 is a plot at high resolution of the x-ray increase near 4 km MSL. On the electric field plot, the breakeven field strength (E_{BE}) and 2/3 E_{BE} are also shown for comparison. As the balloon reached 3.7 km MSL, the x-ray intensity began to increase as the balloon entered the positive electric field region at 4 km, and peaked at about 3.9 km. At this point, a lightning flash occurred at an unknown distance reducing the local electric field, as shown by the abrupt change in the electric field (marked with an "L" in Figure 5.3). At the same time, the x-ray intensity abruptly returned to background levels. About ten seconds later, another lightning flash, again at an unknown location, increased the local electric field, with a simultaneous increase in the x-ray intensity. The total duration of this event was about 90 seconds. Figure 5.4 shows the individual energy channels for the event. The majority of the observed x rays were in the center (60 to 90 keV) channel. During the period that the x-ray levels returned to background, the spectrum is similar to that of the background observed below and above the region of increased x-ray intensity.

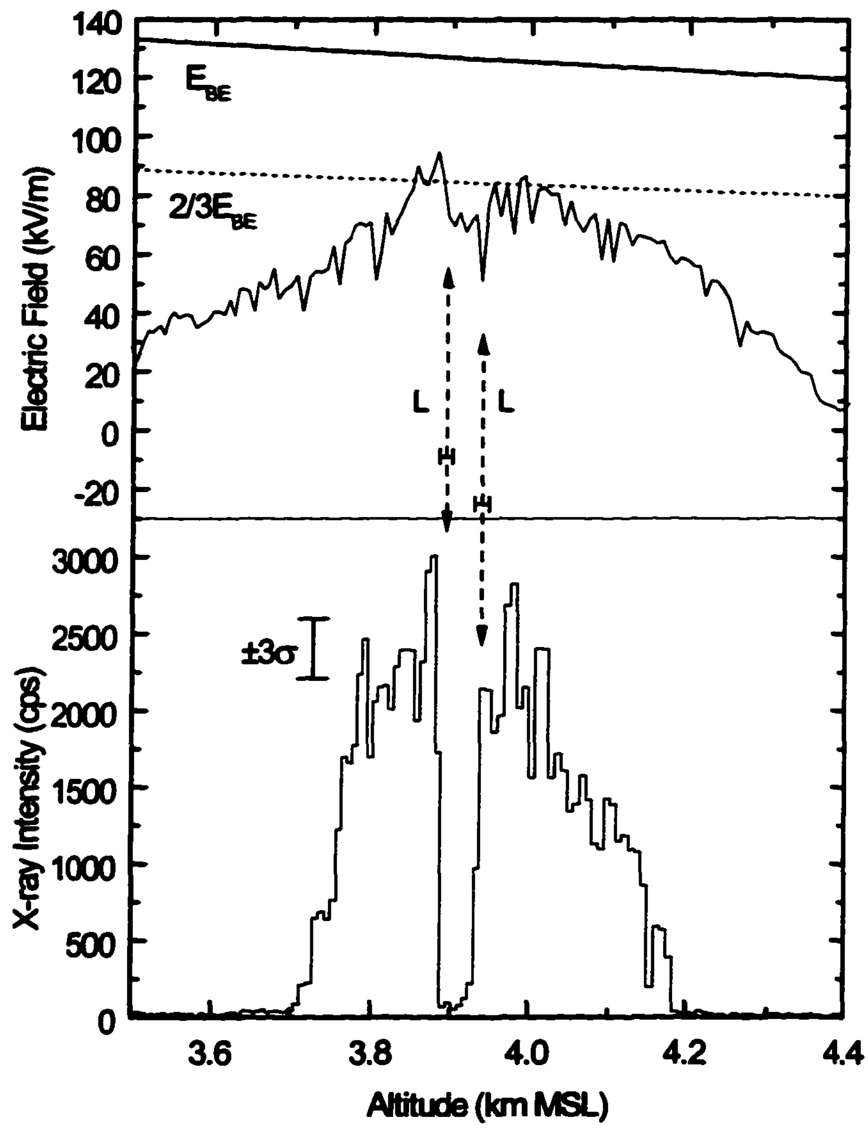

Figure 5.3. Detail of x-ray event observed near 4 km MSL. Electric-field transients due to lightning flashes are indicated by an "L." The x-ray event begins near 3.7 km and lasts for nearly 1 minute. The time between the two flashes is 10 seconds. Horizontal error bars result from the ±1 second error in timing between the x-ray and electric-field data sets. E_{BE} is the breakeven field discussed in Chapter 2.

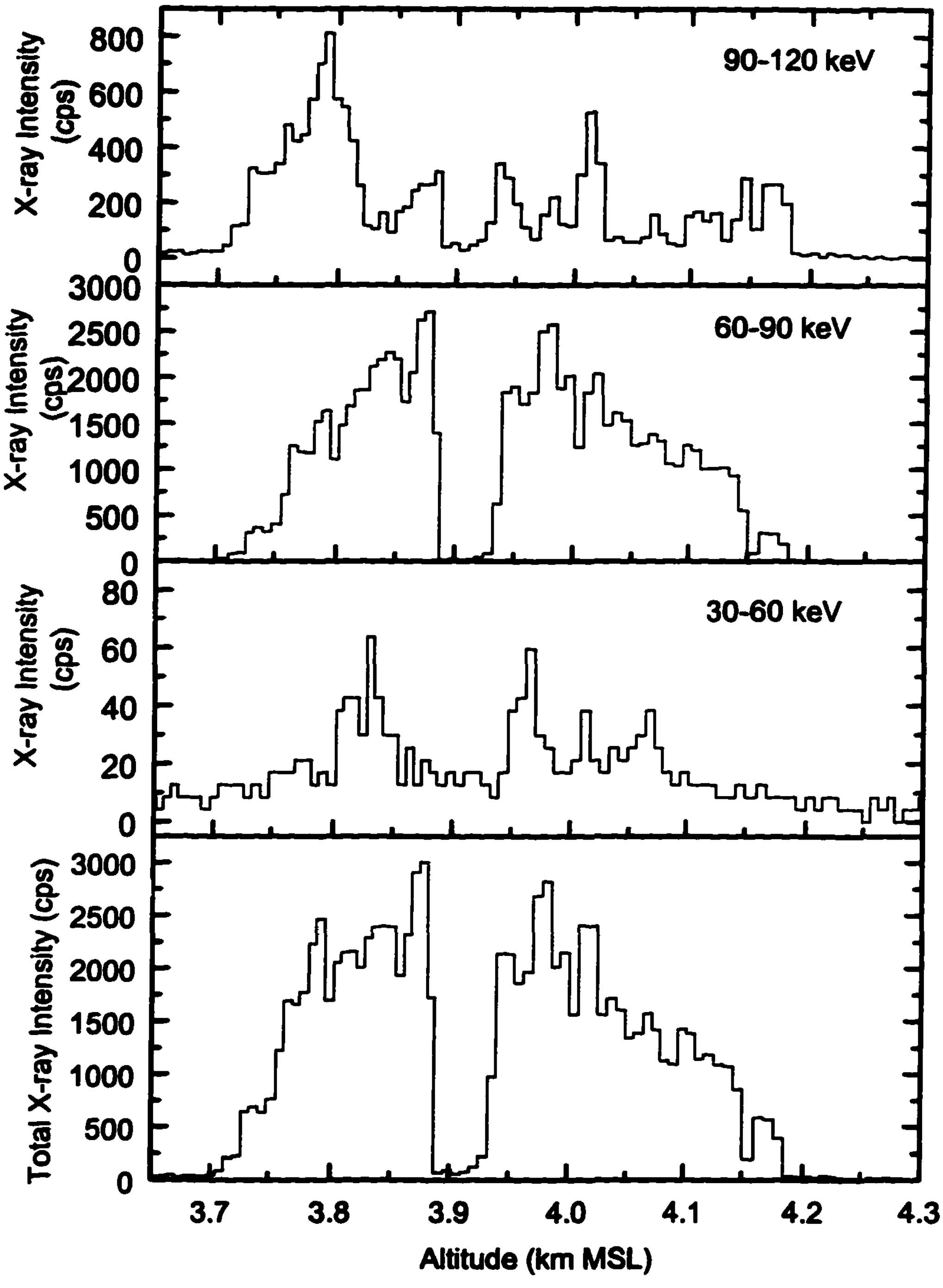

Figure 5.4. X-ray intensity in each energy channel and the total intensity observed by all three channels (lower most panel). Note that the low x-ray intensity near 3.9 km has a spectra similar to that of the background that was observed before and after the event.

Using the spectral information and assuming that the source was constant during the observation time, an estimate can be made of what would be expected for a detector moving towards and then away from a source. To do this, the location and height of the peak x-ray intensity is found for each channel. For each channel, the average attenuation length is used for each channel (42 keV for channel 1, 73 keV for channel 2, and 104 keV for channel 3; at 4 km M.S.L. the attenuation lengths are 65m, 87m, and 131m respectively). Figure 5.5 shows the observed x-ray intensity and the estimated intensity using the above assumptions. It appears that the slow increase and decrease at the beginning and end of the event are a result of the vertical ascent of the balloon.

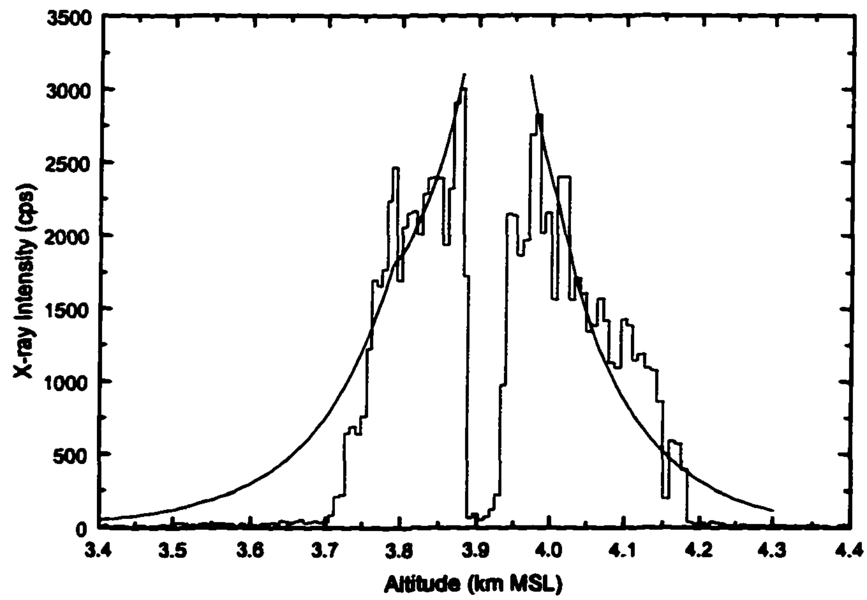

Figure 5.5. Estimated x-ray intensity superimposed on to the observed x-ray intensity. The estimated flux was calculated by using the peak flux and then attenuating it to account for the distance between the detector and the peak location. This estimate shows that the slow rise and fall of the event appears to be due to the motion of the detector towards and away from the x-ray source.

The previous estimate used only the observed x-ray peak locations to gain some insight into the temporal behavior of the observation. This assumes that the source is in the path of the balloon as it flies through the thunderstorm. There is no reason *a priori* to assume this. Instead assume a source at 4 km MSL that is located some distance away from the balloon flight path. Total source strength in the simple model is left as a free parameter and is adjusted so that the estimated peak intensity at the balloon is the same as the observed peak intensity. Figure 5.6 shows the observed data with two model plots for a horizontal distance of 250 m and 500 m from the x-ray source. Although the match is not perfect, especially for the rise to peak, the best fit is for a source located approximately 250 m away from the balloon path. A chi-square fit (Appendix D) estimates the distance at 230±30 m.

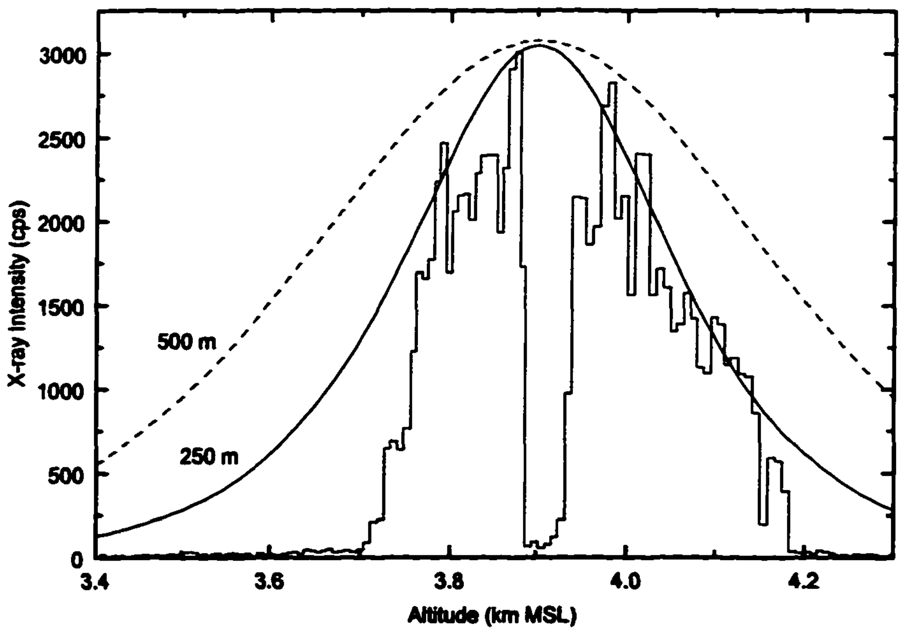

Figure 5.6. Estimates of x-ray intensity for a source located 250 m and 500 m from the flight path of the balloon. The observed x-ray intensity is shown for comparison.

Estimates using the relative intensities of the each energy channel at peak x-ray flux cannot be estimated using my calculations, most likely a result of neglecting Compton scattering effects on the spectrum. The method of *Gurevich et al.* [submitted, 1997] estimates the distance to be 500 m and also does not include Compton scattering.

In all of the estimates, only attenuation between the source and the detector was considered, with no inclusion of Compton scattering. Compton scattering may prove to be an important effect, especially for the rise to peak, since the detector looked down, away from the source as the instrument approached the source region.

5.2.2 Electric Field

As the plot in Figure 5.3 shows, the observed electric field does not appear to support either type of x-ray production theory. Since the electric field strength reaches only 2/3 E_{BE} for a vertical distance of about 200 meters, the electron "gathering" model [*McCarthy and Parks*, 1992] does not appear to be a suitable explanation. The x-ray flux observed is about 44 $(cm^2\ s\ Sr)^{-1}$, similar to the 50 $(cm^2\ s\ Sr)^{-1}$ that *McCarthy and Parks* [1985] observed. The number of energetic electrons produced by a "gathering" mechanism is too small to account for x-ray fluxes in this range [*McCarthy and Parks*, 1992]. Two possible explanations (other than instrumentation related errors) for this are that (1) runaway electrons may occur in weaker electric fields than predicted, and (2) the electric field elsewhere in the storm is greater than the breakeven field strength. The first explanation appears to be very unlikely, since the energy loss in matter and energy gain in an electric field for energetic electrons are well known. I will concentrate on the possibility that the electric field was stronger at some distant point, but not so distant that the x-ray signal is not observable.

In the previous section, the source to detector distance was estimated using the attenuation of a source located off the balloon path (Figure 5.6) and was determined to be about 250 meters. During the x-ray event observed the horizontal field was about 50 kV/m. For a spherical charge distribution centered 250 meters away from the balloon path, the total charge required for a 50 kV/m horizontal electric field is 0.35 C. This results in a charge density of 83 nC m^{-3} for a sphere with radius 100 m, and 10 nC m^{-3} for a 200 m radius. The 200 meter sphere has a charge density a factor of 2-3 times greater than measurements in the stratiform region have estimated [*Stolzenburg et al.* [1994]. Figure 5.7 shows the electric field along a path through the source location and the field that should be observed by the balloon calculated from the simple charge distribution. For the 100 meter sphere, the electric field reaches nearly 2.2 E_{BE} and exceeds breakeven over a vertical distance of about 100 meters, where the field of the 200 meter sphere peaks just above the breakeven field strength. The 100 meter sphere has two problems. First, the charge density is excessive, a factor of 10 greater than previous measurements [*Stolzenburg*, 1993]. The 100 meter sphere should also create a second region where runaway breakdown can occur at 4.1 km MSL. The x-ray measurements do not indicate occurred. From this argument, it seems plausible that a runaway electron process occurred within 250 meters of the balloon resulting from an reasonable variation in the charge density of the horizontal layer.

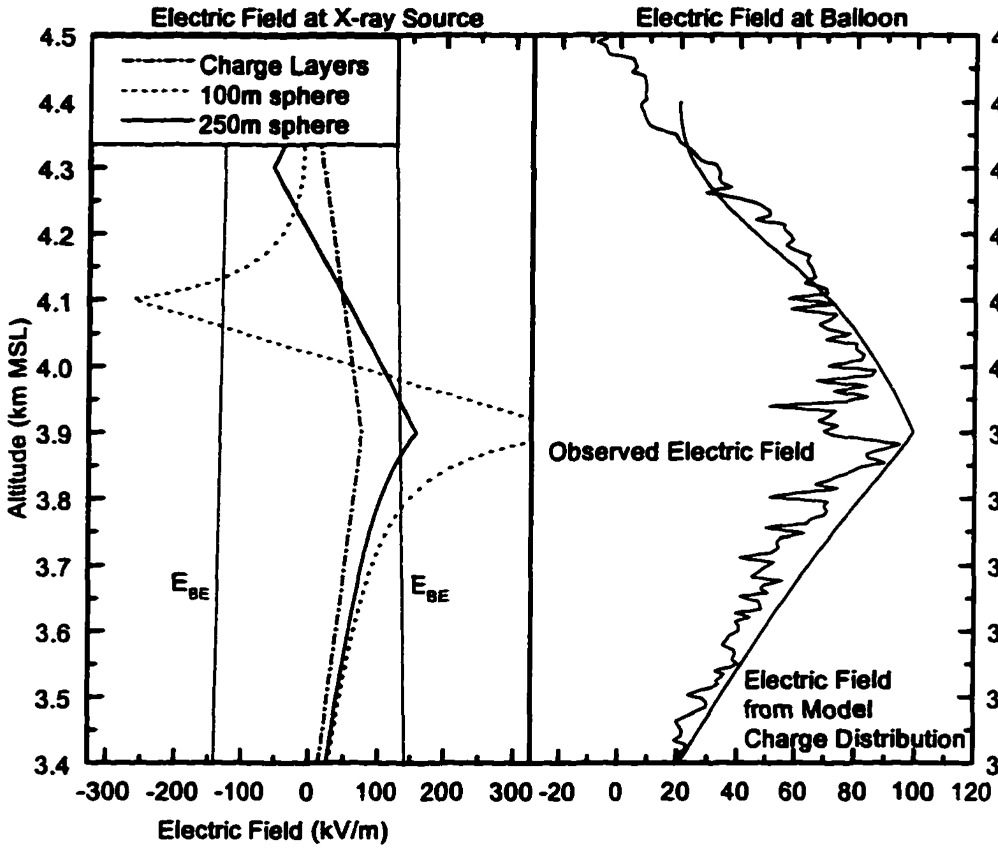

Figure 5.7. Left panel shows calculated electric field for a path through the center of the spherical charge (not the balloon path) for two spherical charges with the same total charge and different radii. This is added to the field from horizontal layers, which is shown separately for comparison. Electric field has no horizontal component due to symmetry. The right panel shows a comparison between the observed electric field at the balloon, and the total electric field calculated from the model charge distribution along the flight path of the balloon. The two compare very well, considering the simplicity of the charge distribution.

5.3 Flight 2: 24 May 1995

5.3.1 X-ray Event

The x-ray event observed on this flight (Figure 5.8), made shortly after Flight 1, was much weaker and associated with a negative electric field. The x-ray event at 4 km MSL has a peak intensity of about 70 cps, with a background rate of about 10 cps. Again, as in flight 1, the x-rays abruptly decreased nearly to background levels at the time of a lightning flash. After this flash there appears to be a slow increase in x-ray count rate to approximately 40 cps. This second increase also terminated at the time of a lightning flash when the balloon was near 5 km MSL. A third increase, although extremely weak with only a few to 10 cps above background level appears to be coincident with the positive electric field region at 5.3 km to 5.9 km MSL. This last event is more easily discernable in the individual channel data (Figure 5.7). The majority of this increase, as well as the previous two, occurs in channel 3 (90 to 120 keV).

The three events are much weaker than that observed in Flight 1. Most of the increases for the Flight 2 event occur in the higher energy channels. A higher proportion of counts in the upper channels could indicate greater distance to the source, since higher energy x-rays have longer attenuation distances. Also the longer distance between source and detector would attenuate the x-ray signal so that it would have a lower peak intensity. In order to estimate the source to detector distance, the procedure described in section 5.1 and in section 5.2.1 are repeated. Using the peak locations from each channel, an estimate of the profile (for the first event) that would be expected due to balloon motion alone is found and is shown in Figure 5.10.

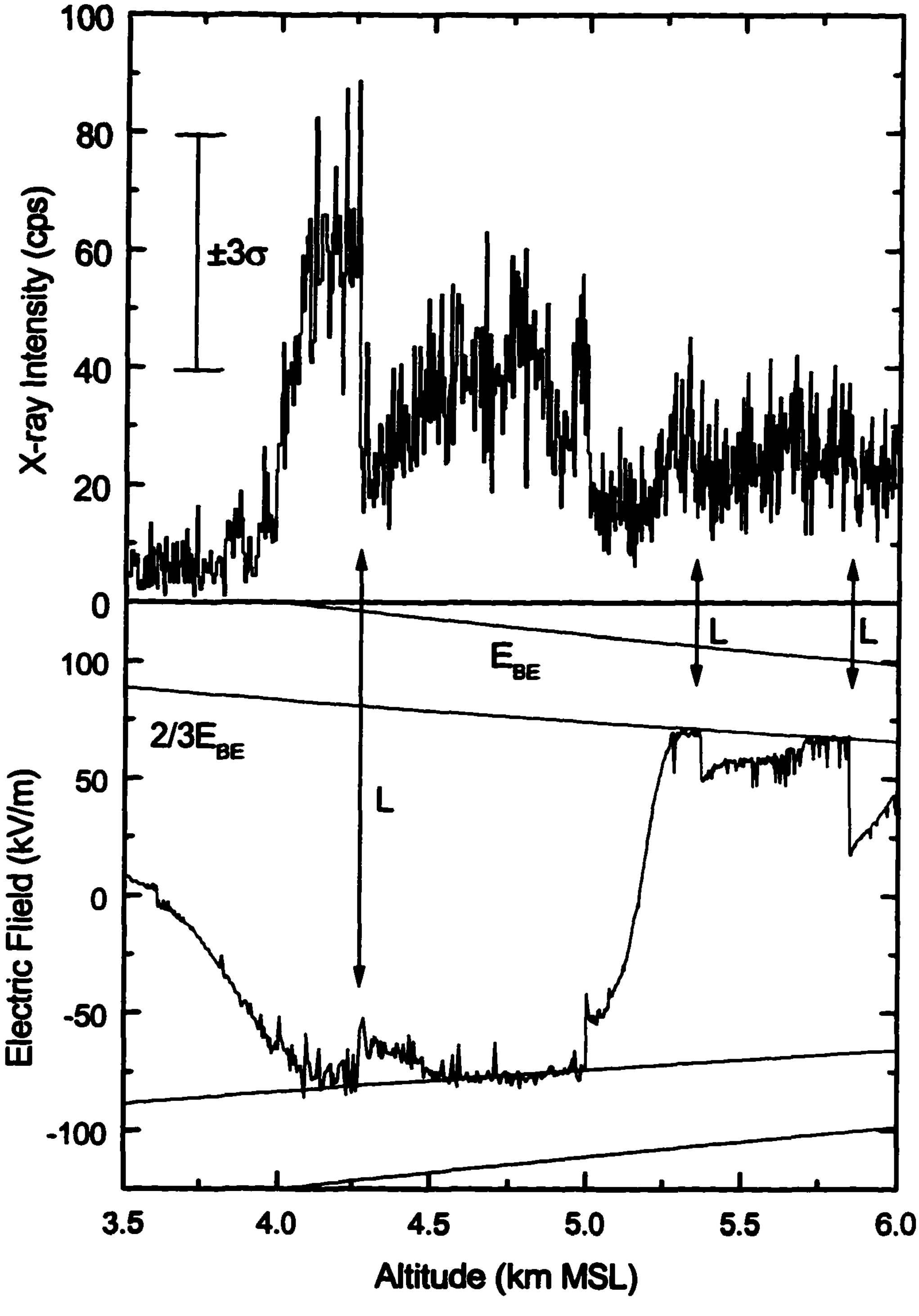

Figure 5.8. Detail of x-ray event observed near 4.2 km MSL. Electric-field transients due to lightning flashes are indicated by an "L.".

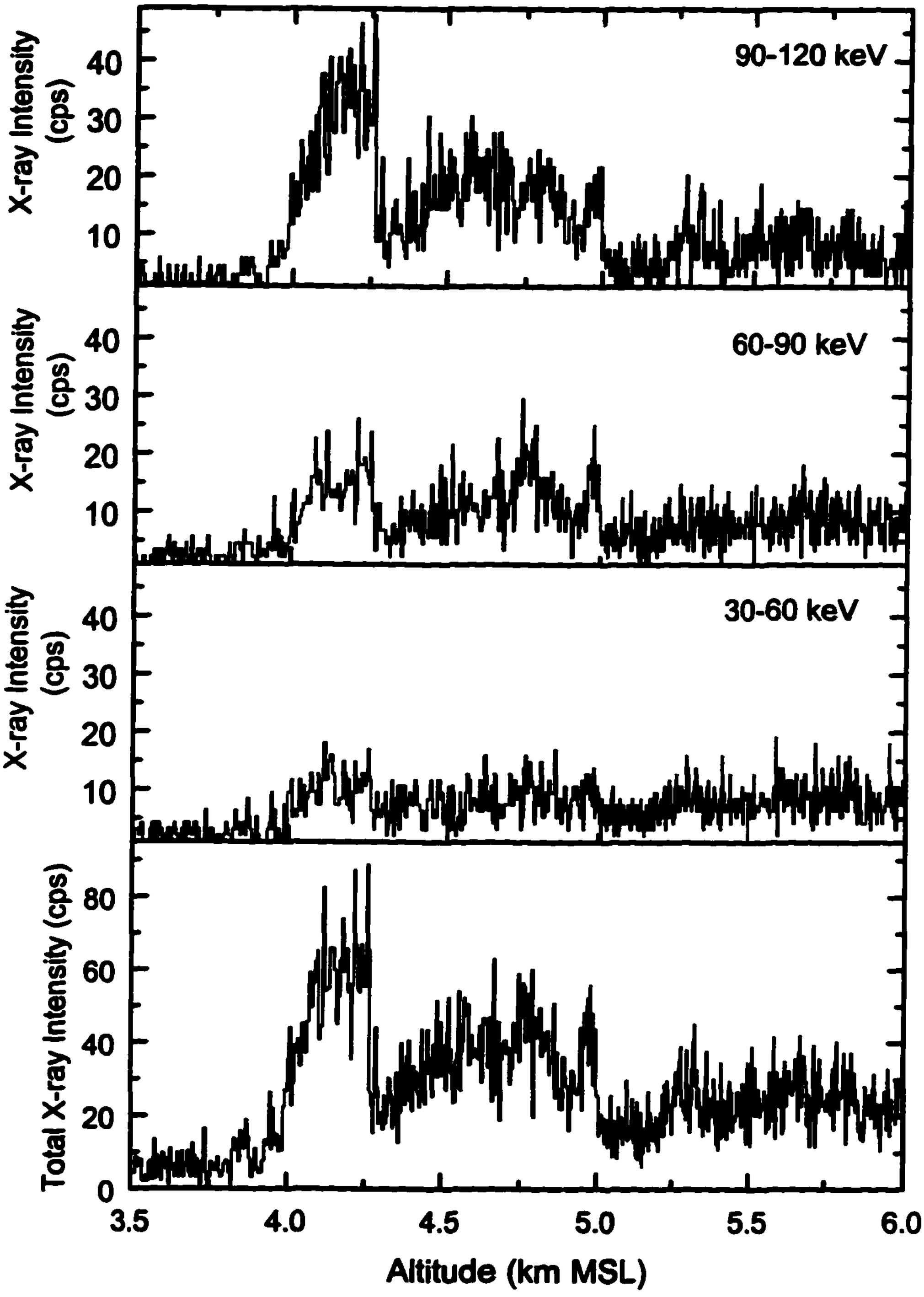

Figure 5.9. X-ray intensity in each energy channel and the total intensity observed by all three channels (lower most panel). The majority of the counts during the event were observed in the 90 to 120 keV energy channel.

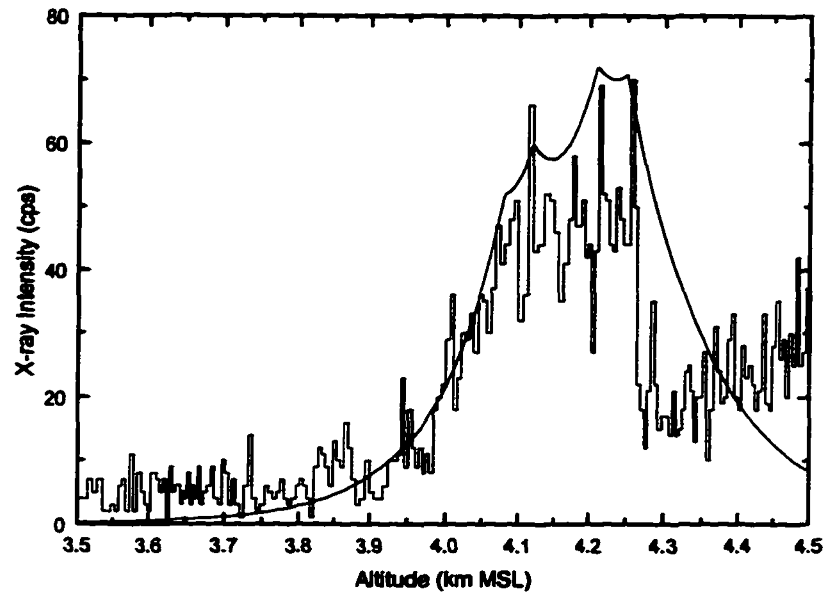

Figure 5.10. Estimated x-ray intensity superimposed on to the observed x-ray intensity. The method used to calculate the estimated flux is same as Figure 5.3. The slow rise of the event appears to be due to the motion of the detector towards the x-ray source

The profile generated matches the observations much better than in Flight 1, and appears to indicate that the slow variations are due mostly to the change in detector to source distance as the balloon ascends. Again, there is no reason to assume the balloon flew directly into the source, so additional expected profiles are generated with a source located horizontally away from the balloon flight path. Figure 5.11 shows this profile for horizontal separations of 250 and 500 meters. The profile for 250 meters matches the observed profile better. Both estimates do not indicate that the source was located any farther away than in Flight 1. The chi-square estimate is 200±30 m.

Relative spectral intensities estimate a distance of 275 m by my calculations, and 250 m by those of *Gurevich et al.* [submitted, 1997].

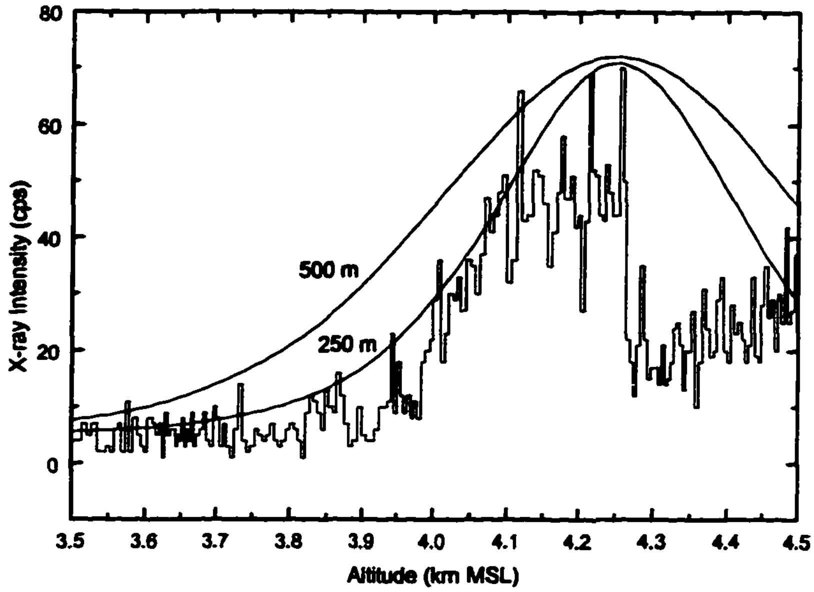

Figure 5.11. Estimates of x-ray intensity for a source located 250 m and 500 m from the flight path of the balloon. The observed x-ray intensity is shown for comparison.

5.3.2 Electric Field

As in Flight 1, the horizontal electric field is used to estimate the amount of charge necessary at the estimated source to detector distance determined above. For a distance of 250 meters at closest approach and a horizontal electric field of 25 kV/m, a charge of 0.17 C is required. Distributing this charge in spheres with radii of 100 and 200 meters results in a charge density of 42 and 5 nC/m^3. The vertical field from this spherical charge is less than 5 percent of the observed vertical field. Most of the vertical electric field is produced by a horizontal charge distribution. Figure 5.12 shows the vertical electric field from the two charge distributions as a function of distance from the center of the spherical charge, and the expected field as observed at the balloon. For the 100 meter sphere, the maximum electric field is about 1.4 E_{BE} and breakeven is exceeded over a vertical distance of about 50 meters. The 200 meter spherical charge reaches a maximum of 0.8 E_{BE}. In comparison to Flight 1, it seems rather unlikely that a runaway electron x-ray source would be operational in both Flights 1 and 2 at similar distances and produce an x-ray intensity a factor of 50 smaller. Also the charge density for the 100 meter sphere is large relative to previous estimates [*Stolzenburg*, 1993].

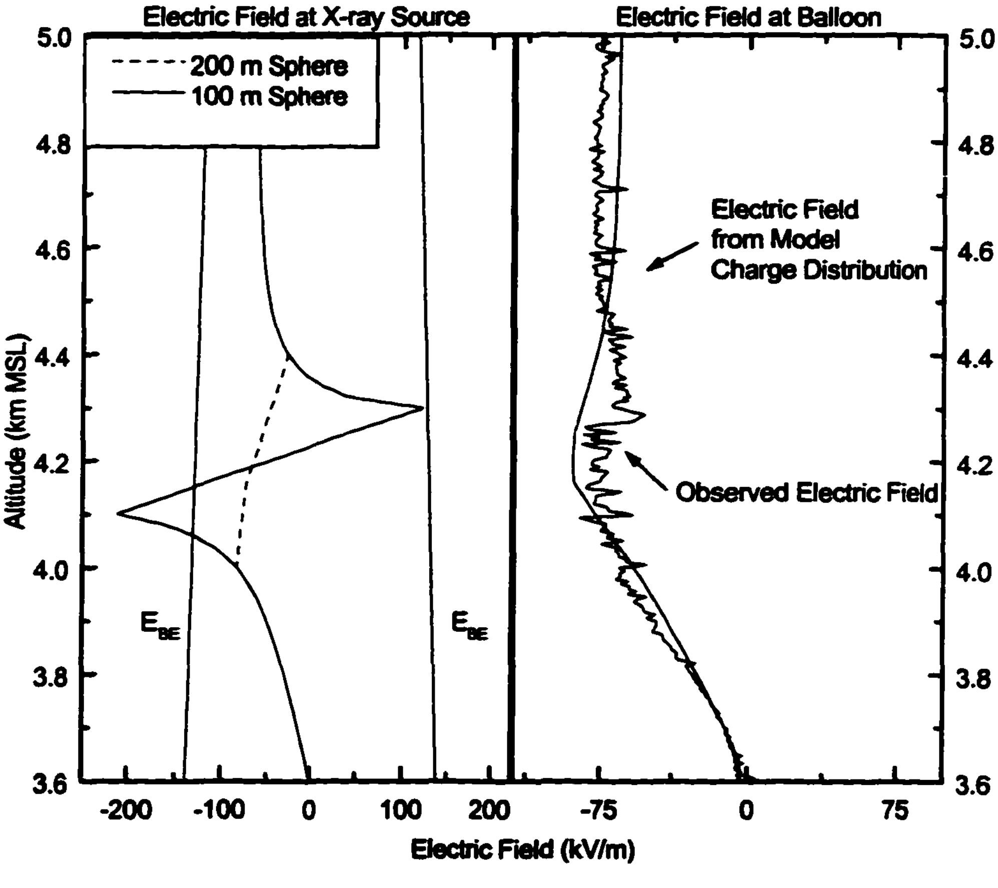

Figure 5.12. Left panel shows calculated electric field for a path through the center of the spherical charge (not the balloon path) for two spheres containing the same amount of charge but with different radii. Electric field has no horizontal component due to symmetry. The right panel shows a comparison between the observed electric field at the balloon, and the electric field calculated from the model charge distribution along the flight path of the balloon. The two compare very well, considering the simplicity of the charge distribution.

However, the electric field profile observed may work well for the electron "gathering" model. The electric field was measured to be close to $2/3E_{BE}$ between 4 and 5 km MSL and again between 5.5 and 6.5 km MSL. This profile fits with the model proposed in *McCarthy and Parks* [1992]. This model did not appear to be able to explain the high x-ray fluxes observed by aircraft observations similar to those observed in the first flight [*McCarthy and Parks*, 1985], because the number of electrons available was too small by a factor of 8. Considering that the model also predicted each electron would produce approximately 10 x-rays over a 1 km path length, the x-ray intensity predicted is a factor of 80 smaller than the aircraft observations or balloon Flight 1. However, it may account for the weak x-ray event observed during Flight 2, which is a factor of 50 smaller than observed in Flight 1.

5.4 Flight 3, Event A: 27 May 1995

5.4.1 X-ray Event

Figure 5.13 shows the detail of the first x-ray event observed during Flight 3. A region of strong negative electric field was measured at about 4 km MSL. The peak electric field reached about 0.85 E_{BE}. Coincident with the strong electric-field was a significant increase in the x-ray intensity, reaching nearly 2000 cps. From the geometry factor of the instrument, the peak flux was calculated to be 32 $(cm^2\ s\ Sr)^{-1}$. During the x-ray event, two changes in the electric field, one at about 3.9 km MSL and the other at about 4.3 km MSL caused a large change in the measured x-ray intensity. The first was an abrupt decrease in the electric field accompanied by a decrease in x-ray intensity. The second change in electric field caused a change in x-ray intensity from nearly 1800 cps to 200 cps. Figure 5.14 shows the individual energy channels for this event. Most of the increase occurred in channel 2 (60 to 90 keV). One interesting feature of the spectra is that the peak flux in channel 3 (90 to 120 keV) occurs right before the event turns off at 4.3 km MSL. One explanation for this might be a change in the source to detector geometry. Since electrons in a negative electric field are accelerated upward, the bremsstrahlung photons emitted will also have an upward momentum. For a downward looking detector located below the source, upward moving x-rays will have to scatter at least twice before they have any chance to be detected. These two Compton scattering events will degrade the energy spectrum. Once the detector is above the source, x rays emitted from the source can be detected without any scattering. The x-ray event ended shortly after the increase in 90 to 120 keV x-ray count rate.

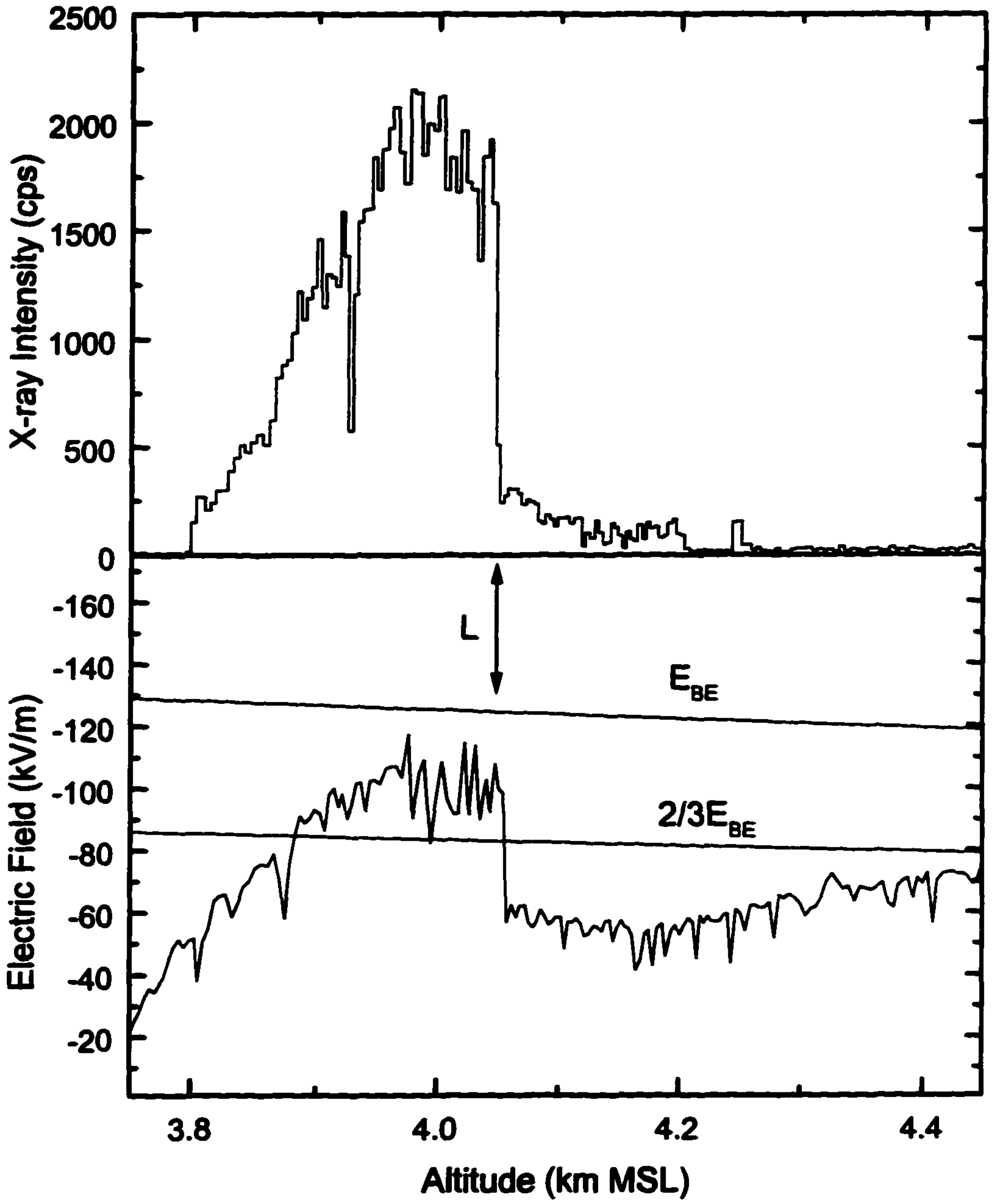

Figure 5.13. Detail of the first x-ray event observed during Flight 3. The electric-field transient from a lightning flash is indicated by an "L." The event lasted for about 45 seconds until the time of the flash.

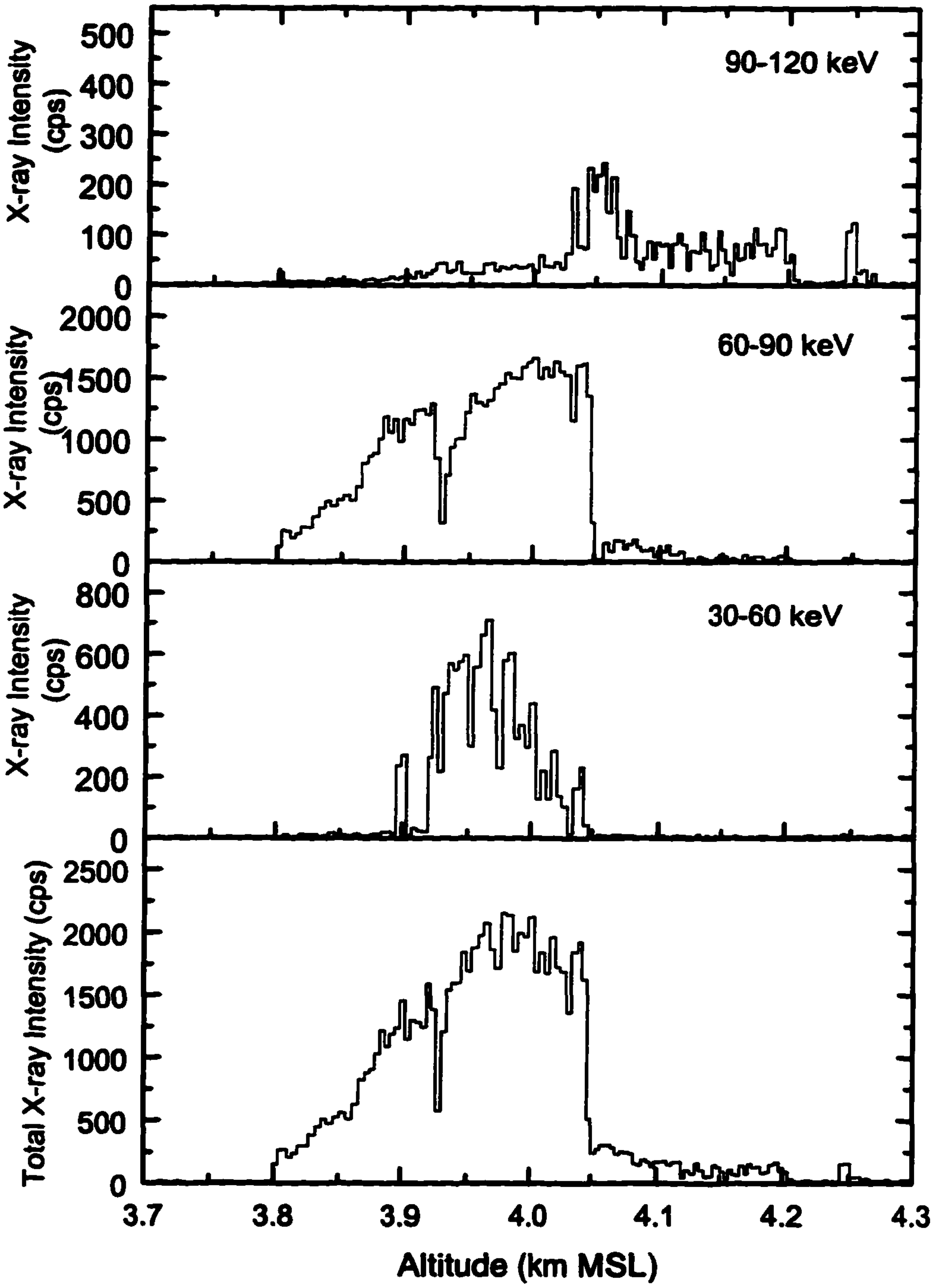

Figure 5.14. X-ray intensity in each energy channel and the total intensity observed by all three channels (lower most panel). Most counts during the event were in the 60 to 90 keV channel. The cause of the increase in counts in the highest energy bin near the end of the event is not known. It is possible that this is a result of the detector reaching a position where scattering was unnecessary for the x-rays to reach it.

Once again, the slow increase to peak can matched by taking into account the motion of the balloon. Figure 5.15 shows the expected curve for a detector moving directly towards a source with peak locations determined by the individual energy channels. Again, there is no reason to assume that instrument went directly through the source. Using the relative intensity of the bremsstrahlung source for each channel, a model curve is generated for a source located at some horizontal distance from the balloon flight path. Figure 5.16 shows these curves for distances of 100 and 250 meters. For this case, the best match is the 100 meter curve. The chi-square calculation gives an estimate of 40±10 m.

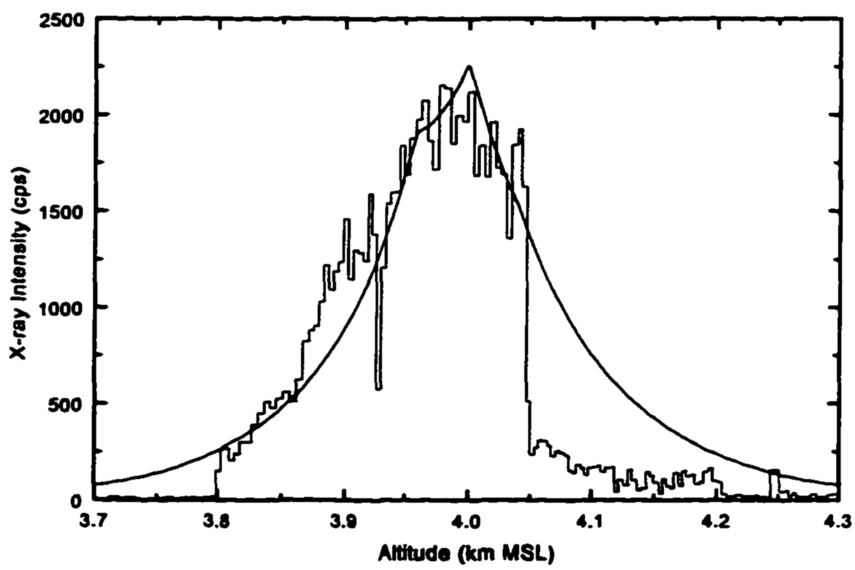

Figure 5.15. Estimated x-ray intensity superimposed on to the observed x-ray intensity. The method used to calculate the estimated flux is same as Figure 5.5. The slow rise of the event appears to be due to the motion of the detector towards the x-ray source

Estimates using the relative spectral intensity at peak are 200 m from the calculation of *Gurevich et al.* [submitted, 1997]. No estimate could be made using my calculations (Appendix D), indicating that the effects of scattering on the spectrum are important.

5.4.2 Electric Field

During this flight, the electric field reached nearly 0.9 E_{BE}. The horizontal field at the time of the peak x-ray flux was about 65 kV/m. Since the source is estimated to be only about 100 meters away, the 200 meter spherical charge distribution used for the previous two flights will not be used. For a spherical charge distribution with a radius of 100 m located 100 meters away from the balloon, a horizontal field of 65 kV/m requires a total charge of 0.12 C, and gives a charge density in the spherical region of 29 nC/m^3. The field from the spherical charge is added to the vertical field from the horizontal charge layers. The total vertical electric field from this configuration is shown in Figure 5.17. The electric field reaches a peak of about 1.4 E_{BE} and exceeds breakeven over a vertical path of about 75 meters. Again it seems reasonable to believe that a runaway process could have occurred near the balloon that produced the observed x rays. Although the electric field profile exceeded $2/3E_{BE}$, it did so only for about 200 meters, so it does not seem likely that the x rays were generated by an electron "gathering" type of mechanism. The high flux similar to the aircraft measurements [*McCarthy and Parks*, 1985] also appears to make this mechanism unlikely.

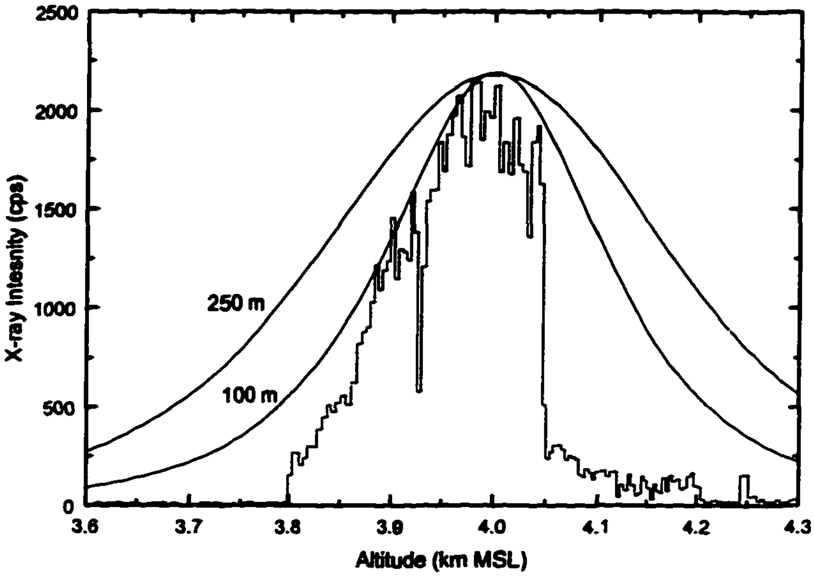

Figure 5.16. Estimates of x-ray intensity for a source located 100 m and 250 m from the flight path of the balloon. The observed x-ray intensity is shown for comparison

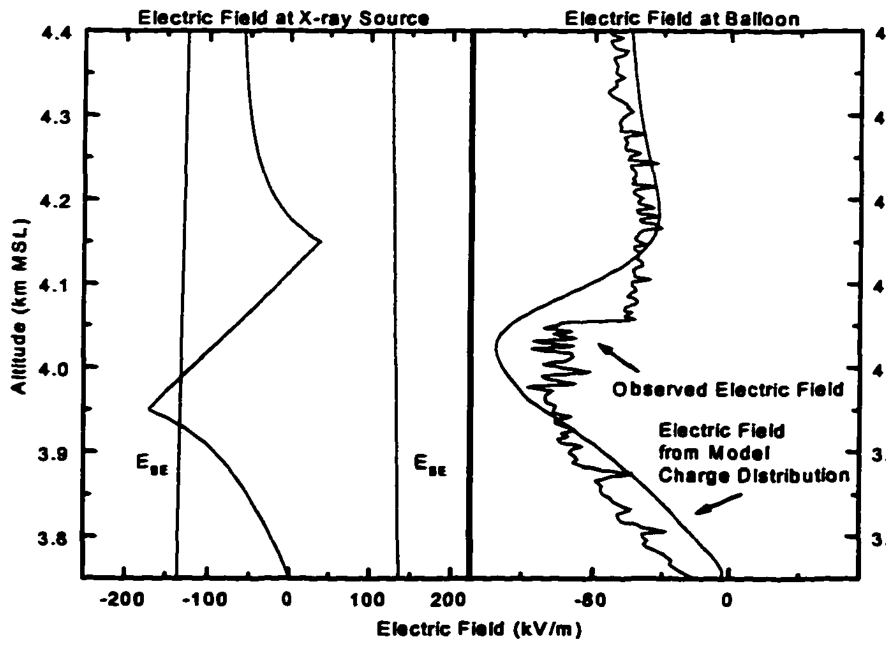

Figure 5.17. Left panel shows calculated electric field for a path through the center of the spherical charge (not the balloon path) for a 100 m sphere with 0.12 C total charge. The right panel shows a comparison between the observed electric field at the balloon, and the electric field calculated from the model charge distribution along the flight path of the balloon.

5.5 Flight 3, Event B: 27 May 1995

5.5.1 X-ray Event

The second event observed on Flight 3 has a much different character from that of the previous three events. A plot of this event and the observed electric field is shown with higher resolution in Figure 5.18. Since models of the runaway mechanism predict exponential electron multiplication over the distance in which the electric field exceeds breakeven, the x ray production would be strongly affected by small variations in the electric field [*M.P. McCarthy*, private communication]. This may indicate that the electric field in the source region was very close to the threshold needed for the x-ray production.

Assuming the source is in the direct flight path of the balloon, a model curve is generated to compare the observation to what might be expected for a balloon moving towards the source. The location of the peaks was determined from the spectral data plotted in Figure 5.19. The model curve in Figure 5.20 matches the overall profile of the event fairly well, but with the assumption of a constant source, the fast variations are not accounted for. The analysis used previously for a source horizontally distant from the balloon flight path is again applied. In the case shown here, the model curve is matched with the second peak. The first peak was also tried, and gives a similar result. Figure 5.21 shows the model curves for 250 and 500 meters, with the 250 meter curve providing the best match. The chi-square method estimates the distance to be 470±50 m. The spectral method of Gurevich et al. [submitted, 1997] gives an estimate of 500 m. My spectral method is unable to produce an estimate. Again indicating that scattering may be playing an important role.

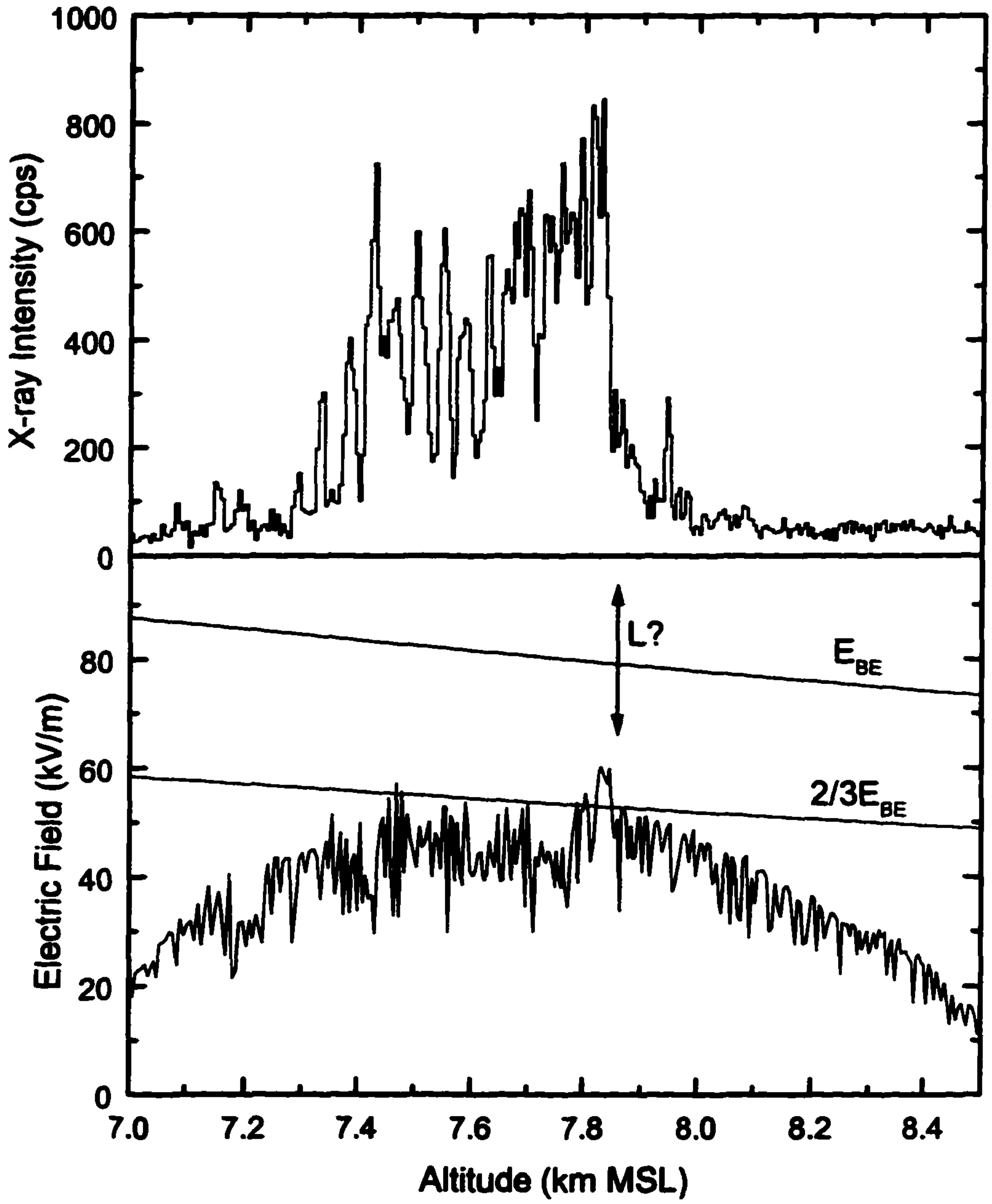

Figure 5.18. Detail of the second x-ray event observed during Flight 3. An electric-field transient, possibly due to a lightning flash is indicated by an "L."

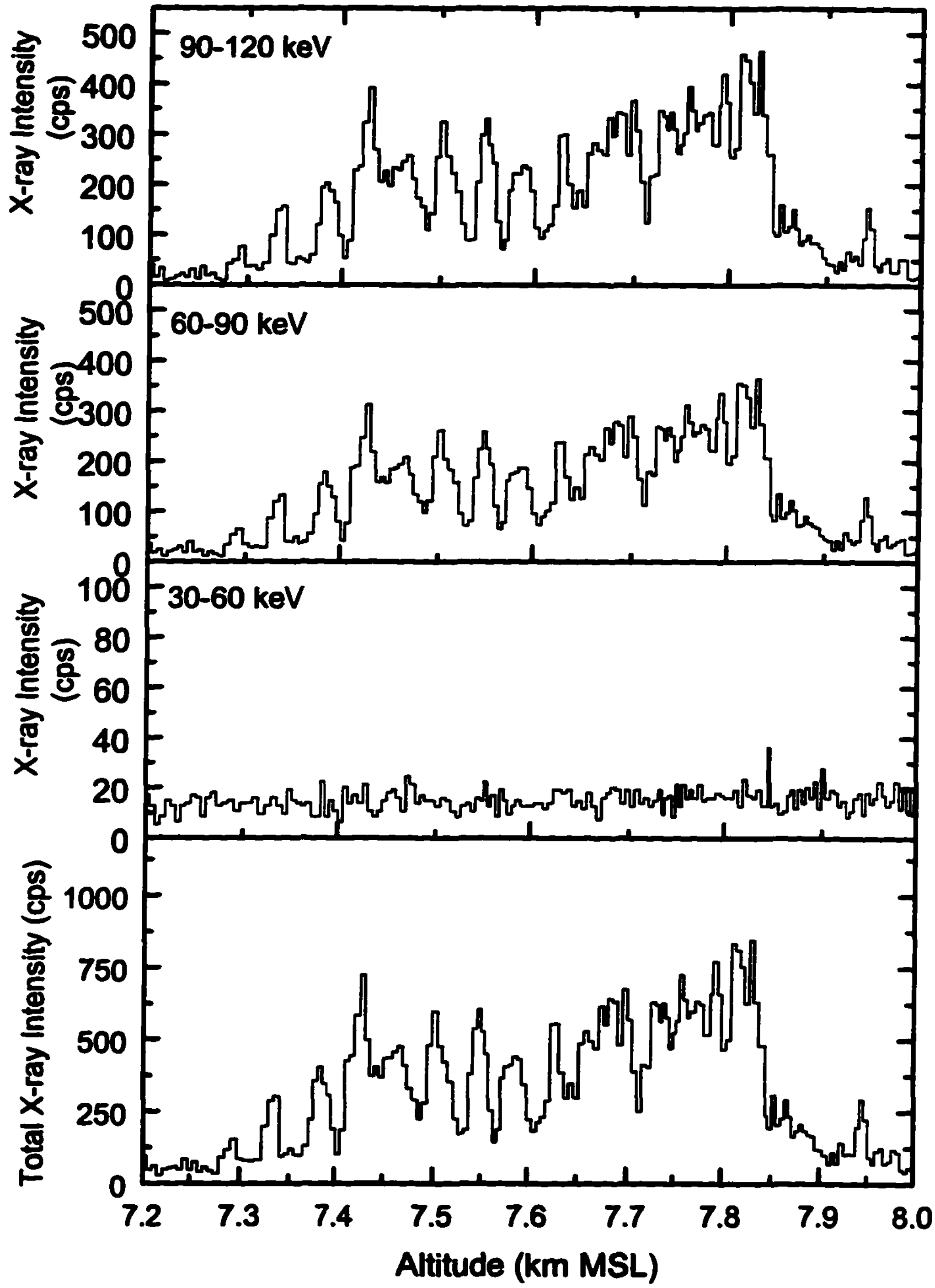

Figure 5.19. X-ray intensity in each energy channel and the total intensity observed by all three channels (lower most panel) for the second event observed during Flight 3.

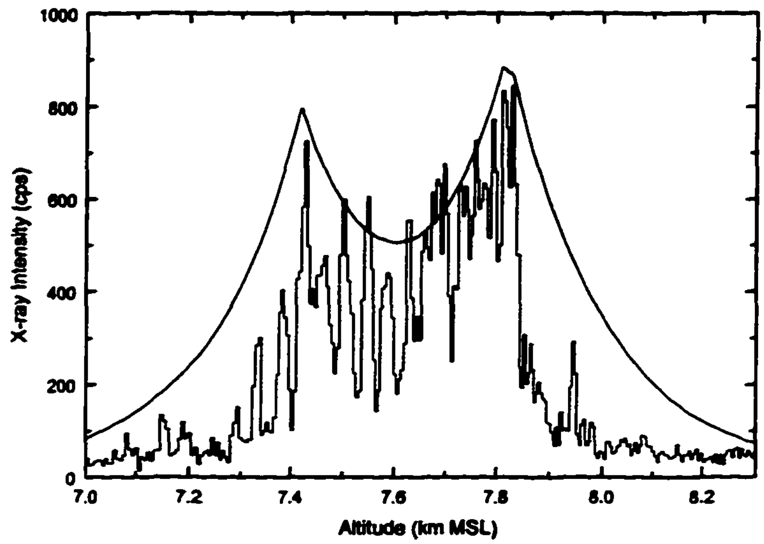

Figure 5.20. Estimated x-ray intensity superimposed on to the observed x-ray intensity. The method used to calculate the estimated flux is same as Figure 5.3. As before, the slow rise of the event appears to be due to the motion of the detector towards the x-ray source

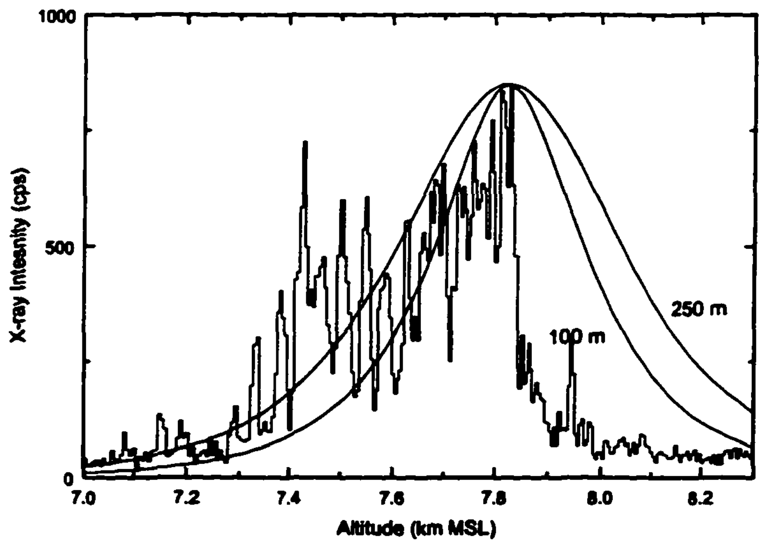

Figure 5.21. Estimates of x-ray intensity for a source located 100 m and 250 m from the flight path of the balloon. The observed x-ray intensity is shown for comparison

5.5.2 Electric Field

The electric field observed at the balloon during the event reached 2/3 E_{BE} over a vertical extent of about 500 meters. During this time, the horizontal field was 35 kV/m. For a spherical charge region centered 250 meters away, a total charge of 0.25 C is required, giving a charge density of 60 or 7.5 nC/m^3 for a spherical region with radii of 100 or 200 m. The electric field from this charge is then added to the field from the horizontal layers, and the result is shown in Figure 5.22. The 100 meter spherical charge region produces a region of electric field that exceeds breakeven for about 100 meters and reaches a peak of about 2.4 E_{BE}, and the 200 meter sphere also produces a field that just reaches breakeven for a limited vertical extent. The excessive charge density in the 100 m sphere appears to make it an unlikely possibility. The sphere with a radius of 200 meters provides a plausible explanation for x-ray production with an electric-field profile on the edge of producing a runaway avalanche. As a result small variations in the field could create large variations in the numbers of electrons and x rays produced.

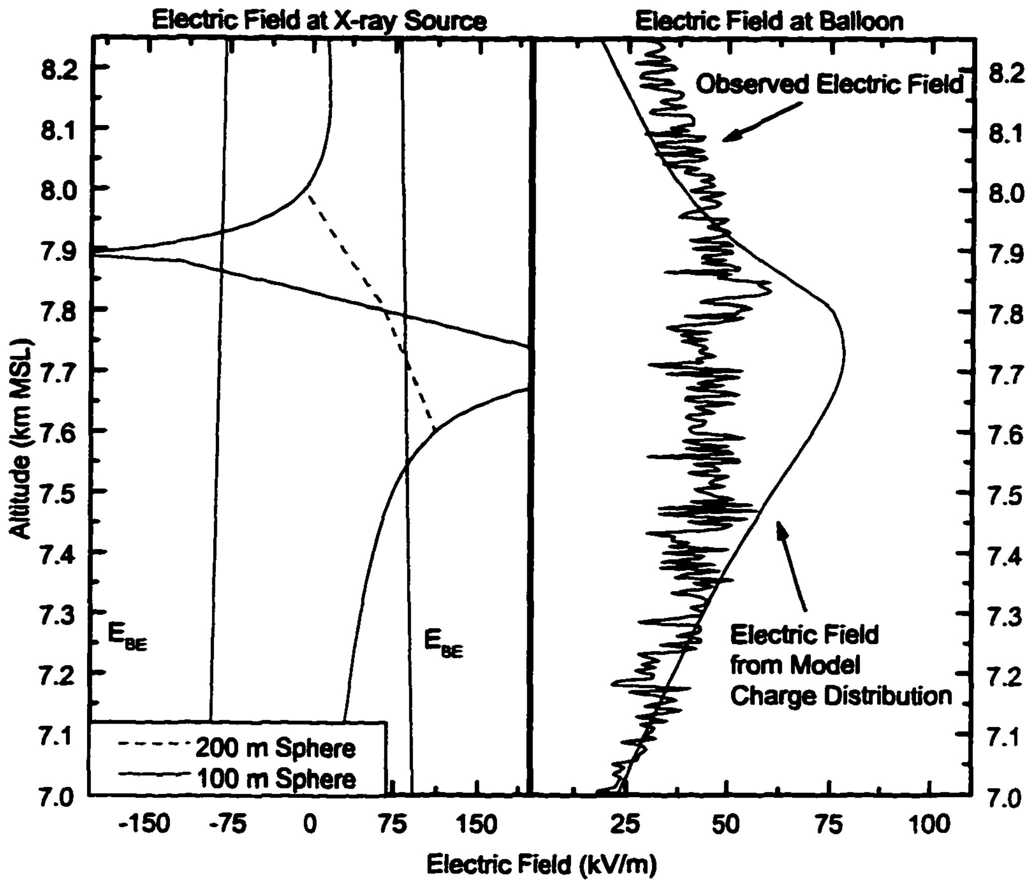

Figure 5.22. Left panel shows calculated electric field for a path through the center of the spherical charge (not the balloon path) for 100 and 200 m spheres with 0.25 C total charge. The right panel shows a comparison between the observed electric field at the balloon, and the electric field calculated from the model charge distribution along the flight path of the balloon.

5.6 Flight 4: 29 June 1995

There were no increases in the x-ray count rate observed while Flight 4 was inside the thunderstorm. Figure 4.5 shows that there were two regions of strong electric field observed during this flight. The first was at 4 km MSL and was about 1 km thick. The magnitude of the electric field in this region was nearly constant at 75 kV/m, with a vertical component of about 45 kV/m. The second region has a peak magnitude of about 70 kV/m and a vertical component ranging from 50 to 70 kV/m. Appendix C has details on the x-ray pulses observed while the balloon was above the thunderstorm.

5.7 Flight 0: 27 May 1994

The flight made in 1994 (Flight 0, 24 May 1994) briefly mentioned in Chapter 4 was not a complete failure, in the sense that it helps show that the source and detector must be relatively close in order to observe significant x ray count rates. Figure 5.23 shows the x-ray and electric-field observations for Flight 0. The x-ray instrument telemetry stopped at about 3.5 km MSL. Note that a strong negative electric field region was located 500 meters higher. This field in this region had a peak magnitude of about 70 kV/m and a vertical component of 50 kV/m. This was slightly weaker than the field observed during the event of Flight 1, and might be enough of a difference that runaway did not occur in this first region of strong electric field. However the second electric-field region of interest was located about 900 meters above the failure point of the telemetry. The electric field had a peak magnitude of 100 kV/m and a vertical component of 80 kV/m. This is similar in magnitude and altitude to the field observed during the first event of Flight 3. It seems reasonable that there might have been an increase in x-ray count rates associated with this strong electric field. Since the distance of 900 meters is almost 9 e-folding lengths for the high energy channel, and more for the lower channels, the x-ray source would have to have been very strong to be observable at this distance.

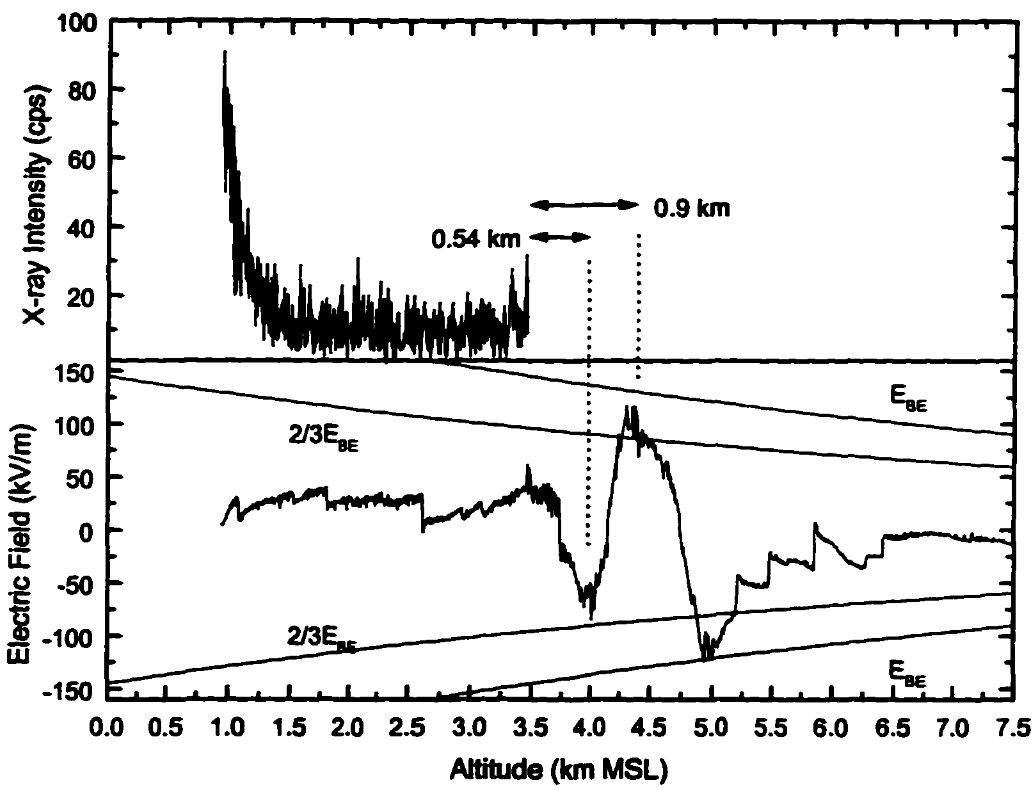

Figure 5.23. X-ray and electric-field sounding from Flight 0 made on 24 May 1994. Note that the peak magnitude of the electric field was larger than observed in the later flights. Although strong electric-fields were located less than 1 km away (assuming the electric-field profile remained somewhat constant) there was no observable increase in x-ray intensity.

Table 5.1 Estimate of source-to-detector distances using four methods.

Method	Flight 1	Flight 2	Flight 3A	Flight 3B
Rate of Rise/Fall	250 m	250 m	100 m	250 m
Chi-square Rate of Rise/Fall	230±30 m	200±30 m	40±10 m	470±50 m
Spectral Intensity Gurevich et al. [1997]	500 m	250 m	200 m	500 m
Spectral Intensity Appendix D	No Estimate Possible	275 m	No Estimate Possible	No Estimate Possible

Chapter 6

Concluding Remarks

6.1 Summary

The five flights presented here are (at this time and to the best of my knowledge) the only simultaneous observations of x-ray intensity and electric field inside thunderstorms. Although the data set is small, the x-ray observations are similar to those previously made from aircraft [*Parks et al.*, 1981; *McCarthy and Parks*, 1985]. Because of the duration of the x-ray events observed and of the coincidence between the reduction in the local electric field and the return of x-ray intensity to or near background levels, I conclude that the x-ray production mechanism responsible for these observations is driven by the large-scale thunderstorm electric field.

The question of exactly how thunderstorm electric-fields can produce enough electrons to account for the observed x-rays is difficult to answer with the present data set. The analysis presented demonstrates that the x-ray events observed (except for Flight 2) can be reconciled with the runaway electron model (electron multiplication) using estimates of the horizontal electric field and the estimates of source distance based on the rate of change with height of the x-ray intensity (Table 6.1). However, the data from a single detector observing a source with an unknown energy spectrum, spatial size, and location cannot be used to derive a unique explanation of the observations. Also, since the electric-field measurement is valid only for the point at which it was measured, there is no way to know exactly what the electric field was at any distant point.

Table 6.1 Summary of analysis of x-ray events and the possible mechanisms behind their production.

Event	Non-Runaway	Local Runaway	Distant Runaway
Flight 1	No Intensity too great E-field region small	No $E<E_{BE}$	Yes Distance = 250 m
Flight 2	Yes $E \approx 2/3\ E_{BE}$ for 1 km Low x-ray intensity	No $E<E_{BE}$	Yes If Distance≈ 600 m and not at estimated 200 m
Flight 3A	No Intensity too great E-field region small	No $E<E_{BE}$	Yes Distance≈100 m
Flight 3B	No Intensity too great E-field region small	No $E<E_{BE}$	Yes Distance≈250 m

6.2 Concerns

The result of this analysis seems to indicate that all of the sources were located 100 to 300 meters away from the balloon. Although physically plausible, this is certainly not the only possible explanation. This may simply be a result of the high attenuation of x-rays in the lower atmosphere. It does raise some issues that at least need to be considered.

If the production mechanism only occurred in small localized areas in the storm, it would seem rather fortunate that two out of four flights observed large increases in x-ray intensity. It is more likely that x-ray production occurs over a large area (at least in the stratiform region of MCS storms) or that there are numerous localized "pockets" of x-ray production. If this is true, is a 100 meter scale length a characteristic of the inhomogeneity of the electric charge distribution in MCS stratiform regions? Yet another possibility is that x-ray production was much closer but did not require electric fields in excess of breakeven.

A final possibility is that the presence of the balloon and instrument train reduces the field locally, and that the undisturbed electric field is larger than what is observed. Calibration of the electric-field meter does not indicate that this is the case for an isolated instrument [*Stolzenburg*, 1993]. *Jonnson* [1990] measured the conductance of materials used for balloon rigging under various conditions and found that currents on the order of 1 nA could flow through the rigging material. *Jonsson* [1990] argued that current flowing through the rigging would have a significant effect on the measured electric field. Since the conductance measurements were made on comparatively short pieces of line and in a laboratory environment, they do not completely represent balloon flight situation. Based on a line current measurement made during a balloon flight and a few calculations, the effects of the small current that flows through the rigging (orders of magnitude less than reported in *Jonsson* [1990]) and the enhancement of the electric field due to the presence of a long thin dielectric (balloon rigging) are at worst case one-percent effects [*Bateman, et al.*, "An instrument to measure balloon rigging line current inside thunderstorms, submitted to *Journal of Oceanic and Atmospheric Technology*, 1997].

6.3 Future Observations

Additional observations are needed not only to characterize the x-ray source better, but also to provide more information on the electric-field strength and vertical profile necessary for the production of the large numbers of energetic electrons thought to be responsible for the x-ray production observed. Improvements on these observations can be made in a number of ways. First using dual detectors to look both upward and downward or to look for both x-rays and electrons at the same time should provide additional information on the location and nature of the x-ray source. Multiple balloon flights into the same storm, separated by a few hundred meters would also aid in locating the source. Finally improved resolution of the horizontal electric-field measurements in conjunction with multiple flights would give additional insight into the electric field that produces the energetic electrons and x rays.

References

Appleton, E.V., and E.G. Bowen, Source of atmospherics and penetrating radiation, *Nature*, **132**, 965, 1933.

Blakeslee, R.J., H.J. Christian, and B. Vonnegut, Electrical measurements over thunderstorms, *J. Geophys. Res.*, **94**, 13135-13140, 1989.

Clay, J., H.F. Jongen, and A.J.J. Aarts, High energy electrons produced in thunderstorms, *Physica*, **18**, 801-808, 1952.

D'Angelo, N., On x-rays from thunderclouds, *Ann. Geophys. Ser. B*, **5**, 119-122, 1987.

Dejnakarintra, M., and C.G. Park, Lightning-induced electric fields in the ionosphere, *J. Geophys. Res.*, 79, 1903-1910, 1974.

Eack, K.B., W.H. Beasley, W.D. Rust, T.C. Marshall, and M. Stolzenburg, X-ray pulses observed above a mesoscale convective system, *Geophys. Res. Lett.*, **23**, 2915-2918, 1996a.

Eack, K.B., W.H. Beasley, W.D. Rust, T.C. Marshall, and M. Stolzenburg, Initial results from simultaneous observations of x rays and electric fields in a thunderstorm, *J. Geophys. Res.*, **101**, 29637-29640, 1996b.

Evans, R.D., *The Atomic Nucleus*, McGraw-Hill, New York, 1955.

Fishman, G.J., P.N. Bhat, R. Mallozzi, J.M. Horack, T. Koshut, C. Kouveliotou, G.N. Pendleton, C.A. Meegan, R.B. Wilson, W.S. Paciesas, S.J. Goodman, and H.J. Christian, Discovery of intense gamma-ray flashes of atmospheric origin, *Science*, **264**, 1313-1316, 1994.

Gurevich, A.V., G.M. Milikh, and R. Roussel-Dupre, Runaway electron mechanism of air breakdown and preconditioning during a thunderstorm, *Phys. Lett. A*, **165**, 463-468, 1992.

Gurevich, A.V., G.M. Milikh, and R.A. Roussel-Dupre, Nonuniform runaway air-breakdown, *Phys. Lett. A*, **187**, 197-203, 1994.

Halliday, E.C., Thunderstorms and penetrating radiation, *Proc. Cambridge Phil. Soc.*, **30**, 206-215, 1934.

Hill, R.D., Investigation of electron runaway in lightning, *J. Geophys. Res.*, **68**, 6261-6266, 1963.

Jonnson, H.H., Possible sources of errors in electrical measurements made in thunderclouds with balloon-borne instrumentation, *J. Geophys. Res.*, **95**, 22539-22545, 1990.

Knoll, G.F., *Radiation Detection and Measurement,* Wiley, New York, 1979.

Lockhart, L.B., R.A. Baus, P. King, and I.H. Blifford, Atmospheric radioacivity studies at the U.S. Naval Research Laboratory, *J. Chem. Ed.*, **36**, 291-295, 1959.

Lyons, W.A., Characteristics of luminous structures in the stratosphere above thunderstorms as imaged by low-light video, *Geophys. Res. Lett.*, **21**, 875-878, 1994.

Macky, W.A., An attempt to detect radiation in thunderclouds, *Proc. Cambridge. Phil. Soc.*, **30**, 70-73, 1934.

Marshall, T.C., M.P. McCarthy, and W.D. Rust, Electric field magnitudes and lightning initiation in thunderstorms, *J. Geophys. Res.*, **100**, 7097-7103, 1995a.

Marshall, T.C., W. Rison, W.D. Rust, M. Stolzenburg, J.C. Willett, and W.P. Winn, Rocket and balloon observations of electric field in two thunderstorms, *J. Geophys. Res.*, **100**, 20815-20828, 1995b.

Marshall, T.C., W.D. Rust, M. Stolzenburg, Electrical structure and updraft speeds in thunderstorms over the southern Great Plains, *J. Geophys. Res.*, **100**, 1001-1015, 1995c.

Marshall, T.C., M. Stolzenburg, and W.D. Rust, Electric field measurements above mesoscale convective systems, *J. Geophys. Res.*, **101**, 6979-6996, 1996.

McCarthy, M., and G.K. Parks, Further observations of x-rays inside thunderstorms, *Geophys. Res. Lett.*, **12**, 393-396, 1985.

McCarthy, M.P., and G.K. Parks, On the modulation of x ray fluxes in thunderstorms, *J. Geophys. Res.*, **97**, 5957-5864, 1992.

Parks, G.K., B.H. Mauk, R. Spiger, and J. Chin, X-ray enhancements detected during thunderstorm and lightning activities, *Geophys. Res. Lett.*, **8**, 1176-1179, 1981

Pasko, V.P., U.S. Inan, Y.N. Taranenko, and T.F. Bell, Heating, ionization and upward discharges in the mesosphere due to intense quasi-electrostatic thundercloud fields, *Geophys. Res. Lett.*, **22**, 365-368, 1995.

Roussel-Dupre, R.A., A.V. Gurevich, T. Tunnell, and G.M. Milikh, Kinetic theory of runaway air breakdown, *Phys. Rev. E*, **49**, 2257-2271, 1994.

Roussel-Dupre, R.A., and A.V. Gurevich, On runaway breakdown and upward propagating discharges, *J. Geophys. Res.*, in press, 1996.

Schery, S.D., R. Wang, K. Eack, and S. Whittlestone, New models for radon progeny near the Earth's surface, *Rad. Prot. Dosim.*, **45**, 343-347, 1992.

Schonland, B.F.J., Thunderstorms and the penetrating radiation, *Proc. R. Soc. London A*, **140**, 314-333, 1933.

Schonland, B.F.J., and J.P. Viljoen, On a penetrating radiation from thunderclouds, *Proc. Roy. Soc. London, A*, **140**, 314-333, 1933.

Sentman, D.D., E.M. Wescott, D.L. Osborne, D.L. Hampton, and M.J. Heavner, Preliminary results from the Sprites94 aircraft campaign: 1. Red sprites, *Geophys. Res. Lett.*, **22**, 1205-1208, 1995.

Shaw, G.E., Background cosmic count increase associated with thunderstorms, *J. Geophys. Res.*, **72**, 4623-4626, 1967.

Stolzenburg, M., *Electrical and meteorological conditions in the stratiform cloud region of a mesoscale convective system*, M.S. Thesis, University of Oklahoma, 153 pp., 1993.

Stolzenburg, M., *An observational study of electrical structure in convective regions of mesoscale convective systems*, Ph.D. Dissertation, University of Oklahoma, 137pp. 1996.

Stolzenburg, M., T.C. Marshall, W.D. Rust, and B.F. Smull, Horizontal distribution of electrical and meteorological conditions across the stratiform region of a mesoscale convective system, *Mon. Wea. Rev.*, **122**, 1777-1797, 1994.

Suszcynsky, D.M., R. Roussel-Dupre, and G. Shaw, Ground-based search for x-rays generated by thunderstorms and lightning, *J. Geophys. Res.*, **101**, 23505-23516, 1996.

Taylor, J.R., *An Introduction to Error Analysis*, p.207-209, University Science Books, Mill Valley, 1982.

Taranenko, Y., and R. Roussel-Dupre, High altitude discharges and gamma-ray flashes: A manifestation of runaway air breakdown, *Geophys. Res. Lett.*, 23, 571-574, 1996.

Wescott, E.M., D. Sentman, D. Osborne, D. Hampton, and M. Heavner, Preliminary results from the Sprites94 aircraft campaign: 2. Blue jets, *Geophys. Res. Lett.*, **22**, 1209-1212, 1995.

Whitmire, D.P., Search for high-energy radiation near lightning strokes, *Lett. Nuovo Cimento*, **26**, 497-501, 1979.

Wilson, C.T.R, The acceleration of β-particles in strong electric fields such as those of thunderclouds, *Proc. Cambridge Phil. Soc.*, **22**, 534-538, 1925.

Winn, W.P., G.W. Schwede, and C.B. Moore, Measurements of electric fields in thunderclouds, *J. Geophys. Res.*, **79**, 1761-1767, 1974.

Winn, W.P., C.B. Moore, C.R. Holmes, and L.G. Byerley, Thunderstorm on July 16, 1975 over Langmuir Laboratory: A case study, *J. Geophys. Res.*, **83**, 3079-3092, 1978.

Winn, W.P., C.B. Moore, and C.R. Holmes, Electric field structure in an active part of a small isolated thundercloud, *J. Geophys. Res.*, **86**, 1187-1193, 1981.

Appendix A

X-ray Spectrometer Details

A.1 X-ray Detector Vendor and Parts List

HV supply and Pre-amp EG&G ScintiPack Model 296 Price: $940

EG&G Ortec
100 Midland Road
Oak Ridge TN 37831-0895
800-251-9750 (Val Johnson)

Gain X1 or X6 preamp
Output time constant: 50 μs

Photomultiplier Hamamatsu R1847-05 (flying leads) Price: $360

Hamamatsu Corp.
380 Foothill Rd.
P.O Box 6910
Bridgewater NJ 08807-0910
908-231-0960
800-524-0504 (Tech Asst.)

10 stage 2" diameter
Gain: $3x10^5$
Dark current: 2 nA

NaI Scintillator Bicron 2xr.080A (Deltaline) Price: $340

Bicron
12345 Kinsman Rd.
Newbury OH 44065-9577
216-564-2251
216-564-8047 (Fax)

2" diamter x 2 mm thick
1 mil (0.001") Al window
0.125" thick optical window

Microcontroller Micro-485 Price: $299

Blue Earth Research
165 W. Lind Ct.
Mankato MN 56001-0400
507-387-4001
507-387-4008 (Fax)

Transmitter AIR AS-1A-T (Temp only radiosonde) Price: $48

Atmospheric Instrumentation Research
8401 Baseline Rd.
Boulder CO 80303
303-499-1701
303-499-1767 (Fax)

Frequencies: 403.4, 403.5
403.6, 404.4, 404.5 ,404.6 MHz

A.2 Amplifier and Discriminator Circuit

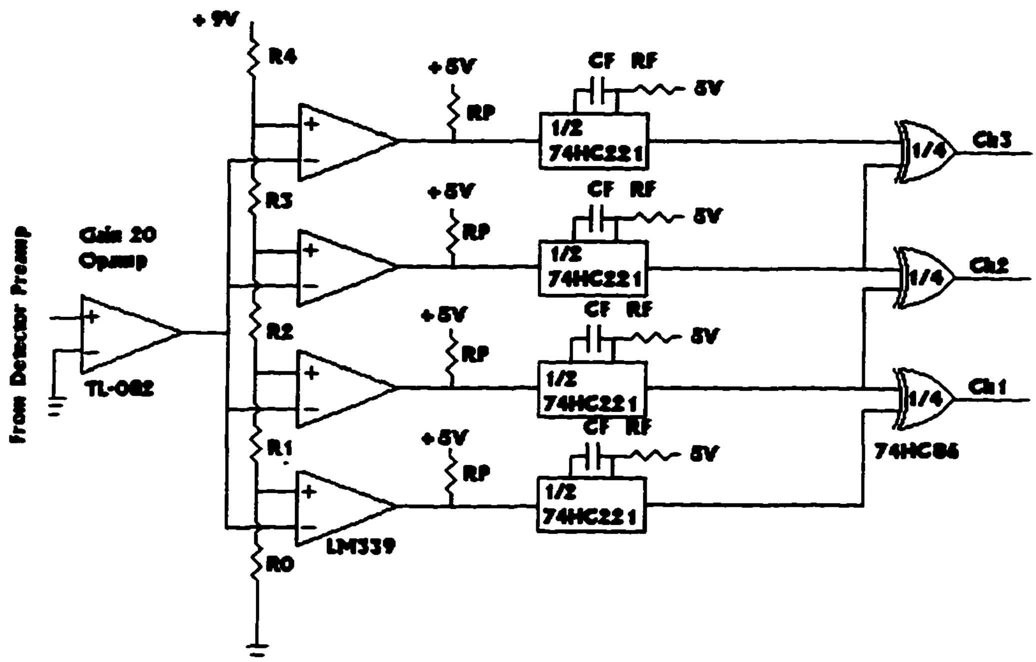

Figure A.1. Schematic of distriminator and amplifier circuit. Pin numbers and power connections for the integrated circuits are not shown. 74HC221 monostable multivibrators (one-shots) are set to leading edge triggering. CF is 100 pF and RF is 20 kΩ giving and output pulse duration of 1.4×10^{-6} s. RP is a pull-up resistor with a value of 5.6 kΩ. R0 to R4 form the voltage divider that sets the energy bins of the discriminator. Typically R0-R3 are 3 kΩ for 30 keV bin spacings. R4 is chosen to calibrate the circuit and is different for each detector, since each has a different calibration.

Appendix B

Electric-Field Meter Data

The electric-field meter (EFM) measures both the vertical and horizontal components of electric field. The total electric-field vector is assigned the polarity of the vertical component. A positive electric field vector points upward and will accelerate an electron downward. The instrument senses both components by rotating about two axes (Figure B.1). Driven by a small motor, rotation about the horizontal axis at about 2.5 Hz allows measurement of the vertical electric field. A mercury switch is used to determine the orientation of the two spheres and therefore the polarity of the electric field. Rhomboid vanes made from Styrofoam on the ends of the instrument rotate the instrument about the vertical axis as the instrument ascends at a speed of about 5 m s^{-1} (in still air). Rotation frequency is about 0.125 Hz. Horizontal orientation is determined by a simple magnetic compass [*Stolzenburg*, 1996]. Typically the horizontal electric field is unresolved, although recently a technique has been developed to deconvolve the vertical and horizontal components (*Bateman*, private communication).

Although unresolved, the horizontal field can be estimated using the electric field plots in Chapters 4 and 5. In many cases, the electric field plot has what appears to be a significant width to the trace. This results from the instrument sensing only the vertical electric field at some points and the total electric field at others. In Figure B.2. a sample electric field sounding is shown. The outer part of the trace represents the total electric field, the sum of the horizontal and vertical components. The inner portion of the trace is the vertical electric field only [*Stolzenburg*, 1996]. The difference between these two, or the width of the trace is representative of the horizontal component. This is calculated using the Pythagorean theorem and the magnitudes of the vertical and total electric-field vectors.

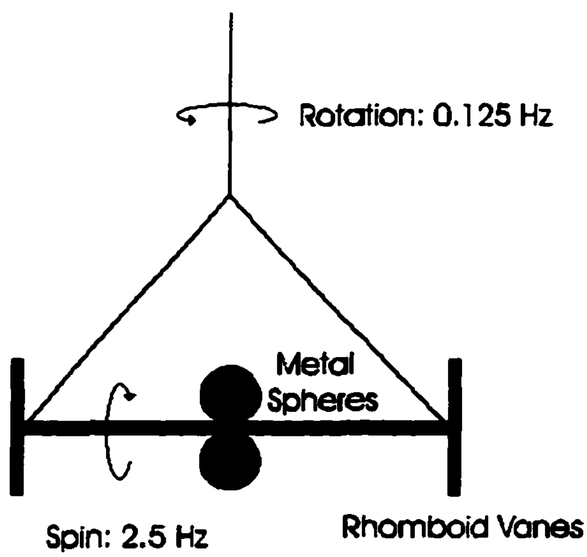

Figure B.1. Diagram of electric field meter. Spin around the horizontal axis and rotation about the vertical allow the instrument to measure both the vertical and horizontal components of the electric field. The metal spheres are used to sense the electric field and as the telemetry antenna.

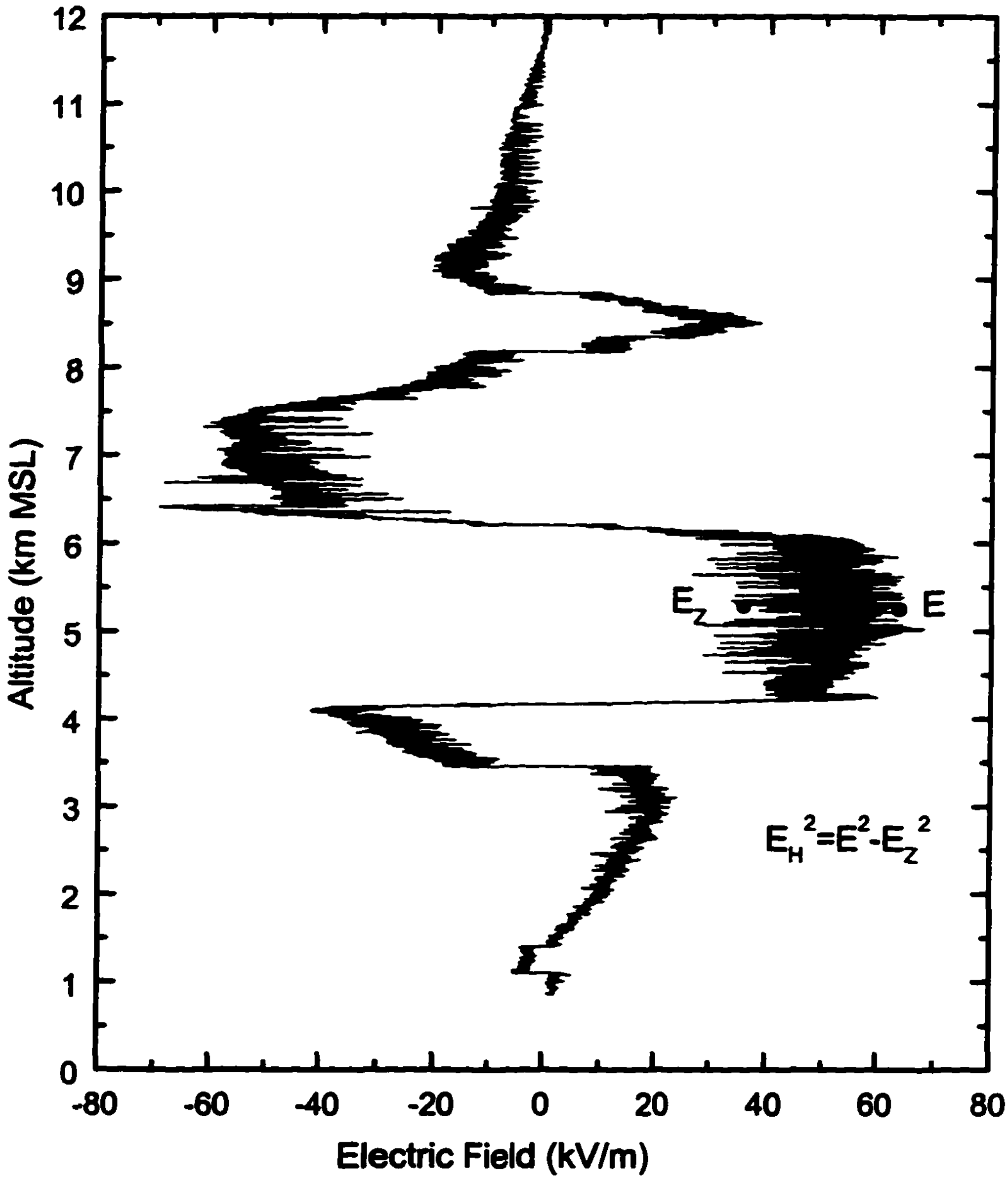

Figure B.2. Sample electric field sounding. The inner envelope of the trace is the measurement of the vertical component, while the outer envelope of the trace is the measurement of the total electric field. The dots marked E_Z and E show the measurement at a single point of the vertical and total electric field respectively.

Appendix C

X ray Pulses

C.1 Observations

At an altitude of about 15 km MSL (about 3 km above the electrical cloud top), and a measured pressure of 130 mb, we observed three x-ray pulses with peak fluxes of 37, 39 and 270 $(cm^2\text{-}s\text{-}sr)^{-1}$, each with a duration of about one second (Figure C.1). We define electrical cloud top as the altitude at which the electric field becomes insignificant, in this case at about 12 km MSL (Figure C.2). Time series plots of each energy channel are shown in Figure C.3. Note that in the lowest energy range (30 to 60 keV), the pulses are slightly longer (by a few counting intervals) than in the higher energy ranges. In the case of the first pulse, the low energy channel has a second peak 0.75 seconds after the first. With a single x-ray detector we cannot determine the location or spatial extent of the x-ray source. Although the detector field of view was upward, x-rays from a source located below the detector could have reached the detector as a result of Compton scattering.

The x-ray pulses occurred at 0654:50, 0655:24 and 0655:26 UT. More than 100 cloud-to-ground lightning flashes were reported within 350 km of the balloon by the National Lightning Detection Network (NLDN) during a two minute period from 06:54:00 to 06:56:00 UT (Figure C.4). Eleven of these were positive flashes. Two of the positive flashes occurred at 06:55:22 and 06:55:24 UT (within two seconds of the last two x-ray pulses). These were both single-stroke flashes with reported peak currents of

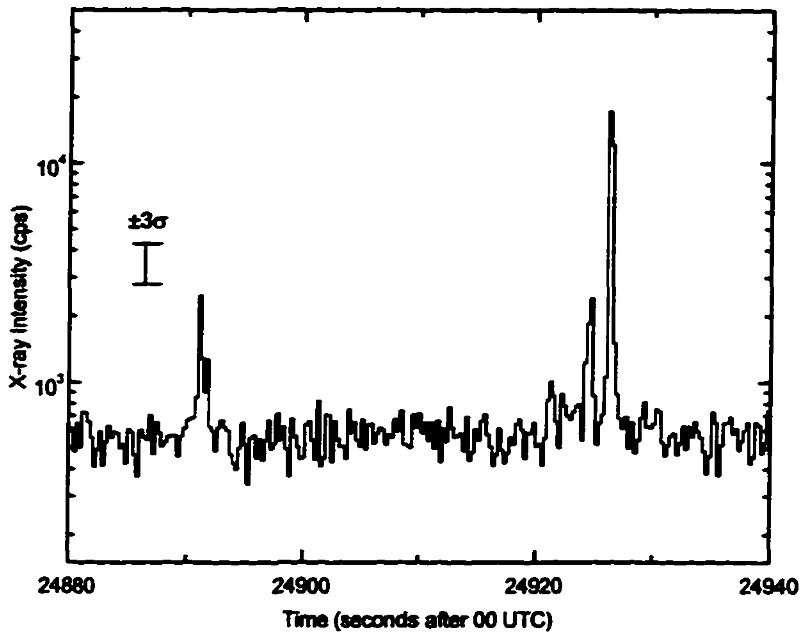

Figure C.1. Plot of three x-ray pulses observed near 15 km MSL on 29 June 1995. Each data step is 0.25 second. Pulses have a duration of about 1s.

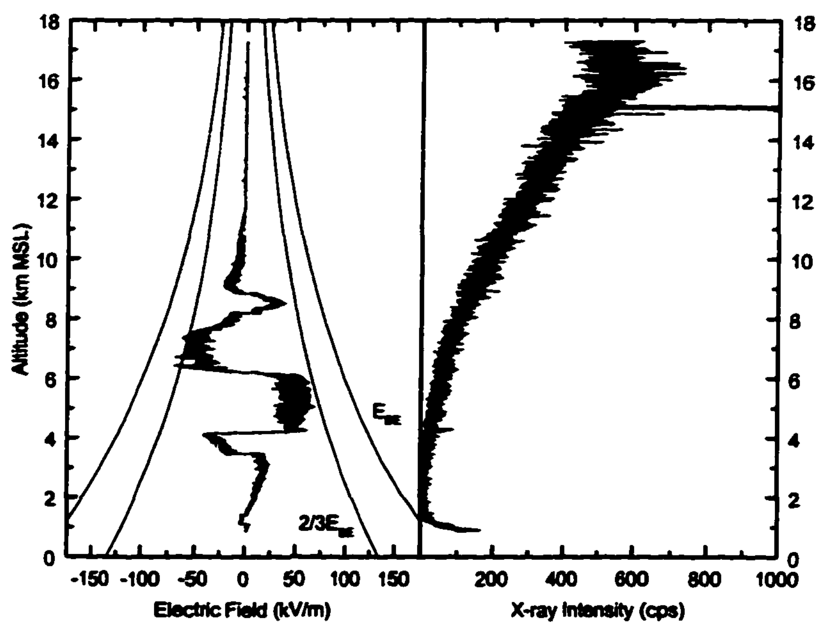

Figure C.2. Complete ascent sounding of x-ray intensity and electric field.

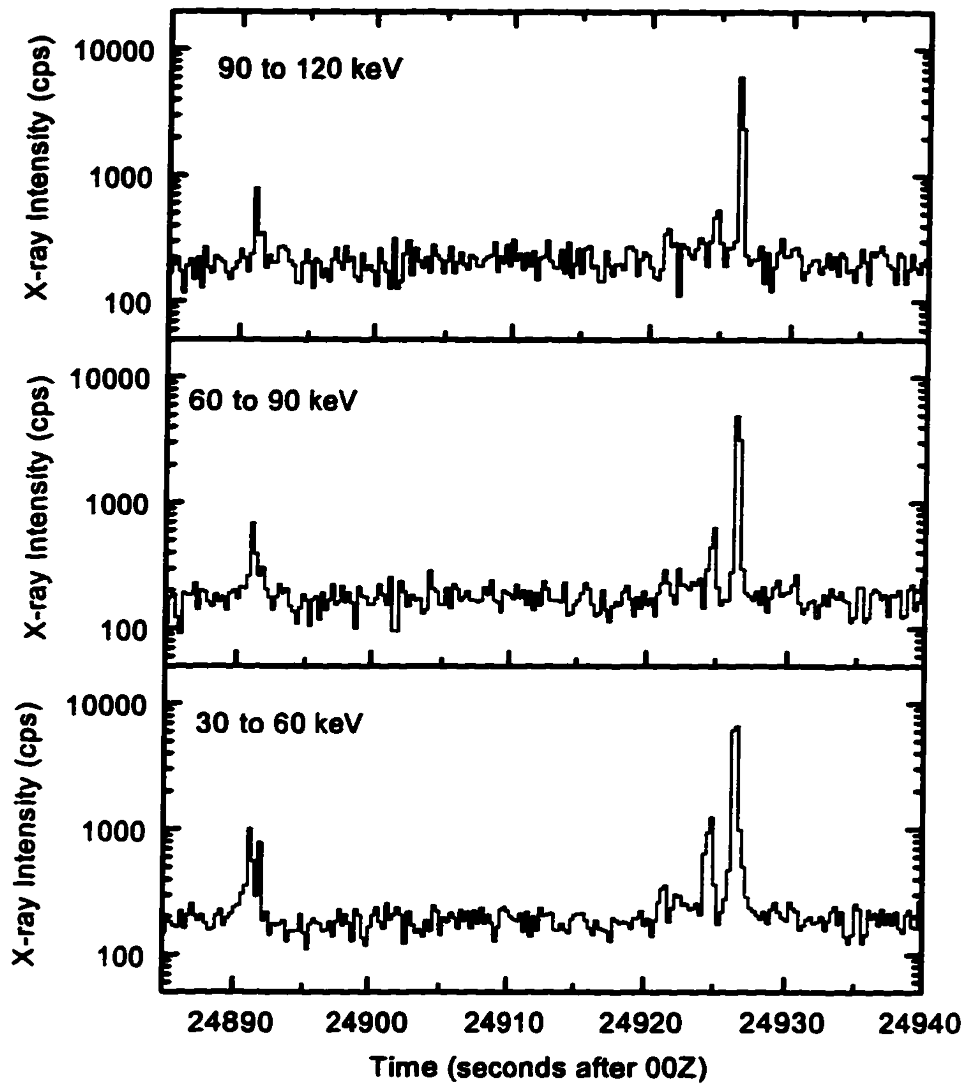

Figure C.3. Three channel time series plot for the three x-ray pulses. Each step is 0.25 seconds in length. The pulses have slightly longer duration in lowest energy channel.

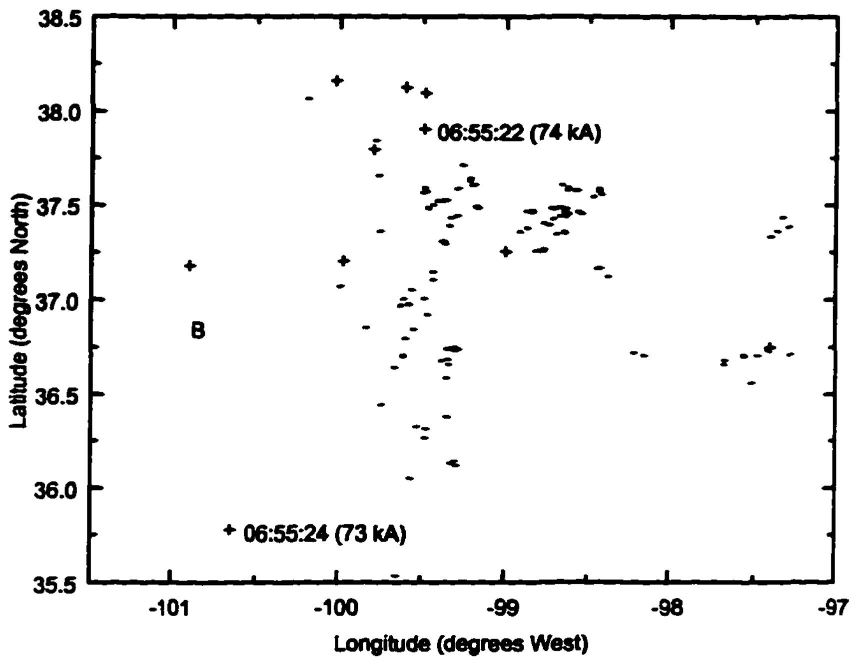

Figure C.4. Cloud-to-ground lightning locations as determined by the NLDN for a two minute period (0654 to 0656 UTC). Positive flashes are marked with a "+" and negative are marked with a "-". The balloon's position at the time of the x-ray pulses is denoted by the letter "B". Balloon motion during this two minute period is negligible on this plot.

about 75 kA. The first was 170 km from the balloon location, while the second was about 110 km distant. Negative flashes also occurred at the time of each x-ray pulse, and in each case had peak currents of about -20 kA and located about 125 km from the balloon's position. We also visually observed a horizontally extensive lightning discharge northeast of the launch site at 0655:23 UT.

At the time of the x-ray pulses, the steady electric field measured at the balloon was about -500 V/m (electric-field vector directed downward). No significant changes in electric field were observed at the time of the x-ray pulses. However, in other balloon measurements [*Marshall et al.*, 1996] electric-field "discontinuities" have been observed above the cloud. These appear to be associated with lightning and have durations ranging from several seconds to several tens of seconds and field-change magnitudes of 1.1 to 4 kV m^{-1}.

C.2 Discussion

The measurement of no significant electric field or field change at the times of the x-ray pulses is puzzling when viewed with the current theories on runaway electrons and the resulting production of x-rays. Instrumentation problems are always a possibility, but we are confident that both the x-ray and the electric-field instruments were working properly. If so, then the lack of significant electric field at the balloon at the time of the x-ray pulses suggests that either (1) some unknown x-ray production mechanism was responsible, (2) a runaway breakdown occurred some distance from the balloon, where the electric field was sufficient for runaway, or (3) the electric field driving the runaway process near balloon was not measured by the electric field meter. Since theories for new production mechanisms are beyond the scope of this paper, we will examine the last two suggestions.

To address the second suggestion, that a runaway breakdown occurred at some distance from the balloon, we need to consider possible locations of the sources. A source could have been located in the thunderstorm cloud or above the position of the balloon. The electrical cloud top was about 3 km below the balloon. X-rays with energies of 100 keV have an exponential attenuation length of about 300 meters at an altitude of 15 km. If we assume this attenuation length for the entire path between the source and detector (underestimating the attenuation) then the x-ray flux at the source would have to have been a factor of 10^5 greater than we measured. In this case we have assumed a large planar x-ray source, which without atmospheric attenuation, provides a constant flux irrespective of distance. Other source geometries would suffer a reduction in x-ray flux with distance, requiring even greater source intensity.

For a source located above the balloon's position, we consider the results of *Taranenko and Roussel-Dupre* [1996]. They have modeled a runaway breakdown which is initiated at 25 km MSL and predict gamma-ray emissions that are in agreement with the CGRO measurements. They predict that the CGRO detector should detect 800 gamma-rays (with energies of 100 keV, and assuming no attenuation) at a distance of 500 km [*Taranenko and Roussel-Dupre,* 1996]. We calculate that a source of this strength would produce about 10^4 counts in our detector 10 km away. This is similar to our measurements, but this calculation only includes the r^{-2} factor for distance effects on flux from a point source with no atmospheric attenuation. At an altitude of 25 km the attenuation length is about 1 km. Using this attenuation for a source 10 km above the detector, the source would need to be a factor of about 10^5 stronger to account for our observations.

Now we address the third suggestion, that the electric field transient was somehow missed by the electric-field instrument. Since we believe that the instrument was working properly, two possibilities exist for this case. The first is that the transient had a duration less than 200 ms, but this seems unlikely given that the x-ray pulses had durations of nearly 1 s. The second possibility is that the electric field driving the runaway process may have been horizontally oriented. The electric field instrument is primarily responsive to vertical electric fields and could miss a 1 s horizontal field transient as a result of the instrument orientation. However, it is unlikely that this would occur for each of the three pulses.

For both possibilities discussed above, the electric field is driving the runaway breakdown. This will occur if the electric field exceeds a threshold value over a distance of at least a few electron doubling lengths, which is dependant upon the atmospheric pressure and the strength of the electric field (see *Roussel-Dupre and Gurevich*, [1996] or *Gurevich et al.* [1992] for a discussion of the runaway process). The threshold is given by E_{TH}=218 (P/P_0) kV/m, where P is the atmospheric pressure, and P_o is the pressure at sea level [*Roussel-Dupre and Gurevich*, 1996]. At 15 km the threshold electric field is about 40 kV/m, and at 50 km altitude it is about 500 V/m. A necessary result of a runaway process is the emission of bremsstrahlung radiation with a spectrum dependant upon the energy of the electrons. The runaway process should continue to operate as long the electric field exceeds the threshold over a long enough path length. The electric-field profile may become unsuitable for the continuation of the runaway breakdown as a result of the runaway process itself [*Taranenko and Roussel-Dupre*, 1996], which separates electrons from positive ions and produces an electric field opposite in direction to the original field. Runaway processes driven by the large-scale electric field inside a thunderstorm may end as a result of lightning discharges or leakage between charge regions due to increased conductivity that results from the runaway process [*Marshall et. al*, 1995a]. Observations made inside thunderstorms appear to support these possibilities [*Eack et al.*, 1996; *McCarthy and Parks*, 1985]. Runaway might also end as a result of the rearrangement of space charge in the weakly conducting atmosphere.

Measurements made above thunderstorms [*Marshall et al.*, 1996; *Blakeslee et al.*, 1989] have shown that the quasi-static electric field is too weak to support a runaway process. However, electric field transients may occur above a storm [*Marshall et al.*, 1996] as a result of the rapid removal or neutralization of charge from the cloud during a lightning discharge (cloud-to-ground or intracloud). As a result, the space charge distribution above the cloud will change in response to the reduction of charge in the cloud on a time scale determined by the local relaxation time (ϵ/σ) of the atmosphere, where σ is the conductivity and ϵ is the permittivity of air. Thus the transient field will decrease with a time constant equal to the local relaxation time, which is altitude dependent. For example, using a conductivity profile of $\sigma(z)=5 \times 10^{-14} e^{z/6km}$ mho m^{-1} (where z is the altitude in km) [*Dejnakarintra and Park*, 1974], the relaxation time is about 30 s near cloud top (about 10 km), 15 s at 15 km, and approximately 40 ms at 50 km. If the transient electric field exceeds the threshold value, then runaway breakdown may occur [*Taranenko and Roussel-Dupre*, 1996]. The transient duration is determined by the relaxation time. Therefore the relaxation time and magnitude of the transient will, in part, determine the time during which a runaway can occur as a result of such a transient.

The gamma ray flashes observed by the CGRO satellite had origins no lower than about 30 km, estimated on the basis of atmospheric scattering and absorption [*Fishman et al.*, 1994]. *Roussel-Dupre and Gurevich* [1996] predict that maximum gamma-ray emissions will occur below 40 km where the majority of the electron avalanche occurs during the runaway breakdown. At these altitudes, from the relaxation time alone, a runaway might be expected to last no longer than 10's or 100's of milliseconds. This is significantly longer than, but not inconsistent with, the CGRO observations of 0.1 to 2 ms. For a runaway process occurring at 15 km, the relaxation time would predict that a runaway process could continue for times on the order of 10 s. The durations of the x-ray pulses we observed at 15 km are not inconsistent with this. However, the measurement of no significant electric field at the balloon indicates that the runaway process would have to have occurred relatively far from the balloon's position.

C.3 Concluding Remarks

With a balloon flying over an MCS, we observed three x-ray pulses that lasted on the order of one second at an altitude of 15 km MSL, 3 km above electrical cloud top. No significant electric field was observed at the time of the pulses. If a runaway breakdown produced these x-rays, our measurements suggest that it had to occur at considerable distance from the balloon. If so, then the source must be strong in order for x-rays to have been detected, since atmospheric attenuation of x-rays at these altitudes is relatively great. Even so, we cannot rule out other mechanisms for x-ray production that do not involve a runaway breakdown driven by an electric field.

This appendix has been excerpted from Eack, K.B., W. H. Beasley, W.D. Rust, T.C Marshall and M. Stolzenburg, "X-ray pulses observed above a mesoscale convective system" published in *Geophysical Research Letters*, volume 23, pages 2915-1918, 1996.

Appendix D

Additional Plots for Source-to-Detector Distance Estimates

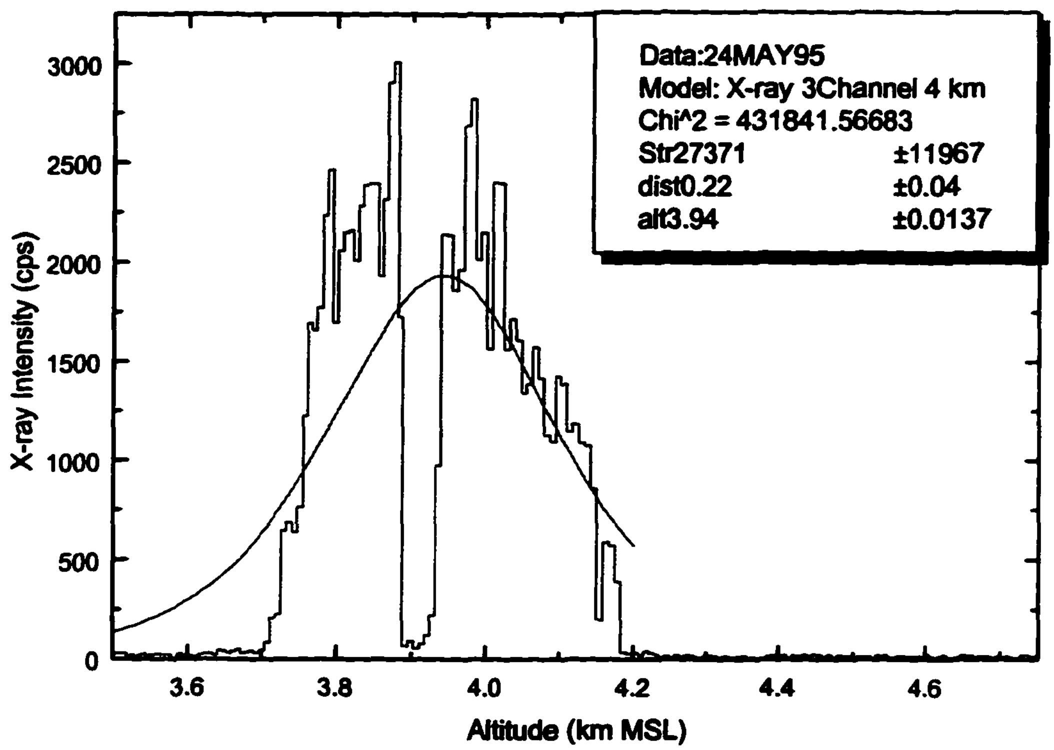

Figure D.1. Minimized chi-square fit for x-ray event observed during Flight 1. Horizontal (source-to-detector) distance is estimated to be 220±40 meters.

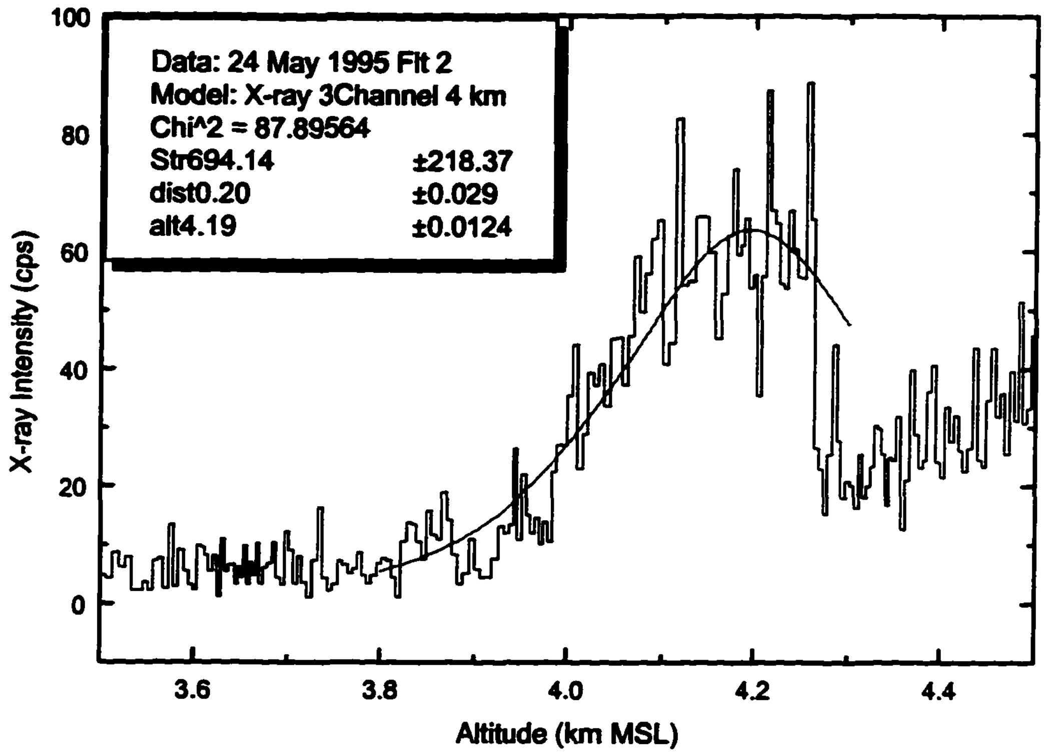

Figure D.2. Minimized chi-square fit for x-ray event observed during Flight 2. The estimated source-to-detector distance is 200±30 meters.

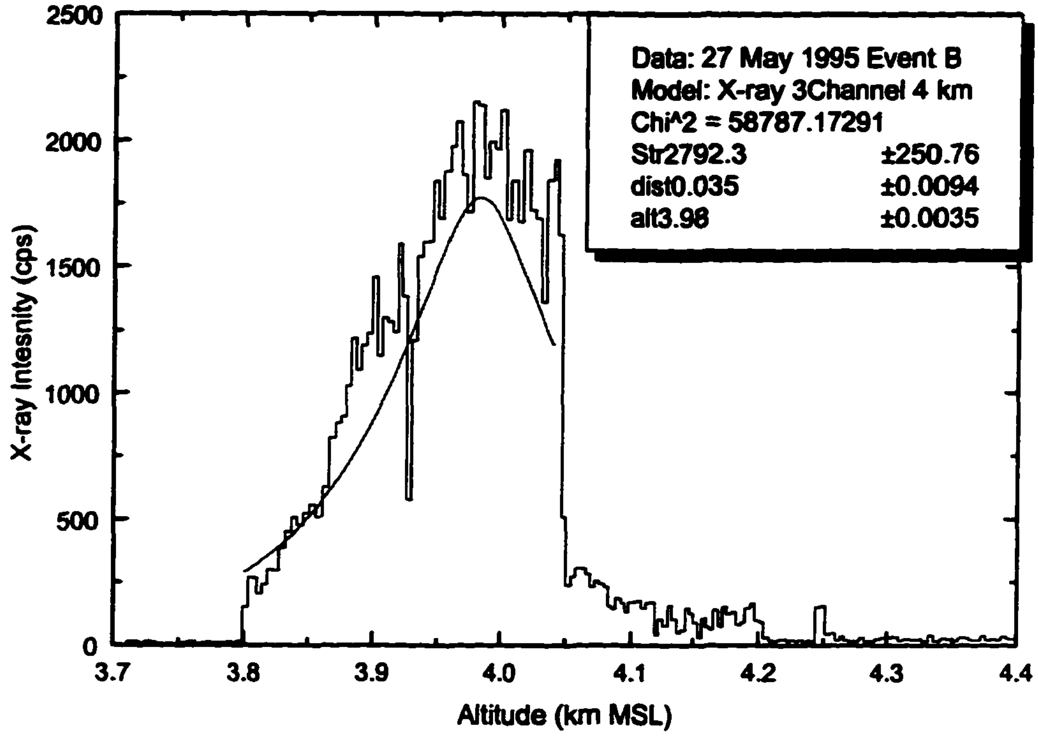

Figure D.3. Minimized chi-square fit for first x-ray event observed during Flight 3. The estimated source-to-detector distance is 35±10 meters.

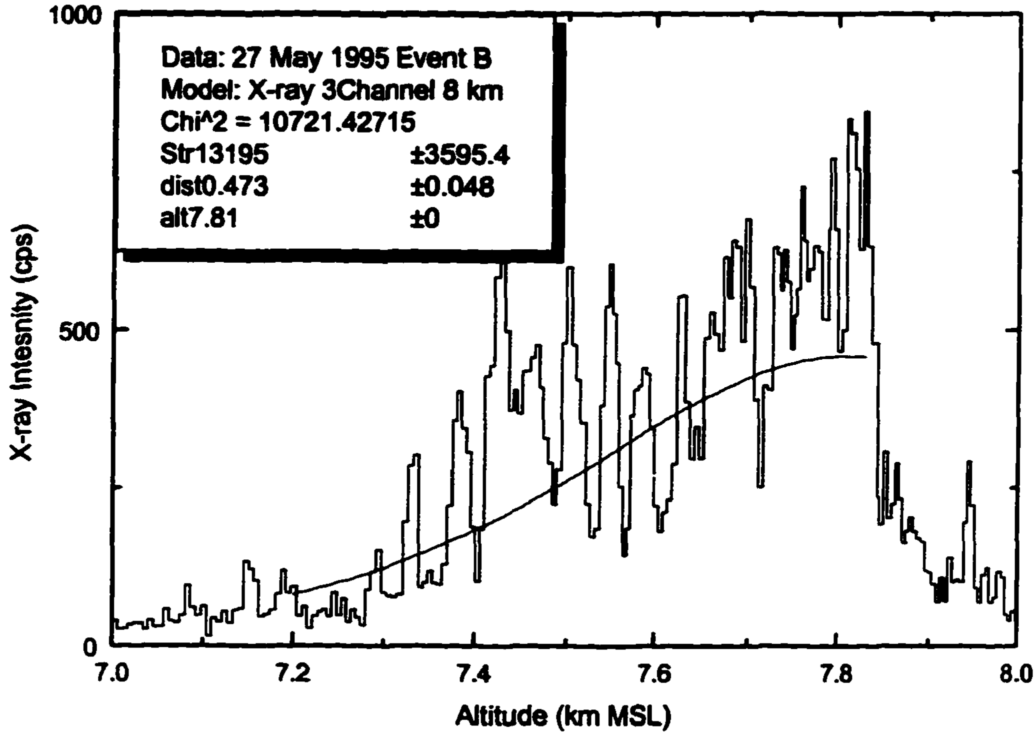

Figure D.4. Minimized chi-square fit for second x-ray event observed during Flight 3. The estimated source-to-detector distance is 470±50 meters.

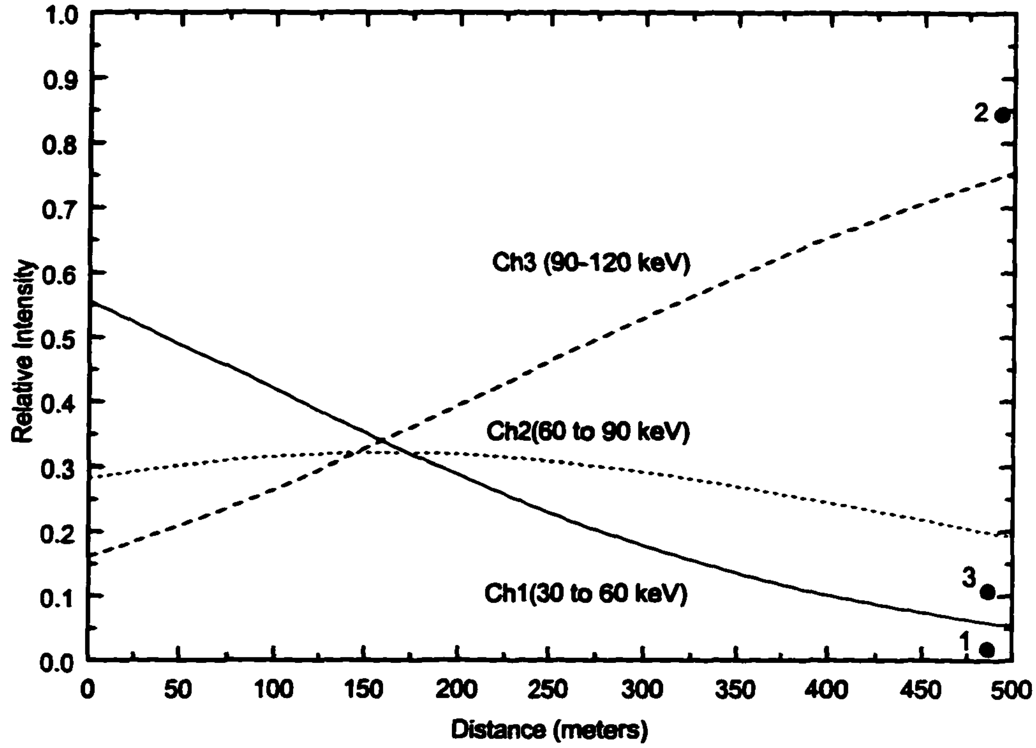

Figure D.5. Relative intensity of each channel as a function of distance from a bremsstrahlung x-ray source. Numbered dots indicate the relative intensities at peak total x-ray intensity for the event observed during Flight 1. Note that channels 2 and 3 are reversed and that a distance estimate cannot be made. This indicates that Compton scattering effects on the spectrum need to be considered.

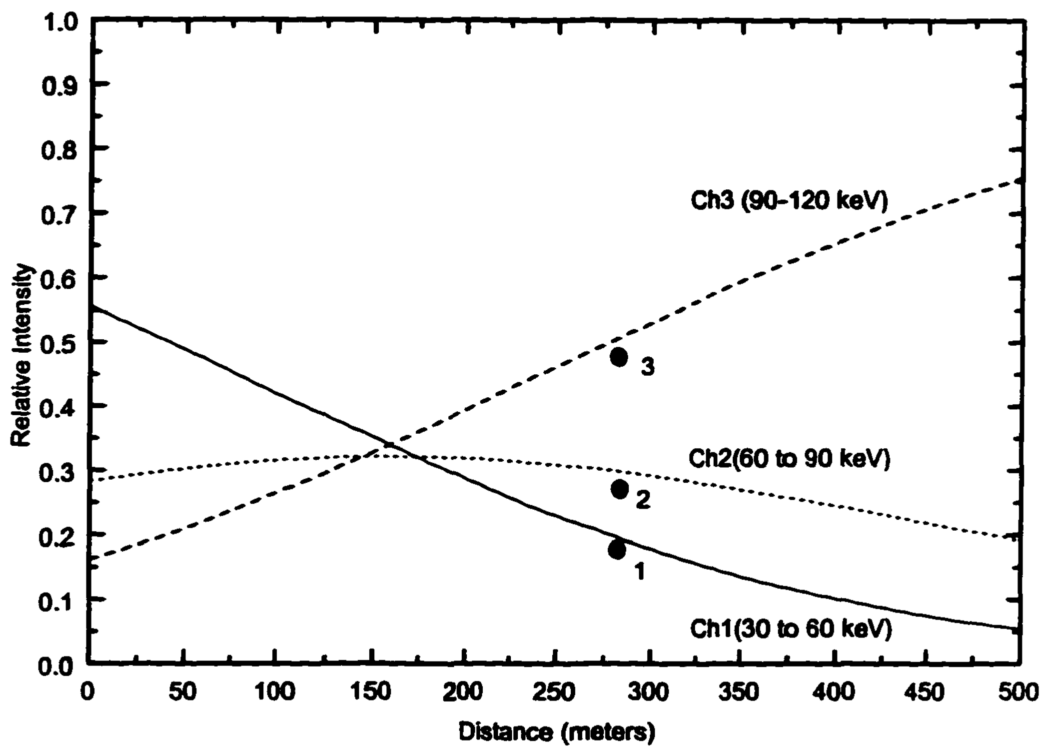

Figure D.6. Relative intensity of each channel as a function of distance from a bremsstrahlung x-ray source. Numbered dots indicate the relative intensities at peak total x-ray intensity for the event observed during Flight 2. From spectral information, the distance is estimated to be about 275 meters in agreement with the estimate from the rate of rise/fall method shown in Chapter 5.

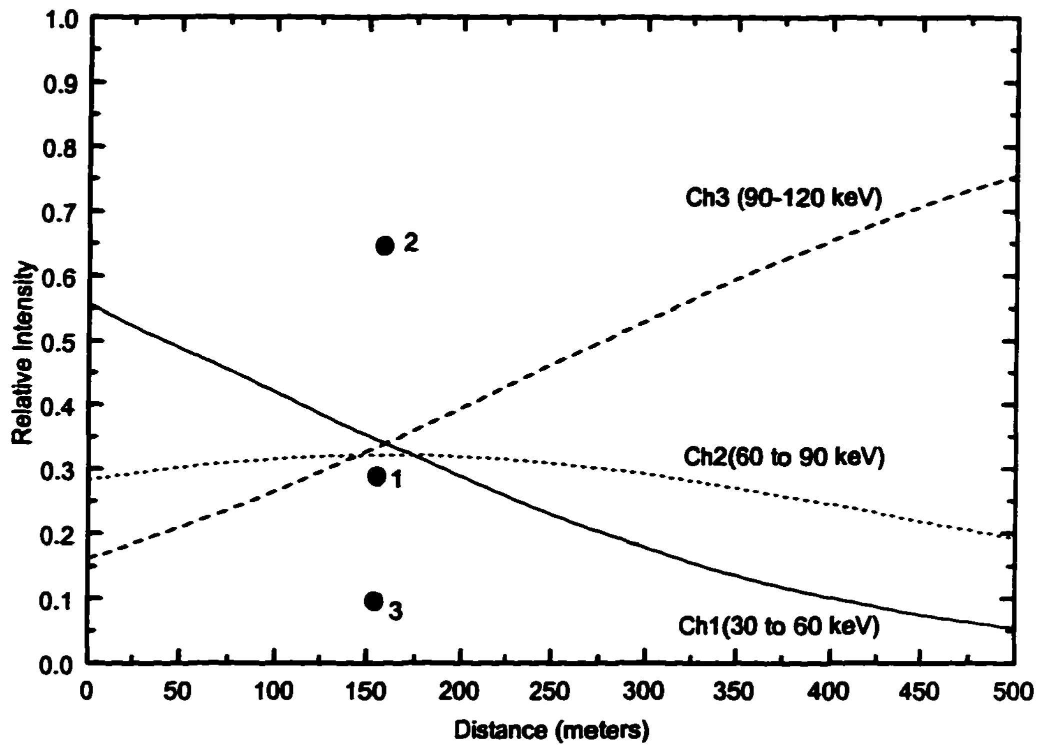

Figure D.7. Relative intensity of each channel as a function of distance from a bremsstrahlung x-ray source. Numbered dots indicate the relative intensities at peak total x-ray intensity for the first event observed during Flight 3. Note that channels 2 and 3 are reversed. A a distance estimate cannot be made. This indicates that Compton scattering effects on the spectrum need to be considered.

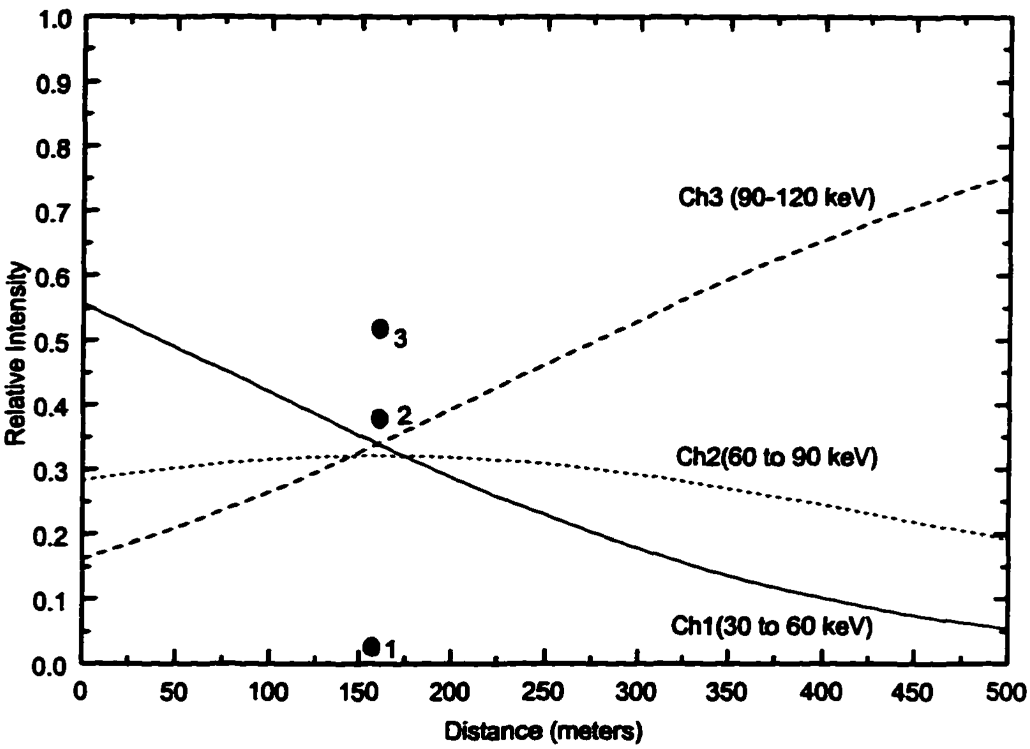

Figure D.8. Relative intensity of each channel as a function of distance from a bremsstrahlung x-ray source. Numbered dots indicate the relative intensities at peak total x-ray intensity for the second event observed during Flight 3. Note that channels 2 and 3 fit well for a distance of nearly 200 to 250 meters, but that x rays in channel 1 are almost completely absent. As for Flight 1, no distance estimate can be made using only absorptive effects on the spectrum.